5-2014

Rapid Condition Assessment of Bridges By Falling Weight Deflectometer

Jeremy David Rawn
University of Arkansas, Fayetteville

Recommended Citation

Rawn, Jeremy David, "Rapid Condition Assessment of Bridges By Falling Weight Deflectometer" (2014). *Theses and Dissertations.* 2290.
http://scholarworks.uark.edu/etd/2290

Rapid Condition Assessment of Bridges
By Falling Weight Deflectometer

Rapid Condition Assessment of Bridges
By Falling Weight Deflectometer

A thesis submitted in partial fulfillment
of the requirements for the degree of
Master of Science in Civil Engineering

by

Jeremy David Rawn
University of Arkansas
Bachelor of Science in Civil Engineering, 2009

May 2014
University of Arkansas

This thesis is approved for recommendation to the Graduate Council.

_____
Dr. Kirk Grimmelsman
Thesis Director

_____   _____
Dr. Panneer Selvam   Dr. Ernie Heymsfield
Committee Member   Committee Member

ABSTRACT

The objective of this thesis is to investigate the feasibility of using a Falling Weight Deflectometer (FWD) as an impact source to rapidly assess the condition of an in service bridge through the evaluation of its modal properties. Tests were conducted on two bridges, a Parker Pony Truss and a modern concrete deck on rolled steel beam bridge. Two full tests were performed on these structures with a hand held impact hammer and a falling weight deflectometer as sources for excitation. The advantage of using a FWD is that many transportation agencies already use these machines for pavement testing and this would provide a means of quantitatively evaluating bridges. This thesis will discuss the advantages and disadvantages of using a FWD and how it compares to the use of a modal impact hammer.

The experimental characterization results indicated that the FWD can be an effective device for the dynamic testing of highway bridges. The FWD enabled the identification of natural frequencies and mode shapes almost identical to those by typical hammer testing. Also, the extracted modal flexibility was in good agreement with modal flexibility extracted from the hammer test and static flexibility from the FE model.

The FWD has some positive qualities that make it attractive for the impact dynamic testing of bridges. First, many departments of transportation already have these devices. Second, the FWD produces an excitation force significantly larger than what can be produced by a standard hand-held impact hammer; the larger force leads to better signal to noise ratios in the measurements and more closely approximates service loads on the bridge. Finally, the FWD provides a fairly consistent impact force from hit to hit and from day to day, which is difficult and labor intensive to accomplish with a hand-held impact hammer.

ACKNOWLEGEMENTS

DEDICATION

This thesis is dedicated to my wonderful wife Molly for her unconditional support and encouragement.

TABLE OF CONTENTS

TABLE OF FIGURES

1.   INTRODUCTION

1.1   PROBLEM STATEMENT

Several full-scale testing methods can be used to characterize and evaluate the global performance and condition of a bridge. These global methods consist of mainly static load tests and dynamic tests that use controlled or uncontrolled dynamic excitation. Each approach has advantages and disadvantages for experimental and logistical considerations, data analysis requirements, and scope and utility of the characterization results obtained. This paper presents a global dynamic characterization program based on controlled impact dynamic testing that was applied to a truss bridge. The impact testing was performed with a hand-held impact hammer and a falling weight deflectometer (FWD) as dynamic excitation sources. The objective of the project was to evaluate whether the FWD, which could produce a broadband dynamic force, could be an effective tool for the quantitative characterization of bridge performance and condition. Many transportation agencies already use FWD devices for their pavement evaluation programs, and it follows that if the device is suitable for the impact dynamic testing of bridges, then agencies also can use FWDs to evaluate bridges quantitatively. Dynamic testing approaches are discussed, and an impact dynamic testing program executed for the truss bridge is presented. The results obtained with the two dynamic excitation devices are presented and compared with each other and with the results from an analytical model of the bridge. Finally, several observations and conclusions related to the efficacy of FWD devices for the impact dynamic testing of bridges are presented and discussed.

The need to monitor and service the nation's infrastructure is an issue that requires constant evaluation and improved research to effectively diagnose the aging infrastructure in the United States. One major concern that will be put into focus in this report is the need for rapid assessment of the nation's bridge population. The most commonly used method of evaluation is through the use of visual inspection. The limitations to visual inspection are just that, only visual damage can be reported. Damage that may be present in locations that are not visible or accessible to inspectors can go undetected. There are over 600,000 bridges in the United States and all of these bridges require inspection to assure that they are safe for daily use. Inspectors are responsible for evaluating and diagnosing the condition of the bridge's deck, superstructure, and substructure over a span of 24 months when inspections occur. While these means of inspection are effective, the results tend to be qualitative and not quantitative. To assist in these inspections it is being proposed that the use of dynamic tests can help in identifying the condition of bridges in a rapid manner by extracting the structures modal parameters. This can be accomplished by using a falling weight deflectometer to impact a bridge and evaluate the bridges condition based on the reaction from the bridge. These methods of evaluation are aimed at assisting the inspectors while also developing a system that will quickly and effectively evaluate these bridges.

The current bridge population in the United States has aged to what is close to their original design life. AASHTO states that nearly one in four bridges in the United States is either structurally deficient, in need of repair, or functionally obsolete (AASHTO, 2008). These bridges that are currently in need of evaluation were designed with a life span of 50 years, and today the average bridge age is 43 years. The National Bridge Inspection Standards (NBIS) uses a rating scale of 0 to 9 to rate the condition of bridges, from zero being in the worst condition and nine

being in the best condition (AASHTO, 2008). To assign a rating the bridges superstructure, deck, and substructure must be inspected. If the condition rating for a bridge is 4 or less, the bridge is determined to be structurally deficient. Of the close to 600,000 bridges inventory, 12% were found to be functionally obsolete and about 13% were found to be structurally deficient. This is not to say that these structures cannot be used but they must be observed with caution. AASHTO acknowledges that improvements are needed in the inspection of bridges where more than just visual inspection can be used. Specifically mentioned is the use of accelerometers by the Iowa DOT to measure vibrations that occur (AASHTO, 2008). The methods of how these vibrations can be acquired and analyzed will be discussed in this report.

The ASCE's report card for America's Infrastructure is another influential resource that gauges the current condition of the infrastructure in the United States. The report card released in 2009 by the ASCE rates the condition of the nation's overall infrastructure as well as individual pieces including roads, bridges, and water and sewer systems. The overall grade for the infrastructure received was a D, although the bridge's received a grade of a C (ASCE, 2009). As a solution to this problem, the ASCE recommends updating bridge-inspection standards. As the ASCE reports from the Department of Transportation in 2008, 12.1% of the bridges were considered structurally deficient and 14.8% of the bridges are considered to be functionally obsolete. The reports from both AASHTO and the ASCE draw the same conclusion that the nation's bridges are in need of repair and an efficient means of inspection to prioritize the bridge's that are in the most need.

In a 2001 report from the FHWA regarding reliability of visual inspections, five types of bridge inspection are described (Moore, 2001).

- Initial Inspection

- Routine Inspection

- In-Depth Inspection

- Damage Inspection

- Special Inspection

For bridge evaluation, AASHTO discusses specific methods that can be used to evaluate a structures condition. AASHTO has two classifications of load tests: diagnostic tests and proof tests (AASHTO, 2011). The diagnostic test is a quantitative test, meaning that the results can be analyzed and quantified in a way that will provide a means of measurement for future evaluation. A proof test is more qualitative in that it is a function of visual defects and the ability of the inspector to identify damage. The results from a proof test would determine a bridge's load capacity and the location of external damage, but may not indicate the true extent of the bridges in-situ capacity. In comparison, the results from a diagnostic test, would determine a bridge's response to specific loadings as well as the identification of internal damage that may not be visible from visual inspection. For this report and for the benefit of furthering testing alternatives, the importance and benefits of diagnostic testing will be discussed further.

Diagnostic testing is performed by applying various dynamic loads and static loads to a bridge in order to gage a response. The results from the tests are quantitative measurements because they are measured, analyzed, and assigned a mathematical and rational meaning. These two methods, static testing and dynamic testing, provide a means of global analysis that is not available with visual inspection. Quantitative inspections can be much more beneficial than qualitative inspections in determining the real condition of a structure. Qualitative evaluations are based on visual inspection, and do not provide analysis of the performance the bridge

experiences under loading. The results from these types of inspections can provide results that can identify and assess local conditions. The results can then be extrapolated to produce a global analysis of the bridges condition. Static testing and dynamic testing can both be used to produce these results, although the constraints of static testing make it less beneficial in the need for rapid assessment of bridges.

Dynamic testing methods are classified as operational modal analysis (OMA) and experimental modal analysis (EMA). The difference between EMA and OMA is the means of excitation used to cause the vibrations. OMA consists of uncontrolled vibrations, where EMA uses a controlled means of excitation. The uncontrolled methods of vibration are ambient sources such as traffic and wind. These sources of vibrations are difficult to quantify, but it is the response from the bridge that is needed for analysis. Using OMA mode shapes, damping, and frequencies can be established, but these parameters alone do not allow for accurate detection of damage. By properly analyzing the results from EMA the modal parameters can be scaled to provide the modal flexibility of the structure.

AASHTO lists dynamic testing as a means of evaluation but does not apply enough depth into the means and methods to show that the test can be performed efficiently and effectively. The objective of this report is to show that these methods can be used to effectively diagnose bridge and provide the bridges global condition. The collected data can be used as a baseline for future testing where a database can be established to record the bridges behavior over time. The depth at which AASHTO discusses dynamic bridge testing lists that frequencies, mode shapes, and damping can be determined from vibration testing. AASHTO also discusses the use of shakers, the sudden release of applied deflections, and the sudden stopping of vehicles by breaking as sources of excitation, but these are not effective means of providing rapid condition

bridge assessment. This is due to the impracticality of closing the bridge in order to acquire ideal testing conditions. The use of an impulse caused by a hammer, provide a more rapid evaluation, especially if the number of impact locations can be limited. One major benefit of using hammer impacts is through the use of modal analysis to acquire the information that is available within the frequencies, mode shapes, and damping. These parameters can be used to identify local damage within the structure and further more acquiring a global condition of the bridge. The use of the modal impact hammer will be discussed in this report as it has been proven to be a reliable excitation source. The hammer's reliability and accuracy is the basis of furthering the research in impact testing of bridges through the use of falling weight deflectometers.

1.1.1   Quantitative Inspection

By performing quantitative inspections as opposed to qualitative inspections the bridges will be characterized based on their behavior and not only on their visual appearance. There are two methods that can be used to acquire quantitative results: static testing and dynamic testing. Using these two methods of evaluation, a global characterization can be made for the structure and it can be defined in terms of flexibility. Defining the structure in terms of flexibility provides engineers with a relatable value to common engineering principles. Both methods are useful for evaluation but using dynamic testing has the promise of showing more reliability and accessibility than static testing.

1.1.1.1   Static Testing

Static testing on a bridge can be time consuming and requires a bridge to be closed through the duration of the test. The issues caused by the closing of selected bridges causes interference with the daily flow of traffic and are an inconvenience to the general public. In order to perform static tests the bridge must be instrumented with displacement gages and strain gages in several locations to measure how the bridge performs under a variety of loading conditions. Initial tests are run to establish baseline readings without any load applied to the bridge. The initial test is followed by a series of load test where the bridge is incrementally loaded. In order to acquire accurate readings the bridge must be properly instrumented with sensors that can detect minor changes in the structure. The application of the sensors on the bridge is very complicated and time consuming and varies depending on the type of bridge being tested. Strain gages must be attached to a clean surface on the bridge so that there is no slippage between the sensor and the surface of which the sensor is being applied. Having to thoroughly clean the locations where the strain gages are to be placed requires extra labor and increases the time needed to complete the test. Displacement transducers require a reference point that the bridges displacement can be measured against. This can prove difficult because in general a bridge is constructed over terrain that would usually be difficult to navigate. Once these sensors are connected to the bridge, they then require cabling to be run to a data acquisition system that is located some distance away. To acquire accurate readings there must be significant loadings applied to the bridge. One method is the use of loaded dump trucks that can be used to manually load the bridge. The trucks must be weighed so that the applied load is known for the resulting displacements. Using these measures the flexibility of the bridge can be determined and then the

stiffness can be defined. These methods require that the bridge be closed to traffic while testing is being performed. This is an inconvenience in high traffic areas where a stoppage in traffic flow would have unfavorable implications on the public in general.

1.1.1.2   Dynamic Testing

Using dynamic testing can be much more advantageous in terms of time and the ease of testing. The materials required for dynamic testing include sensors, a method of excitation, and a data acquisition system. An accelerometer is the most common sensor used for dynamic bridge testing. The accelerometer uses gravity as a reference point to measure the response of the bridge. Where in static testing the sensors must be attached to a fixed point and be restricted from movement. The accelerometers can easily be mounted to the structure by magnets either on the bridge's deck or superstructure. By attaching the sensors to the superstructure, testing can occur while preventing traffic stoppage or keeping the stoppage at a minimum. The methods of excitation can be from controlled or uncontrolled sources. The uncontrolled sources include ambient vibration that would come from traffic or wind. The controlled sources include impact testing, shaker testing, or by displacing the bridge and releasing it to free vibration. With dynamic testing the sensors are used to measure the response from these controlled or uncontrolled sources of excitation. The way in which the bridge vibrates is a result of its global condition, and any damage will show up in its flexibility. The measured responses can be used to find the mass and stiffness properties of the bridge and the bridge can then be defined in terms of flexibility.

1.1.1.3   Dynamic vs. Static

Dynamic testing has much more feasibility as a means of bridge evaluation because the test requires less man power, ease of instrumentation, and the structure can remain open through testing. In static testing there are many more variables in the outcome due to difficult sensor instrumentation and the acquisition of an available load that is large enough and to cause a significant deflection in the bridge. By using accelerometers, the issue of having a physical reference point is diverted because of its reference to gravity. Applying sensors to the bridge in this manner reduces the amount of time needed to fix a displacement transducer to a secure and grounded location. Several options are available that can be used to excite modes depending on the specific needs of the test. Long term monitoring can be achieved using ambient testing while rapid condition assessment can be achieved by impact testing. Having the ability to perform impact testing will allow for a larger sample of bridges to be evaluated for current and future reference. Initial tests are performed to acquire a baseline reading of the bridge so that a model can be built for future evaluations. Once an initial model is built, the use of rapid impact testing can be used to evaluate damage that occurs.

1.2   OBJECTIVES

AASHTO describes damping, frequencies, and mode shapes as the parameters that can be obtained through dynamic testing as a means of assessing damage. Much research has been performed, and will be discussed in this report to show that these three characteristics can be acquired and also used to extrapolate more information about the bridge's condition through the

modal parameters by the use of modal analysis. These modal parameters are beneficial in developing a modal flexibility, which is equivalent to the static flexibility, and performing rapid bridge evaluations.

The purpose of this study is to investigate the feasibility of effectively using a falling weight deflectometer (FWD) to perform impact tests on a bridge. Because most transportation departments already own FWD devices and are familiar with their operation, it could be advantageous to also use this tool for multi reference impact testing of bridges. Generally, a modal hammer is used to impact the bridge at a variety of locations where sensors have been placed. One major problem with the impact hammer is that there is a good potential for human error to influence the quality of the experimental results. Because of the requirement that several hits are needed at every location where an impact must occur, several inconsistencies can be caused through the lack of attention and consistency of impact. By using the FWD, this human error could be removed from the test by replacing impacts of various force and duration with impacts that are consistent and known. The range of force provided by FWD drops can potentially be useful on both small and large bridges and single and multi-span bridges. Two different bridges located near the University of Arkansas were tested for this study using both an impact hammer and a FWD as sources of impact. The results are compared to verify that the proposed methods can be used for bridge evaluation. There is very little discussion given to this by AASHTO and it is not discussed in a way that shows that these tests can be performed with accuracy, consistency, and reliability. With a better understanding of modal testing and a greater understanding of how the results can be used effectively will provide AASHTO with another effective tool of evaluating an infrastructure that is rapidly deteriorating.

1.3   SCOPE

This main scope of this research project consists of dynamic testing of two in-service bridges using a falling weight deflectometer to characterize the bridges in terms of their flexibility matrices. The FWD is used as an excitation device to perform multi-reference impact testing (MRIT) of a multi-beam bridge and a simply supported truss bridge. The overall research process included laboratory testing and evaluations of a very simple cantilever beam structure and a more complicated steel grid model structure. The experiments with the cantilever beam and steel grid models are used to design and implement a testing scheme for field testing portion of this research. The laboratory tests are also used to determine the most advantageous locations for sensor placement and impact locations in the field. The research presented herein consisted of a three stage process:

      1) Quantitative characterization of a simple cantilever beam model.

      2) Quantitative characterization of a more complex steel grid structure.

      3) Quantitative characterization of two full-scale bridges by multiple-reference impact
         testing methods.

The cantilever beam model was characterized and evaluated first because it is a very simple structure that can be analyzed with very little uncertainty. The simplicity of this structure is helpful for validating the proposed testing and analysis methods and for developing a rational testing scheme. The grid model is a structure that has been designed to resemble a bridge and it can be characterized three dimensionally. Impact and static testing is performed on both the cantilever beam and the grid models. The experimental and data analysis methods employed in the laboratory are then applied to two in-service bridges to identify their dynamic properties and

to characterize their present condition in terms of their flexibility matrices. These results provide a quantitative baseline description of their in-situ performance. When testing a bridge in the field, there will be more uncertainty than in the laboratory. This is why the laboratory testing is a critical step in the verification of the proposed method. Using the modal hammer for the impact test in the lab and verifying the results with the static load tests, enables more confidence in comparing the hammer results with the FWD results for the full-scale bridges. The field tests provide a real world evaluation that can be applied to a wide range of bridges across the state for condition assessment.

2.   LITERATURE REVIEW

2.1   GLOBAL CHARACTERIZATION OF BRIDGES

A bridge can be globally characterized by defining the structure in terms of its overall flexibility. Local damage and deterioration will be automatically reflected in this global characteristic thereby enabling more rational and reliable assessments of bridge condition. Flexibility is used as a tool to globally describe a structure based on the Maxwell-0Betti theory of reciprocity (Hibbeler, 2006), where the displacement at several locations is measured as a result of a single unit load. By repeating this process on several locations, a flexibility matrix can be obtained that will define the global condition of the bridge based on several load points. If damage has occurred after an initial baseline test has been performed, that damage can be located through future tests. It should also be noted that global flexibility is, by definition, the inverse of the global stiffness matrix for a structure. Thus, it is possible to determine a structure's stiffness by first determining its flexibility.

There are two primary ways to experimentally determine the flexibility of a bridge structure: (1) static load testing, and (2) through controlled dynamic testing. In a static load test, known loads are placed at known locations on the structure and the resulting deflections are measured at various points of interest. The results are normalized to a unit load to develop the flexibility matrix. Flexibility is determined from controlled dynamic testing by identifying the modal parameters (natural frequencies, mass normalized mode shapes, and damping ratios) which can be related to the flexibility of the structure through its frequency response function (FRF). The modal parameters of the structure are considered structural properties as they are

mathematically related to the structure's mass and stiffness characteristics. Identifying a structure's flexibility through dynamic testing may appear to be a more elaborate and complicated approach than through static load testing, however, in many instances, the experimental requirements for a controlled dynamic test can be significantly more practical and cost effective than those required for a static load test. The details of each testing approach and the procedures required for computing the flexibility of a bridge are presented in the following sections through a review of the available published literature.

2.1.1   Static Load Testing

Static load testing is a very direct method in defining the global characteristics of a structure. A load is applied to the bridge at one location and the bridge responses to that load are measured at every location that a sensor is placed. The location of each sensor is specifically planned so that the bridge will be accurately represented once analysis is performed. The deflections of the structure at various points can be measured directly using displacement sensors, or they can be computed from tiltmeter measurements or strain gages using structural mechanics relations. The flexibility is defined and reported in matrix form by determining the deflections at several output locations (matrix rows) for loads placed at various input locations (matrix columns). The testing approach is a very straightforward and there are limited calculations involved, but static testing has several complications that make it time consuming and labor intensive (Levi et al., 1997; Catbas et al., 2001b; Alampalli and Kunin, 2003).

Static load testing of a bridge to determine its flexibility requires that the structure be instrumented with numerous displacement transducers and/or strain gages. Strain gages must be

carefully installed and securely fastened to the structural members so that accurate measurements are recorded. The sensors can be micro dot welded or bonded with adhesives. When attaching the strain gage, the surface of the structure where the attachment is made must be carefully prepared and cleaned at the time that the strain gage is installed. To utilize strain measurements to compute deflections and ultimately flexibility, the moment at the strain gage location must first be determined using linear-elastic stress-strain relations and the geometry of the member cross section. This generally requires more than one strain gage be installed on the member cross section at the point of interest for computing the deflection. A similar approach can be implemented for tiltmeter measurements using analytical slope-deflection relationships for the bridge members. Displacement transducers can be used to directly measure the deflections of various points on the structure under applied loads, but these sensors require some fixed point of reference. Securing such a fixed point of reference is often problematic for bridges located over water, active roadways, and for bridges having large vertical clearances.

The known loads used for a static load test are typically heavy loaded dump trucks. The trucks are placed at various known positions on the bridge deck while the bridge is temporarily closed to normal traffic, and the sensor measurements are recorded. This loading scheme can be problematic for bridges with questionable structural capacities, those with load restrictions, and bridges with lots of traffic. Large loads are generally required to attain the necessary signal-to-noise ratios in the measurements to obtain reliable results.

2.1.2   Dynamic Testing

Dynamic testing offers a more simplified approach for experimentally determining the flexibility of a bridge. Dynamic testing is different from static testing in that the bridge is excited by some controlled or uncontrolled dynamic (time-varying) force that activates the structure's inertia forces. The time-varying bridge responses due to this excitation are usually measured with accelerometers, although velocity transducers (geophones) are sometimes used for this purpose. The use of accelerometers to measure the bridge's dynamic response has several important advantages including: (1) the sensors are much more sensitive than strain gages or displacement transducers; (2) the installation requirements for the sensors are very simple are require minimal surface preparation (accelerometers can be attached to steel bridges using magnets); and (3) the external frame of reference for the sensor is the Earth's gravitational field.

Dynamic testing can be accomplished using either controlled or uncontrolled methods of excitation. Controlled excitation testing requires a mechanical device to supply known or measureable random, harmonic or impulsive dynamic forces to the structure. These devices can include impact or drop hammers, and linear and eccentric mass shakers. (Douglas and Richardson, 1984; Farrar et al., 1999; KRÄMER and DE, 1999). Controlled dynamic testing using shakers or impact devices are the most suitable approach for determining a bridge's flexibility. Both the input (dynamic excitation force) and the corresponding bridge accelerations (outputs) are measured and utilized in the data analysis stage. The measurements from a controlled vibration test can be used to determine the natural frequencies, mode shapes, damping ratios and modal scaling for the bridge. Modal scaling can be determined as a result of the input-

output measurement pairs and is a key parameter used in computing the flexibility of a bridge from the measurements.

Dynamic testing by uncontrolled excitation takes advantage of the unmeasured ambient excitations due to traffic, wind, and other natural sources. This testing approach is commonly referred to as ambient vibration testing (AVT), operational modal analysis (OMA) or output-only vibration testing. AVT is generally easier, cheaper and more practical to implement for in-service bridges than controlled dynamic testing. It is also a very desirable approach for monitoring the dynamic properties of a bridge over long periods of time since it does not interfere with the normal operation of the bridge. Only the measured vibration responses of the bridge are used in the subsequent analysis of the data. The measurements can be analyzed to determine the natural frequencies, mode shapes, and damping of the structure. Because uncontrolled testing does not measure the input to the structure, this approach cannot be directly used to obtain modal scaling, and hence, the flexibility of the bridge.

All of the dynamic testing methods described above are adequate if the objective is to identify the dynamic properties (frequencies, mode shapes and damping) for a bridge. Changes in the dynamic properties have been investigated by many researchers as indicators of structural damage or deterioration; however, these parameters have not been found to be reliable indicators of damage in specific locations on a structure. The modal parameters for a bridge can also change over time due to temperature changes and other environmental effects (Farrar et al., 1997; Liu and DeWolf, 2007), and these changes can often be larger than those that occur due to damage or deterioration.

Static and dynamic testing are both valid experimental approaches that can be used to quantitatively characterize the in-situ properties of a bridge. Dynamic testing has several

experimental and practical advantages that make it more practical and rapid for evaluating most in-service bridges. Of the available dynamic testing methods, controlled dynamic testing provides a means for identifying the modal properties of a bridge and for computing its flexibility. Uncontrolled dynamic testing is more cost-effective and practical to implement than controlled dynamic testing, but it is somewhat more limited in capabilities than controlled dynamic testing is since the output-only measurements cannot be used to directly compute the flexibility of the structure from the test measurements.

2.1.2.1 Dynamic Impact Testing

Of the controlled dynamic testing approaches described above, the most cost-effective and practical approach to implement for bridges is multiple-reference impact testing (MRIT). This approach requires an excitation device that can provide impulsive type dynamic loads to a bridge structure. The excitation devices that have traditionally been used for impact dynamic testing of bridges include hand-held impact hammers (instrumented sledges), drop weights, and drop hammers. The use of a large drop weight can cause issues because of its mobility (Krämer and De, 1999). Due to their portability and low-cost, hand-held impact hammers are the most commonly used device for impact testing. A modal impact hammer has a dynamic force sensor attached to the head of the hammer that measures the generated impact force when the hammer strikes the bridge (usually on the deck surface). A larger hammer can also be used in conjunction with a dynamic force sensor that is attached to a rigid surface and is used to measure the impact force from the hammer. The use of impact hammers is popular because they are lightweight and mobile. Mobility is important when bridge testing and is beneficial in being able collect input-

output measurements from many locations rapidly. The main drawbacks of impact hammers are that are labor intensive (someone must swing the hammer to provide the impact force), and inconsistencies of the impact due to human operation. The operator often must deliver multiple impacts at several designated locations for averaging purposes to mitigate the inconsistencies between independent hammer strikes. When this is performed manually; the amplitude, location, and time of impact can vary.

A falling weight deflectometer (FWD) device was investigated as a potential impact excitation device for dynamic testing of bridges in this Thesis. The use of an FWD as an impact device for controlled dynamic testing is an approach that has not be extensively evaluated, although it does have promise as being a viable tool for MRIT evaluations of in-service bridges. A significant advantage associated with the use of FWD devices is that most departments of transportation already own and use these devices for their pavement evaluation programs, and extending the use of these devices as a tool for also characterizing their bridges has obvious economic and practical benefits.

There are very few examples in the literature describing the use of FWD devices for bridge testing. Hoadley and Gomez (1996) used an FWD with its installed geophones to measure the local deflections of bridge decks. Catbas et al. (2001a) describe using a FWD device to capture the natural frequencies of a bridge which would be compared with prior test results to identify and evaluation damage. The research project presented in this report explored the use of the FWD strictly as a potential excitation device for impact dynamic testing of bridges since it offers advantages of mobility and consistency of the impact forces generated. Based on their vibration testing results for a multiple span bridge using traditional excitation approaches, Turnage and Baber (2009) suggest that a FWD could be used to provide larger impulsive forces

for locating natural frequencies during preliminary vibration testing of bridges. In a research report published for the Kansas DOT, the FWD was proposed as a tool for bridge rating, but was not actually applied to an actual bridge (Melhem et al., 1996).

2.2   MODAL FLEXIBILITY

Modal flexibility is the accumulation of modal vectors and describes how they contribute to the flexibility matrix of the structure. The concept of modal flexibility was introduced as a way to compute an approximation of the static flexibility using the dynamic properties of a structure. The modal flexibility concept has been explored in several prior studies as a means for characterizing and evaluating bridges (Raghavendrachar and Aktan, 1992; Toksoy and Aktan, 1994; Pandey and Biswas, 1994; Doebling and Peterson, 1997; Zhang and Aktan, 1998; Patjawit and Kanok-Nukulchai, 2005; Catbas et al., 2006). Modal flexibility is frequently computed using the results acquired from controlled dynamic testing methods such as MRIT. Modal flexibility was first formulated using unit mass normalized mode shape vectors and their associated natural frequencies. Calculating the modal flexibility in this form is difficult due to problems with approximating an accurate mass model for the system. Due to the variations of age and degree of deterioration of a test specimen, approximating the mass may be a difficult task without accurate plans and specifications. When experimental data is used to calculate modal flexibility, unit-mass-normalized modal vectors are not used. The mass is instead approximated from the captured and scaled data. The concept of using modal flexibility to detect damage has been tested and shown to be successful in the laboratory and field by the researchers previously discussed.

2.3   DAMAGE DETECTION USING MULTI REFERENCE IMPACT TESTING

Pandey and Biswas (1994) studied the use of modal flexibility as a method of locating damage in structures. They wanted to use the convergence of frequencies and mode shapes to the flexibility. Their research involved laboratory testing of a W12x16 beam and applying damage scenarios. The location of the applied damage was located by a significant jump in the flexibility at that position and the only first two frequencies of the beam were used. The information used to classify damage was recorded directly from the experimental data collected and not from an analytical model.

Toksoy and Aktan (1994) investigated modal flexibility for evaluating bridge condition by acquiring the modal parameters and calculating the modal flexibility for an existing bridge. The bridge was tested in its natural state and after controlled damage scenarios had been induced. Tests were performed in phases by removing a layer of asphalt off of the surface of the bridge. Static testing and dynamic testing were both used to characterize the bridge and the results from both approaches were compared. Loads were applied to the bridge to initiate a damaged state while modal impact testing was performed to detect damage from the test. Damage was detected before failure in an area below an asphalt overlay. This is a location that would not be detected through visible inspection, but was located through the global characterization of the bridge by dynamic testing.

Raghavendrachar and Aktan (1992) mathematically synthesized frequency response functions from the identified modal parameters for a bridge and compared them to the measured frequency response functions from the same structure. Modal flexibility was calculated using unit-mass-normalized modes and compared with the static flexibility. Their results showed great

correlation between the two approaches. The number of scaled modes acquired and used in the modal flexibility calculation was also examined to evaluate the importance of the torsion modes. The authors showed that modal flexibility could be underestimated by not incorporating enough identified modes into the formulation.

Doebling and Peterson (1997) proposed an approach for computing statically complete flexibility from a dynamically measured flexibility. Modal flexibility represents an approximation of static flexibility as it the summation of all of a structure's modal results, some of which may not be experimentally identified. This approximation can lead to modal flexibility that does not accurately reproduce the force-displacement relationships for a structure. The authors present a technique for synthesizing a statically complete flexibility matrix from the measured modal flexibility matrix by analytically reproducing specific partitions of the modal flexibility matrix and scaling them such that they match the predictions of the statically complete partitions modal flexibility matrix. The partitions of the scaled flexibility matrix are combined with the statically complete partitions of the modal flexibility matrix to produce a nearly statically complete flexibility matrix. The authors tested and evaluated their approach both numerically and experimentally using a simple cantilever beam model. This issue may not be as significant for bridge applications as for other more complex mechanical systems. The papers that describe the implementation of modal flexibility for bridges (Raghavendrachar and Aktan, 1992; Zhang and Aktan, 1998) showed that very accurate modal flexibility matrices could be obtained by including the lower order modes that tend to dominate the dynamic response of constructed systems, and that can be easily identified through dynamic testing.

Methods for calculating the modal flexibility directly from identified modal parameters is discussed in Catbas et al. (1997), Catbas et al. (2004), and Catbas et al. (2006). The techniques

described by the authors in these papers included the use of the complex mode indicator function (CMIF) which is comprehensively discussed in Allemang and Brown (2006) and is based on singular value decomposition (SVD) of the measured FRF data acquired from controlled dynamic testing. The CMIF is a zero order, spatial domain algorithm that allows for an accurate amount of modes, including closely-spaced modes, to be identified for subsequent processing and analysis. Animated mode shapes are also used in the evaluation of the results evaluation to detect any inconsistencies in the mode shapes. Catbas et al. (1997) Calculated modal flexibility using modal parameters independent of unit mass normalized vectors (Raghavendrachar and Aktan, 1992). This method allows for the modal parameters to be found using the material properties from acquired test results. This research successfully compared flexibility acquired from static load tests with modal flexibility calculated in terms of the identified modal parameters. Testing was performed before and after damage was induced to the structure by the removal of bearing plates. The induced damage was detected using both static flexibility and modal flexibility. The results discussed in this paper showed that the results can be derived directly from the FRF and not require unit-mass normalized modal vectors.

Patjawit and Kanok-Nukulchai (2005) proposed a method for tracking the condition of a bridge using the modal flexibility matrix. The authors proposed using the spectral norm of the modal flexibility as a Global Flexibility Index (GFI) describing the condition of a bridge. A sharp change in the GFI would signify a rapid weakening trend for the structure. The authors evaluated their method on a simple steel channel beam in the laboratory and with an existing concrete slab bridge.

Using modal flexibility as a tool for bridge evaluation has been shown to be effective in many of the papers listed above; however, the modal flexibility matrix can be complicated to

interpret on its own. Zhegnsheng et al. (2005) and Catbas et al. (2006) utilized a bridge girder condition index (BGCI) to simplify the usage and interpretation of the modal flexibility matrix. The BGCI represents the deflected shape of a bridge girder obtained by virtually loading the modal flexibility matrix obtained from dynamic testing with a load vector corresponding to some real loading condition for the structure. In the two papers listed above, the authors compared girder deflection profiles obtained from the modal flexibility with the values obtained from controlled static load tests. Similar comparisons could be made with results from analytical or finite element models of a bridge.

2.4   ANALYTICAL FORMULATIONS OF STATIC AND MODAL FLEXIBILITY

The literature discussed thus far in this chapter represents developments in both the laboratory and field research that have shown the viability of dynamic testing and modal flexibility for evaluating bridges. In order to better understand the experimental procedures and the corresponding data analysis techniques, it is helpful to first examine the formulations for static and modal flexibility from an analytical perspective.

2.4.1   Static Flexibility

Static flexibility is simply the inverse of stiffness. It can be defined as the deflection at some point i due to a unit load applied to the structure at point j. The individual elements of the static flexibility matrix, f, are denoted by f_{ij}. The individual elements of f are computed using

basic deflection computations. The static flexibility matrix is symmetric due to the Maxwell-Betti theorem of reciprocal displacements, and elements $f_{ij} = f_{ji}$ (Hibbeler, 2006).

Consider the cantilevered beam shown in Figure 2.1. The beam has length of l and a flexural rigidity of EI. The beam can be represented in an idealized manner by discretizing it into four displacement (translation) degrees of freedom that are evenly spaced along the length of the beam as shown in the figure. The static flexibility matrix for the beam can be formulated in terms of these four degrees of freedom (DOF) using closed form deflection equations available from standard references such as the AISC Steel Construction Manual (AISC, 2011) using a concentrated load p with a unit load value:

$$y = \frac{px^2}{6EI} (3a\text{-}x) \quad for \ o < x < a \qquad [2.1]$$

$$y = \frac{px^2}{6EI} (3x\text{-}a) \quad for \ a < x < l \qquad [2.2]$$
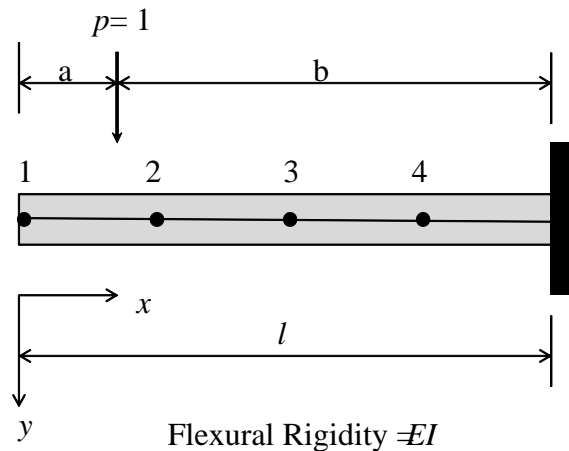
Figure 2.1: Cantilevered beam idealized by four displacement degrees of freedom
Figure by Dr. Kirk Grimmelsman

Equations [2.1] and [2.2] can be used to compute deflections at DOFs 1 – 4 when a unit

load is placed, in turn, at each of the DOF locations. The static flexibility matrix for the

cantilevered beam is a 4 x 4 matrix with elements as shown in equation [2.3]. Each column of

this matrix represents the DOF where the unit point load is placed, and each row entry represents

the resulting deflection that occurs at each DOF.

$$f = f_{ij} = \begin{bmatrix} f_{11} & f_{12} & f_{13} & f_{14} \\ f_{21} & f_{22} & f_{23} & f_{24} \\ f_{31} & f_{32} & f_{33} & f_{34} \\ f_{41} & f_{42} & f_{43} & f_{44} \end{bmatrix} \tag{2.3}$$

The stiffness matrix for the structure is simply the inverse of the flexibility matrix as

shown in equation [2.4].

$$\frac{1}{f} = k = \begin{bmatrix} k_{11} & k_{12} & k_{13} & k_{14} \\ k_{21} & k_{22} & k_{23} & k_{24} \\ k_{31} & k_{32} & k_{33} & k_{34} \\ k_{41} & k_{42} & k_{43} & k_{44} \end{bmatrix} \tag{2.4}$$

2.4.2   Modal Flexibility

The development of the modal flexibility matrix can also be shown for the cantilevered

beam shown in Figure 2.1. In this case, the same four translational degrees of freedom are

considered for the idealized structure. The beam is analyzed as a multiple degree of freedom

(MDF) system in undamped free vibration. Free vibration is simply the motion of the structure

that occurs only as a result of some initial conditions, external dynamic excitations or support

motions are not considered. Free vibration is initiated by disturbing the structure from its equilibrium position by some initial displacements and/or by imparting some initial velocities (Chopra, 2007). The equation of motion for this case is shown in equation [2.5], where m is the mass matrix and k is the stiffness matrix $\ddot{u}$, denotes acceleration, and u denotes displacement.

$$m\ddot{u} + ku = 0$$

[2.5]

It is desired to find the solution $u(t)$ of equation [2.5] that satisfies the initial conditions shown in equation [2.6] at $t = 0$.

$$u = u(0) \qquad \dot{u} = \dot{u}(0)$$

[2.6]

The mass matrix is found by the application of lumped masses to the cantilever at some number, N, degrees of freedom. The degrees of freedom are the number of independent displacements required to define the displaced positions of all the masses relative to their original position (Chopra, 2007). For structures with distributed mass and stiffness characteristics, the degrees of freedom can be an infinite number of nodes, or for this case, lumped masses along the length of the cantilever. The mass is distributed throughout an actual structure, but it can be idealized as lumped or concentrated at the nodes of the discretized structure; usually, such a lumped-mass idealization is satisfactory. The lumped mass at a node is determined from the portion of the weight that can reasonably be assigned to the node (Chopra, 2007).

For the cantilevered beam discretized into 4 DOFs, the lumped masses represent half of the translational mass of the beam located to each side of given node. The lumped masses are then arranged into the mass matrix as shown in equation [2.7]. The masses form a diagonal line through the matrix, leaving all other locations in the matrix as zero. The reason for this is because the masses are treated independently, where when one mass is deflected the effects are

not felt on the others. One of the advantages of using a lumped mass matrix is that the calculations become simplified because of the zero terms.

$$m = \begin{bmatrix} \dfrac{m_1L}{4} & 0 & 0 & 0 \\[2ex] 0 & \dfrac{m_2L}{2} & 0 & 0 \\[2ex] 0 & 0 & \dfrac{m_2L}{2} & 0 \\[2ex] 0 & 0 & 0 & \dfrac{m_2L}{2} \end{bmatrix} \qquad [2.7]$$

The stiffness matrix utilized in forming the equation of motion is the same matrix formed in Equation [2.4]. Once the mass and stiffness matrices have been formed, the dynamic properties of the cantilevered beam can be computed through the eigensolution to the equation of motion.

2.4.3   Eigensolution

The eigensolution to the equation of motion leads to eigenvalues and eigenvectors. The eigenvalues are the squares of the natural frequencies ω_n, and the eigenvectors are the associated natural mode shapes of vibration, φ_{jn}. The term *natural* is used to qualify each of these vibration properties to emphasize the fact that these are natural properties of the structure in free vibration, and they depend only on its mass and stiffness properties. The subscript *n,* denotes the mode number and the first mode ($n = 1$) is also known as the fundamental mode (Chopra, 2007).

A plot of the eigenvectors will display the motion of the structure in each of its natural frequencies. The values inside each vector represent the displacement of the mass of DOF *j* in

each mode n. The frequencies and mode shapes can be found using the characteristic equation given in equation [2.8].

$$\det\ [k\text{-}\ \omega_n^2 m] = 0 \qquad\qquad [2.8]$$

By substituting the **k** matrix and the **m** matrix into equation and solving, the square of the circular natural frequencies, ω_n, can be solved.

2.4.4   Modal Flexibility

In order to determine the modal flexibility matrix for the system, the eigenvectors must first be normalized. Normalizing the modes using equation [2.9] will allow for each mode to be scaled or have a value of unity. Scale factors are sometimes applied to natural modes to standardize their elements associated with various DOFs. This process is called *normalization* (Chopra, 2007). If each mode shape is unit mass normalized according to Equation [2.9], the pre- and post-multiplication of the mass matrix with these modes produces the identity matrix as shown in Equation [2.10]. The form of normalization ensures that the natural modes are both orthogonal and normalized with respect to the mass.

$$\{\phi_n\}^T\ \{m\}\ \{\phi_n\} = 1 \qquad\qquad [2.9]$$

$$\mathbf{M} = \phi^T m\ \phi = \boldsymbol{I} \qquad\qquad [2.10]$$

The final values will be the mass unit normalized mode shape vectors, $\{\hat{\phi}_n\}$. If the modal vectors have been mass unit normalized, then pre- and post-multiplication of the stiffness matrix

with these vectors yields the spectral matrix $\mathbf{\Omega}^2$, which is a diagonal matrix of the N eigenvalues, $\omega_n{}^2$ and is the modal stiffness matrix, $\mathbf{K}$ as shown in Equation [2.11]:

$$\mathbf{K} = \boldsymbol{\phi}^T \boldsymbol{k} \, \boldsymbol{\phi} = \boldsymbol{\Omega^2} = \begin{bmatrix} \omega_1^2 & & & \\ & \omega_2^2 & & \\ & & \ddots & \\ & & & \omega_N^2 \end{bmatrix}$$
[2.11]

Equation [2.11] can be re-arranged as shown in Equation [2.12]

$$[K] = [\hat{\phi}]^{-T} [\Omega^2] \, [\hat{\phi}]^{-1} = \left([\hat{\phi}] \, [\Omega^2]^{-1} \, [\hat{\phi}]^T \right)^{-1}$$
[2.12]

The modal flexibility matrix is the inverse of modal stiffness matrix, so taking the inverse of Equation [2.13] yields:

$$[f]_{modal} = [K]^{-1} = \frac{1}{\left([\hat{\phi}] \, [\Omega^2]^{-1} \, [\hat{\phi}]^T \right)^{-1}} = \frac{[\hat{\phi}] \, [\hat{\phi}]^T}{[\Omega^2]}$$
[2.13]

The result shown in Equation [2.13] represents the contributions of each of the N modes in the system. The individual coefficients in the modal flexibility matrix can also be written as shown in Equation [2.14].

$$f_{ij} = \sum_{k=1}^{m} \frac{\hat{\phi}^k(i)\hat{\phi}^k(j)}{\omega_k^2}$$
[2.14]

Modal flexibility can be determined using Equation [2.14], where k is the mode and *i* and *j* are the masses of the mass normalized mode shape vectors, ϕ. Solving this equation will fill the

flexibility matrix, where f_{ij} at the ith point under the unit load at the point j is the summation of terms related to each mode identified. The numerator of one term in this summation is the product of modal coefficients at points i and j of one mode, respectively. The denominator is the square of the corresponding frequency (Zhang and Aktan, 1998). Equation [2.14] is based on the unit-mass-normalized modal vectors. However, real life structures cannot always be approximated as being proportionally damped (Catbas et al., 1997). When calculating modal flexibility analytically, the contribution that each mode makes to its respective point is observable. The lower modes will very noticeably contribute to the flexibility calculations while the higher frequencies will not show as much contribution. The higher modes will not contribute as much as the lower modes simply because of the increasing size of the denominator.

The relationship between static flexibility and modal flexibility has now been shown. Furthermore, it is observed that modal flexibility can be computed using the modal parameters identified for a structure from a controlled dynamic test, such as MRIT testing. The following section provides an overview of the procedures required to develop the modal flexibility matrix for a structure from impact testing experiment.

2.5   IMPACT TESTING

The impact test is conducted using the same principles as the static load test. In a static load test, displacements are measured at each DOF location while the load is located at one of the DOFs. This process is repeated until all DOFs have been loaded. For impact testing, the load is replaced by an impulse force using a modal impact hammer. The principle of f_{ij} holds true for the development of the modal flexibility matrix. As one degree of freedom is impacted the

response is recorded by the sensors at all degrees of freedom. Through impact tests the modal parameters of the cantilevered beam will be calculated. Using those parameters, the modal flexibility can be calculated. The modal flexibility can then be directly compared to the static flexibility. The process of acquiring modal flexibility requires a series of algorithms that is shown in Figure 2.2 below.

```
┌──────────────┐    ┌──────────────┐    ┌──────────────┐
│Measure Impacts│──▶│  Use FFT to  │──▶│Auto and Cross│
│  & Responses │    │convert all data to│ │power spectrum of│
│              │    │frequency domain│   │    data      │
└──────────────┘    └──────────────┘    └──────────────┘
        │
        ▼
┌──────────────┐    ┌──────────────┐    ┌──────────────┐
│Plot the Frequency│▶│ SVD of FRF to│──▶│  Locate Mode │
│Response Function│  │ plot CMIF for│    │shapes and Natural│
│    (FRF)     │    │ peak picking │    │ Frequencies  │
└──────────────┘    └──────────────┘    └──────────────┘
        │
        ▼
┌──────────────┐    ┌──────────────┐    ┌──────────────┐
│Compute eFRF to│──▶│Calculate Modal│──▶│Compute Modal │
│ Isolate Modes│    │  Parameters  │    │ Flexibility  │
└──────────────┘    └──────────────┘    └──────────────┘
```
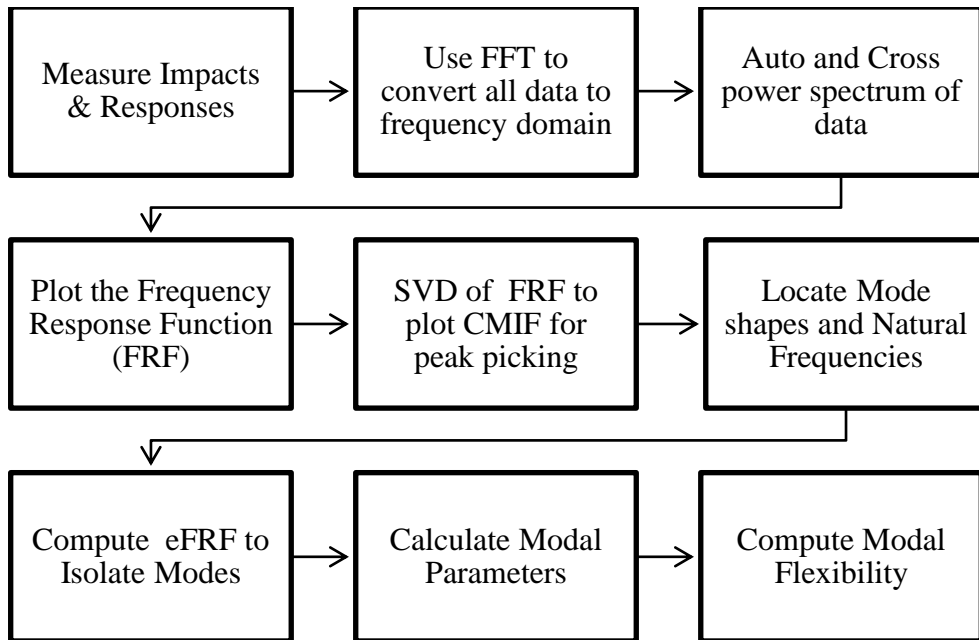
Figure 2.2: Process for the identification of modal flexibility

The accuracy of each step is crucial in acquiring an accurate modal flexibility. The testing process is described as single input multiple output, SIMO, where there is a single input reading from the impact hammer and multiple output readings from the accelerometers placed along the cantilevered beam. A soft tip can be used to excite the lower frequency modes, while a hard tip is needed for exciting the higher frequency modes. The time data is observed during testing so that there is verification that the correct data is being recorded. Issues to be aware of during testing that can be viewed in the time data include: the response data being properly triggered by the impact, double impacts, over ranged sensors, the sensors being powered, and

outside noise being recorded in the response data. It is also necessary to view the coherence with the frequency response functions. These issues will be covered with more depth in the following sections. In order to develop an accurate estimation of the frequency response function, a number of averages, N_{avg} is used to minimize the random errors (variance) (Allemang, 1999). A total of five impacts are typically used at each sensor. It has been determined that using a minimum of five hits at each sensor should be used for averaging to acquire a good data set (Lenett et al., 1997).

2.5.1 Frequency Response Function

To calculate the frequency response function (FRF), the acquired data in the time domain should be converted into the frequency domain using the fast Fourier transform (FFT). The process of conversion is lengthy by hand, but through MATLAB the process is simplified and can be performed rapidly. To properly process the data once it is converted to the frequency domain the frequency response function, FRF, for the cantilever must be calculated. The frequency response function is normally used to describe the input-output (force-response) relationships of any system (Allemang, 1999). The equation for the FRF is shown in equation [2.15].

$$H(\omega) = \frac{X(\omega)}{F(\omega)}$$ [2.15]

Where *X* is the dynamic response and *F* is the force input, both in the frequency domain. The FRF function relates the Fourier transform of the system input to the Fourier transform of the system response (Harris and Crede, 1996). It should be noted that the acquired data from the tests is captured as acceleration, and this data must be converted to displacement, $X(\omega)$. This can

be accomplished easily in the frequency domain by dividing the acceleration at each frequency line (ω_k) by the quantity $(j\omega_k)^2$, in which j is the imaginary unit number. The H_1 and H_2 algorithms will be used to assemble the FRF. Using this method requires the use of the auto- and cross-power spectrums as a function of frequency. The equations for the cross and auto power spectrums according to Allemang (1999) are shown below:

Cross Power Spectra

$$GXF_{pq} = \sum_{1}^{N_{avg}} X_p F_q^*$$

[2.16]

$$GFX_{qp} = \sum_{1}^{N_{avg}} F_q X_p^*$$

[2.17]

Auto Power Spectra

$$GFF_{qq} = \sum_{1}^{N_{avg}} F_q F_q^*$$

[2.18]

$$GXX_{pp} = \sum_{1}^{N_{avg}} X_p X_p^*$$

[2.19]

where:
- $F^* =$ Complex conjugate of $F(\omega)$
- $X^* =$ Complex conjugate of $X(\omega)$

The H_1 technique underestimates amplitude at resonances which causes damping to be overestimated. The H_2 technique overestimates amplitude at resonances and causes damping to be underestimated. The H_1 and the H_2 algorithms differ in that the H_1 method is used to minimize the noise from the output while the H_2 method minimizes noise on the input. Within both of these methods, the phase information is preserved in the cross power spectrum (Allemang, 1999) The H1 and the H2 method also allow for the ordinary coherence function to be determined. The ordinary coherence function indicates the degree of causality in a FRF, where there is a measure

34

between the impact and the response. The coherence for the FRF should fall between zero and one, where if it hits at one there will be perfect causality. If the coherence is zero, the output is caused by sources that are not from the measured input. The coherence function is described in equation [2.20].

$$COH = \gamma^2 = \frac{\left|GXF_{pq}\right|^2}{GFF_{qq}GXX_{pp}} = \frac{GXF_{pq}GFX_{qp}}{GFF_{qq}GXX_{pp}} \qquad [2.20]$$

Having good coherence will help while acquiring and analyzing the data so a determination can be made as to the cleanliness of the data being recorded and processed. During testing, the FRF and the coherence should be closely observed after each impact occurs. It is necessary to have the coherence to be at one where each peak of the FRF occurs.

Using the H_1 and the H_2 methods, individual plots are obtained for the response at each sensor due to an impact at each sensor. For a four degree of freedom system there will be a total of sixteen individual plots containing one plot of the H_1 vs. H_2 methods, a second plot containing the phase and a third plot with the coherence shown. By observing the data collected from the driving points, causality can be observed in all three windows.

2.5.2 Complex Mode Indicator Function

Having a FRF for the response at each node due to an impact at each node, the FRF matrix can be evaluated at each spectral line by using singular value decomposition (SVD) shown below.

$$[H(\omega)]= [U(\omega)][\Sigma(\omega)][V(\omega)]^{H} \qquad\qquad [2.21]$$

$[U]$ = Left singular vector matrix (unitary)

$[V]$ = Right singular vector matrix (unitary)

$[\Sigma]$ = Singular value matrix (diagonal)

The FRF calculated using the H_1 method is used in the SVD calculation. The SVD at each spectral line will produce matrices containing the mode shapes (left singular vectors), singular values, and participation factors (right singular vectors) for each point. Using the singular values and plotting them against the frequency range, the complex mode indicator function (CMIF) can be viewed. The CMIF is based upon the Expansion Theorem in that it assumes that, at every frequency, the long dimension of the frequency response function matrix is made up of a summation of modal vectors (Allemang and Brown, 2006). If singular value decomposition is used to estimate the CMIF, the singular vectors are unitary and the singular values are a measure of the strength or dominance of each mode at the particular frequency and the singular vectors in the long dimension are estimates of the contributing modal vectors associated with every singular value (Allemang and Brown, 2006). The plot of the CMIF will contain a number of lines that is equal to the number of inputs. The locations of the peaks on the CMIF are the possible locations of the mode shapes associated with each natural frequency. In order for the CMIF to be most effective, there should be a good estimation of where the modes exist. This can be done through finite element modeling, through power spectral density (PSD), or from theoretical calculations. Using a finite element program, like SAP 2000, the natural frequencies and mode shapes can be identified for comparison. More details about the CMIF function can be found in Allemang and Brown (2006).

2.5.3   Enhanced Frequency Response Function

In order to find the modal parameters of the cantilevered beam, this multi degree of freedom system, must be reduced to several single degree of freedom systems. This is done by the development of the enhanced frequency response function (eFRF). The eFRF is a virtual measurement, used to identify the modal frequencies and scaling of a single degree-of-freedom characteristic that is associated with each peak in the CMIF (Allemang, 2006). The eFRF will can be calculated according to methods described in Catbas et al. (2004). Here the FRF matrix is pre-multiplied by left singular vector transpose, $\{U\}^T$, and post-multiplied with modified right singular vector, $\{V_{modif}\}$ at each spectral line. The eFRF amplifies the peak associated with each mode being analyzed; this process will isolate the individual peaks, which allows for single degree-of-freedom analysis to be completed. If the modal vectors are mutually orthogonal, then the eFRF will be completely uncoupled, showing a single mode FRF with a strong peak (Catbas et al., 2004). It should be noted that using the right singular vector $\{V\}$ as a post multiplier will not preserve the correct scaling, and results involving the scaling such as unit-mass-normalized modal vectors or modal flexibility will be corrupted (Catbas et al., 2004). An eFRF can be calculated for each driving point. The driving point refers to a location where an impact occurred as well as a response. So, the number of driving points used will be directly related to the number of eFRF's.

Having the eFRF for each driving point, the modal parameters for each point can then be calculated using each eFRF. Using a least squares solution, the poles for each driving point can be solved directly. A system pole is a complex number that contains the damping and the natural frequencies for a given mode. In order to acquire the pole for each driving point location, the

peak of that location is chosen as well as a number of points on either side of that peak. For accuracy, it was found from testing that the use of between five and fifteen points on either side of the peak will give the best results. The least squares approach is shown in the equation below as described in Allemang (1999). The equations represent over determined sets of linear equations that can be solved using any pseudo-inverse or normal equations approach.

$$\begin{Bmatrix} H_{pq}(\omega_p)\text{-}H_{pq}(\omega_1) \\ H_{pq}(\omega_p)\text{-}H_{pq}(\omega_2) \\ H_{pq}(\omega_p)\text{-}H_{pq}(\omega_3) \\ H_{pq}(\omega_p)\text{-}H_{pq}(\omega_4) \\ ... \\ H_{pq}(\omega_p)\text{-}H_{pq}(\omega_s) \end{Bmatrix}_{N_s x 1} \{\lambda_r\}_{1x1} = \begin{Bmatrix} j\omega_p H_{pq}(\omega_p)\text{-}j\omega_1 H_{pq}(\omega_1) \\ j\omega_p H_{pq}(\omega_p)\text{-}j\omega_2 H_{pq}(\omega_2) \\ j\omega_p H_{pq}(\omega_p)\text{-}j\omega_3 H_{pq}(\omega_3) \\ j\omega_p H_{pq}(\omega_p)\text{-}j\omega_4 H_{pq}(\omega_4) \\ ... \\ j\omega_p H_{pq}(\omega_p)\text{-}j\omega_s H_{pq}(\omega_s) \end{Bmatrix}_{N_s x 1} \qquad [2.22]$$

Using this least squares approach and solving for the system poles, λ_r, the modal scaling values can be solved for each mode. The system pole contains the damping, σ_r and the frequency, ω_r. To solve for the modal scaling, the eFRF will be analyzed over the range of the selected peaks chosen from the peak picking process in the CMIF. According to the methods outlined in Catbas et al. (2004), the eFRF will be rewritten to solve for the modal scaling, Q_r. In Equation [2.23], the eFRF equation can be seen written in terms of modal parameters.

$$eH(\omega_i) = \frac{s_{1k} Q_k s_{2k}}{j\omega_i \text{-} \lambda_k} \qquad [2.23]$$

2.5.4   Modal Parameters

Q$_r$ is solved using the two scalar values s$_{1k}$ and s$_{2k}$. By rearranging this equation to solve

for Q$_r$, the modal scaling can be acquired, as shown in the equation below.

$$Q_r = \frac{eH(\omega_i)(j\omega_i - \lambda_k)}{s_{1k}s_{2k}} \qquad [2.24]$$

The s$_1$ and s$_2$ components of Equation [2.24] are the two scalar values for mode *k* and are

defined for each of the selected modes that are to be analyzed. These equations are shown below

and are calculated according to Catbas et al. (2004):

$$S_{1k} = \{U\}_{1xNo}^{T}\{\psi\}_{Nox1} \qquad [2.25]$$

$$S_{2k} = \left\{\psi_{drv.pt}\right\}_{1xNi}^{H}\{V_{scaled}\} \qquad [2.26]$$

The modal scaling term Q$_r$, is directly related to Modal A (M_{A_r}). Modal A is the scaling

term that is used to calculate the modal flexibility. Modal A, which is the reciprocal of Q_r, is

used to estimate the modal mass. The *modal A* scaling factor is also the basis for the relationship

between the scaled modal vectors and the residues determined from the measured frequency

response function (Allemang, 1999). When testing a system that is non-proportionally damped,

the mass and stiffness matrix is very difficult to approximate. Because of these difficulties, the

modal mass will be inaccurately depicted when scaling the frequency response function.

$$M_{A_r} = \frac{1}{Q_r} \qquad [2.27]$$

Modal A is the scaling term that brings the weight to the modal flexibility calculations. Here, M_{A_r} is calculated directly from the physical response of the structure, where the mass matrix does not have to be approximated. The first modes acquired from the impact testing are as necessary as they are in Equation [2.14] with the unit-mass-normalized vectors because of their high participation value to the systems response.

2.5.5   Modal Flexibility from Impact Testing

Using the modal parameters that are listed in the previously discussed equations, the modal flexibility can be calculated strictly from the acquired test data. According to Allemang and Brown (2006), the FRF can be calculated using the acquired modal parameters extracted from data recorded during dynamic tests, shown in equation [2.28].

$$H_{pq}(\omega) = \sum_r \frac{Q_r \psi_{pr} \psi_{qr}}{(j\omega - \lambda_r)} \qquad [2.28]$$

This equation for the FRF uses the modal scaling constant, the mode shapes, and the poles associated with each mode. By taking the above equation and evaluating the FRF at $\omega = 0$, the modal flexibility can be calculated according to Catbas (2006), shown below where the * denotes the complex conjugates. This calculation of modal flexibility differs from Equation [2.14] in that an estimation of the mass matrix is not needed because the scaling comes from the modal A factor and not the unit-mass-normalized vectors.

$$H_{pq}(\omega=0)=\sum_{r=1}^{m}\left[\frac{\psi_{pr}\psi_{qr}}{M_{Ar}-\lambda_r}+\frac{\psi_{pr}^*\psi_{qr}^*}{M_{Ar}^*-\lambda_r^*}\right]$$ [2.29]

The modal flexibility matrix can then be developed and written as shown in equation [2.30].

$$[H]=\begin{bmatrix} H_{11}(\omega=0) & H_{12}(\omega=0) & \cdots & H_{1N}(\omega=0) \\ H_{21}(\omega=0) & \cdots & \cdots & \vdots \\ \vdots & \vdots & \vdots & \vdots \\ H_{N1}(\omega=0) & \cdots & \cdots & H_{NN}(\omega=0) \end{bmatrix}$$ [2.30]

This form of the flexibility matrix is a close approximation of the actual flexibility matrix. Because every structure contains an infinite number of modes, the modal flexibility can only practically be evaluated over the amount of modes being measured or successfully captured.

2.6   SUMMARY

The use of modal flexibility to characterize a structure has been explored. The research has shown that flexibility can not only be obtained through static testing, but also through dynamic testing. Modal flexibility utilizes the measured dynamic responses from the system to approximate the static flexibility. The problems with modal flexibility were discussed, these problems included having an accurate approximation of the mass so that the mode shapes could be unit mass normalized. Although using the unit-mass-normalized mode shape vectors is still currently practiced, the ability to approximate mass through the dynamic properties reduces that uncertainty and also eases the complications of testing. What is being considered in this research is the use of a falling weight deflectometer as an impact source for multiple reference impact tests (MRIT). The use of the FWD has been proposed and attempted by some, but no results

have been fully discussed. In MRIT, the modal hammer has been a proven impact source to perform the tests. The impact hammer can be used in conjunction with the FWD to compare the results. The FWD may prove to add some consistency to an already proven method by eliminating human error and being able to apply a larger and more consistent force. If the FWD proves successful then a process can be established that will enhance the ability to perform MRIT on several state and county owned bridges. With proper instrumentation, a testing scheme can be developed to perform these evaluations quickly and effectively.

3   LABORATORY STUDIES

3.1   INTRODUCTION

In order to validate the experimental and analysis procedures required to conduct multi reference impact tests on an in service bridge, a full range of tests were first conducted in the laboratory using a cantilever beam structure and a large steel grid structure (grid). The physical models were designed and constructed for the purpose of testing and validating experimental and analytical methods for characterizing structures such as bridges under more controlled and less uncertain conditions that what are typically encountered in the field. The cantilever steel beam model represents a very simple and idealized structural form that is not subject to the uncertainties typically associated with the more complex geometric configurations, connection details, boundary and continuity conditions, and material characteristics encountered with full-scale constructed systems. The simply-supported steel grid structure represents a more complex geometric form than the cantilever beam, and incorporates additional complexities and uncertainties through its larger size, connection and boundary condition details.   Since both model structures are located within the closed environment of the laboratory, they are also not subject to the uncertainties associated with a structure interacting with its ambient environment. Both structures can be characterized analytically and experimentally with much greater confidence than is possible for real-world constructed systems.

The cantilever beam model served as a starting point for the research program. The model was tested both statically and dynamically to describe the in-situ mechanical properties of the structure. The flexibility of the structure was computed from both static load testing results

(static flexibility) and dynamic impact testing results (modal flexibility), and these were compared with each other and their analytically derived counterparts.

The more complex grid model structure was characterized and evaluated using a similar procedure. The static and modal flexibility of the grid were identified from the results static load tests and multiple-reference impact testing, respectively. The grid structure was also analytically evaluated using static and dynamic analysis results from a FE model created using the commercially available software package SAP2000. The analytical and experimental results were compared to evaluate and validate the experimental methods that were to be used for the field testing program.

The details and results of the experimental and analytical characterization programs for the cantilever beam and grid model structures are presented and discussed in the following sections.

3.2   CANTILEVER BEAM STRUCTURE

The cantilever beam structure (Figure 3.1) was constructed from a steel 3x2x3/16 Hollow Structural Section (HSS) and has a span length of 180 inches. The beam section was oriented such that it would bend about its weak axis in the vertical plane. The fixed end of the cantilever beam was clamped to a steel pedestal support as shown in Figure 3.2. The beam span was divided into 4 even spaces of 45 inches for the measurement nodes. A measurement node was also located at the fixed support location of the beam although this location was expected to have zero response for static and dynamic loadings. Figure 3.3 shows a schematic of the cantilever

beam and its measurement node locations. The section and material properties for the cantilever

beam section are summarized in Figure 3.1.
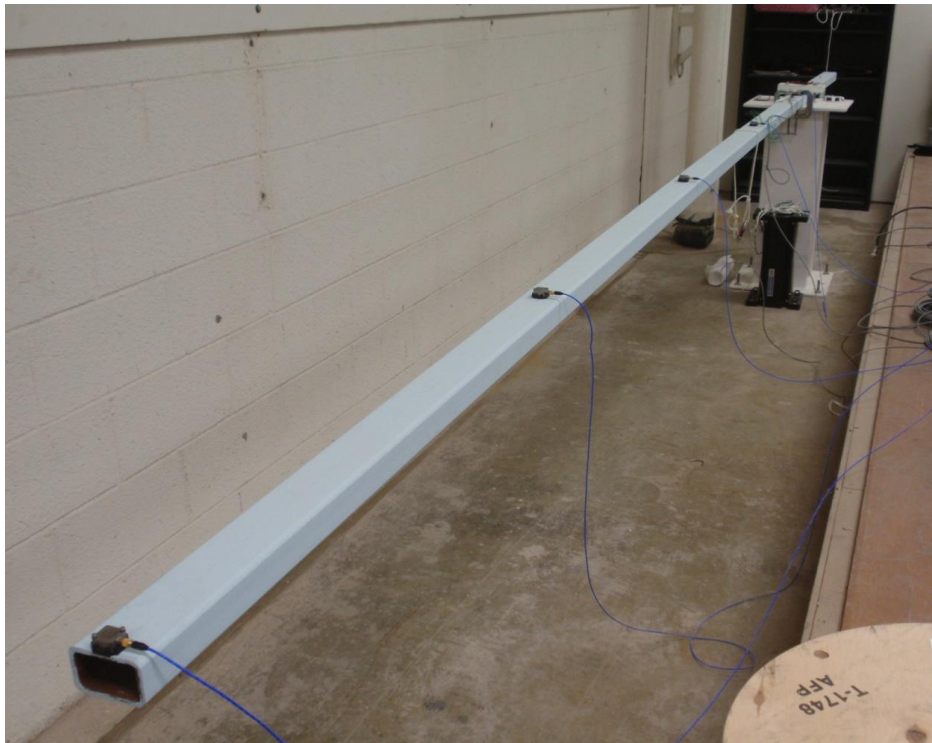
Figure 3.1: HSS cantilever with accelerometers attached
Photo taken by Jason Herrman, Fall 2010 Engineering Research Center

Figure 3.2: Fixed end of HSS cantilever

Photo taken by Jason Herrman Fall 2010, Engineering Research Center
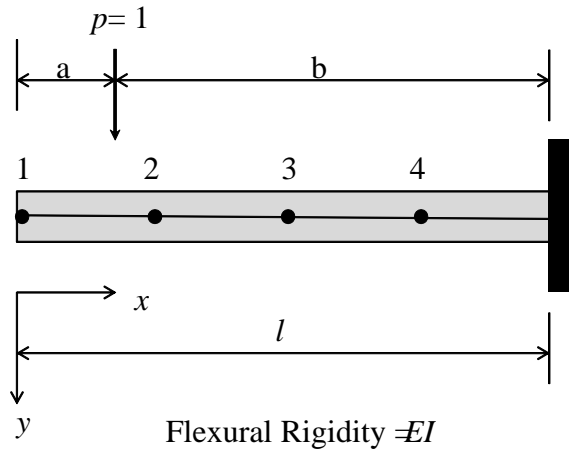
Figure 3.3: Schematic of HSS cantilever setup and measurement nodes

Figure By Dr. Kirk Grimmelsman

Table 3.1: Material and Section Properties of HSS Beam

Property	Value
Span Length (L)	180 in
Moment of Inertia (I)	0.932 in^4
Unit Weight (ρ)	0.2835 lbf/in^3
Cross Sectional Area (A)	1.54 in^2
Mass per unit length (*m*)	1.130 x 10^{-3} lbm/in

3.3   CANTILEVER BEAM EVALUATION AND RESULTS

The cantilever beam has a continuous distribution of mass and stiffness; however, for this characterization program, the model was discretized according to a finite number of measurement nodes or degrees of freedom (DOF) as shown in Figure 3.3. The static load testing of this model consisted of placing a known amount of weight at a single measurement node point and measuring the resulting displacements (with displacement transducers) at all of the defined measurement nodes. This process was repeated until all of the measurement nodes had been loaded. The measured displacements were subsequently scaled using the actual load amount applied to the structure to obtain displacements corresponding to a unit load magnitude. The bending moment in the beam near the clamped support was also computed in each of these load cases from strain gage measurements to independently corroborate the displacement measurements.

The dynamic testing was conducted using accelerometers that were located at the same measurement node locations used for the static load testing. A total of five accelerometers were glued to the beam at a spacing of 45 inches as shown in Figure 3.1. The beam was struck at each measurement node individually using an instrumented hammer and the input (dynamic impulse force) and the outputs (accelerations) at all measurement nodes were recorded. It should be noted

that only the in-plane accelerations of the beam were measured. The measured inputs and outputs were subsequently used to identify the modal parameters of the beam and to assemble the modal flexibility matrix for the structure.

Finally, the cantilever beam structure was analytically represented using fundamental equations of statics and dynamics. This analysis represented theoretical results for the beam structure. A static analysis of the analytical model was performed by applying unit loads at the measurement node locations as a series of separate load cases to determine the static flexibility of the structure. An eigenvalue analysis of the analytical representation of the structure was conducted assuming undamped behavior to identify its modal parameters and to compute the modal flexibility matrix. These analytical results were compared with the experimentally derived results described above.

The results from the cantilever beam testing that were compared included the theoretical static flexibility, theoretical modal flexibility using unit-mass-normalized vectors, measured static flexibility, and modal flexibility from impact testing.

The analytical solution for the modal flexibility of the cantilever beam utilized a lumped mass matrix idealization in the development of the equations of motion. The mass of the beam was lumped at the locations of the measurement node locations from the experimental tests. The mass that is lumped at measurement degree of freedom (DOF) was based on the tributary length between each DOF. In other words, each DOF is assigned the mass associated with half of the 45 inch length of beam to each side of the DOF. The DOF at the free end of the beam is assigned only half as much mass as the other DOFs. The DOF located at the fixed end is excluded from the analysis since it is a support point. The masses determined for each DOF were then arranged into the mass matrix where the masses form a diagonal line through the matrix. This leads to the

equations of motion for the beam being uncoupled in the mass matrix. The lumped mass matrix

for the 4 DOF model of the cantilever beam structure is computed according to Equation [3.1]

where m = the mass per unit length, and L = the distance between the DOFs.

$$[m] = \begin{bmatrix} \dfrac{m_1 L}{4} & 0 & 0 & 0 \\ 0 & \dfrac{m_2 L}{2} & 0 & 0 \\ 0 & 0 & \dfrac{m_2 L}{2} & 0 \\ 0 & 0 & 0 & \dfrac{m_2 L}{2} \end{bmatrix} \qquad [3.1]$$

The stiffness matrix for the beam was both calculated analytically and found

experimentally. The stiffness matrix is calculated using the theorem of reciprocal displacements.

The deflections are computed at each DOF for a unit load applied, in turn, at each DOF. The

analytically computed static flexibility matrix for the 4 DOF cantilever beam is shown in Table

3.2. This static flexibility matrix has units of inches/pound-force. Each column of the matrix

corresponds to the displacements at each of the DOFs due to a unit load applied at the DOF listed

in the column heading. The modal flexibility matrix for the beam was also computed using the

natural frequencies and mass unit normalized modal vectors.

Table 3.2: Analytical static flexibility matrix (in/lbf) for cantilever beam

	DOF 1	DOF 2	DOF 3	DOF 4
DOF 1	0.07193	0.04552	0.02248	0.00618
DOF 2	0.04552	0.03034	0.01573	0.00450
DOF 3	0.02248	0.01573	0.00899	0.00281
DOF 4	0.00618	0.00450	0.00281	0.00112

The inverse of the flexibility matrix (stiffness matrix) shown in Table 3.2 was used with the lumped mass matrix determined previously to form the undamped equations of motion for the 4 DOF cantilever beam. The matrix eigen solution for the analytical representation of the beam was computed using these equations of motion. The eigenvalues are the squares of the circular natural frequencies, ω_n, and the eigenvectors are mode shapes, ψ_{jn}, associated with each frequency. The modal vectors associated with each DOF can be written in matrix form, and this is referred to as the modal matrix, $[\Phi] = [\psi_{jn}]$. The natural frequencies found from this analysis are shown in Table 3.3 and corresponding mode shape vectors are summarized in equation [3.7]

Table 3.3: Undamped natural frequencies of the cantilever beam from analysis

Mode	ω_n (rad/sec)	f_n (Hz)
1	16.3078	2.5954
2	95.85125	15.2552
3	253.8256	40.3976
4	442.4154	70.4126

The modal vectors determined from this analysis are unscaled and thus are relative values. Any vector that is proportional to the modal vector will also satisfy the eigenvalue

solution. Modal vectors are commonly normalized to standardize their elements associated with the various DOFs (Chopra, 2007). One common approach is to normalize the elements in each vector such that the largest element value is unity. The modal matrix of unit normalized modal vectors computed for the cantilever beam is shown in Equation 3.2. The unit normalized modal vectors are also shown as displaced shapes for the 4 DOFs in Figure 3.4.

$$[\Phi]=\begin{array}{|c|c|c|c|}\hline 1 & -1 & 0.8354 & -0.3722 \\ \hline 0.6541 & 0.2725 & -0.9174 & 0.644 \\ \hline 0.336 & 0.8282 & 0.2575 & -0.9835 \\ \hline 0.0959 & 0.4544 & 1 & 1 \\ \hline \end{array} \qquad [3.2]$$

In order to determine the modal flexibility matrix, the eigenvectors must be mass normalized. The relationship between an un-scaled modal vector for a given mode, $\{\psi\}$, and the mass normalized modal vector $\{\hat{\phi}\}$ for that mode is given by Equation 3.3, where α is a scaling factor determined by Equation 3.4 The pre- and post-multiplication of the mass matrix for the cantilever beam with the mass normalized modal matrix, $[\hat{\Phi}]$ yields the identity matrix (Chopra, 2007) as shown in Equation 3.5. Pre- and post-multiplication of the stiffness matrix with the mass normalized modal matrix yields the spectral matrix, Ω^2, which is a diagonal matrix of the natural circular frequencies squared as shown in Equation 3.6. The mass normalized modal matrix for the cantilever beam analysis is given in Equation 3.7.

$${\hat{\phi}} = a * {\psi} \tag{[3.3]}$$

$$\alpha = \frac{1}{\sqrt{{\psi}^T \ [m] \ {\psi}}} \tag{[3.4]}$$

$${\Phi}^T{m}{\Phi} = \begin{bmatrix} 1 & 0 & 0 & 0 \\ 0 & 1 & 0 & 0 \\ 0 & 0 & 1 & 0 \\ 0 & 0 & 0 & 1 \end{bmatrix} \tag{[3.5]}$$

$$\left[\widehat{\Phi}\right]^T [k] \left[\widehat{\Phi}\right] = [\Omega^2] = \begin{bmatrix} \omega_1^2 & 0 & 0 & 0 \\ 0 & \omega_2^2 & 0 & 0 \\ 0 & 0 & \omega_3^2 & 0 \\ 0 & 0 & 0 & \omega_4^2 \end{bmatrix} \tag{[3.6]}$$

Mass normalized mode shape vectors			
Mode 1	Mode 2	Mode 3	Mode 4
4.365	-3.66	2.46	-1.053
2.855	1.007	-2.706	1.822
1.466	3.03	0.7596	-2.787
0.4186	1.663	2.95	2.82

[3.7]

Once the modal vectors have been mass normalized, they can be used in combination with the circular natural frequencies to compute the coefficients of the modal flexibility matrix. This is to accomplish a matrix according to Equation [3.8], where k represents a given mode, *i*

and *j* are the elements of the mass normalized mode shape vector corresponding to the DOFs as defined for the analysis, and m is the total number of natural modes considered.

$$f_{ij} = \sum_{k=1}^{m} \frac{\hat{\phi}^k(i)\hat{\phi}^k(j)}{\omega_k^2} \qquad [3.8]$$

The modal flexibility matrix computed from analysis for the 4 DOF cantilever beam is given in Table 3.4. The percent differences between the individual flexibility coefficients determined by static and modal analysis of the beam analytical model (relative to the static analysis results) are summarized in Table 3.5. The differences between the flexibility coefficients are very small, with most being less than 3%. The difference between the analytical values was largest for the DOF located nearest to the support. This difference is most likely the cumulative result of several factors including the number of DOFs and modes used in the analysis, and the contribution of shear deformation to the total displacements at DOFs located nearest to the support. The closed form displacement equations used to determine the static flexibility matrix and to obtain the stiffness matrix used for the modal analysis assume Bernoulli beam behavior. This assumes that the displacements are mainly due to the bending moment in the beam and that the contribution of shear deformation is negligible. This assumption becomes less valid as DOFs nearer to the fixed support are evaluated.
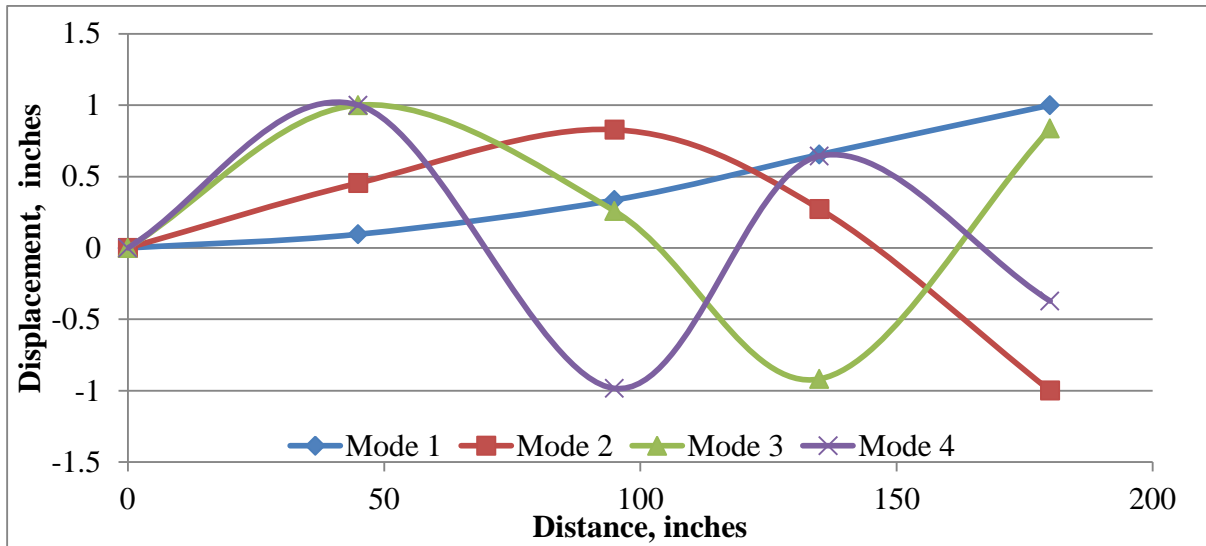
Figure 3.4: Unit normalized mode shape vectors for cantilever beam from analysis

Table 3.4: Modal flexibility matrix for the cantilever beam from analysis

	DOF 1	DOF 2	DOF 3	DOF 4
DOF 1	0.07183	0.04563	0.02243	0.00608
DOF 2	0.04563	0.03021	0.01579	0.00459
DOF 3	0.02243	0.01579	0.00894	0.00282
DOF 4	0.00608	0.00459	0.00282	0.00095

Table 3.5: Percent differences between the analytically determined static flexibility and modal flexibility matrix coefficients

	DOF 1	DOF 2	DOF 3	DOF 4
DOF 1	0.14%	-0.25%	0.20%	1.59%
DOF 2	-0.25%	0.43%	-0.37%	-2.18%
DOF 3	0.20%	-0.37%	0.54%	-0.18%
DOF 4	1.59%	-2.18%	-0.18%	15.66%

3.3.1   Static Flexibility Matrix by Load Testing

The static flexibility matrix coefficients were also determined experimentally by attaching a 10.07 lb. weight to each measurement DOF location in turn and measuring the resulting deflections at all DOF locations. The vertical deflections of the cantilever beam were measured using TML Model CDP-25 displacement transducers placed below each DOF location. The nominal specifications for the displacement transducers are summarized in Table 3.6. The measured displacements were normalized to a unit load value and the resulting flexibility coefficients are presented in Table 3.7.

Table 3.6: Nominal specifications of the TML CDP-25 displacement transducers

Specification	Value
Range	10 V/g
Sampling Rate	10 Hz
Number of Samples	100
Broadband Resolution (1 to 10000 Hz)	0.000004 g rms

Table 3.7: Measured static flexibility matrix coefficients

	DOF 1	DOF 2	DOF 3	DOF 4
DOF 1	0.07249	0.04687	0.02443	0.00765
DOF 2	0.04618	0.03098	0.01668	0.00546
DOF 3	0.02433	0.01738	0.01013	0.00377
DOF 4	0.00765	0.00556	0.00338	0.00159

3.3.2 Modal Flexibility Matrix by Impact Testing

The modal flexibility matrix coefficients for the cantilever beam were also experimentally determined by impact testing to evaluate and validate the dynamic testing approach. The impact testing was performed as described in previous sections. The cantilever beam was instrumented with four PCB Piezotronics, Inc. Model 393B05 accelerometers to measure the vertical vibration responses induced by the impulsive force. A Model 086C03 impact hammer from PCB Peizotronics, Inc. was used to provide the impulse excitation of the cantilever beam. The nominal specifications for both the impact hammer and the accelerometers are given in Table 3.8.

Table 3.8: Specifications of Impact hammer and accelerometers

Parameter	PCB 393B05	PCB 086C03
Sensitivity ($\pm$ 10 %)	10 V/g	10 mV/lbf
Measurement Range	0.5 g pk	$\pm$ 500 lbf pk
Frequency Range ($\pm$ 5 %)	0.7 to 450 Hz	-
Frequency Range($\pm$ 3 dB)	0.2 to 1700 Hz	-
Resonant Frequency	$\geq$ 2.5 kHz	$\geq$ 22 kHz

The impact hammer can be equipped with rubber tips with different hardness values to control the amplitude and frequency band of the impact force produced. The hammer tips include: super soft (red), soft (black), medium (blue), and hard (white). Initial evaluations of the impact hammer hits with the different rubber tips indicated that the red tip provided the best coherence for all of the cantilever beam modes and in particular for the first natural frequency of the beam at 2.49 Hz.

The impact testing data were measured at a sampling rate of 1 kHz and for a sampling duration of 20 seconds. A total of five impacts were made at each measurement DOF location and these results were averaged together to minimize the experimental variance. A pre-trigger of 30 seconds was also used with the measurements to ensure that the complete impact force generated would be captured. The time domain measurements and the FRFs and coherence functions were observed during each measurement to ensure that good data was captured. Viewing the FRF and coherence functions during testing enables verification that the recorded signal from the driving point locations were from the impact force and not from outside noise. A FRF matrix was assembled and each FRF was compared to check for matching peaks locations to verify linear reciprocity existed between the different measurement DOFs.
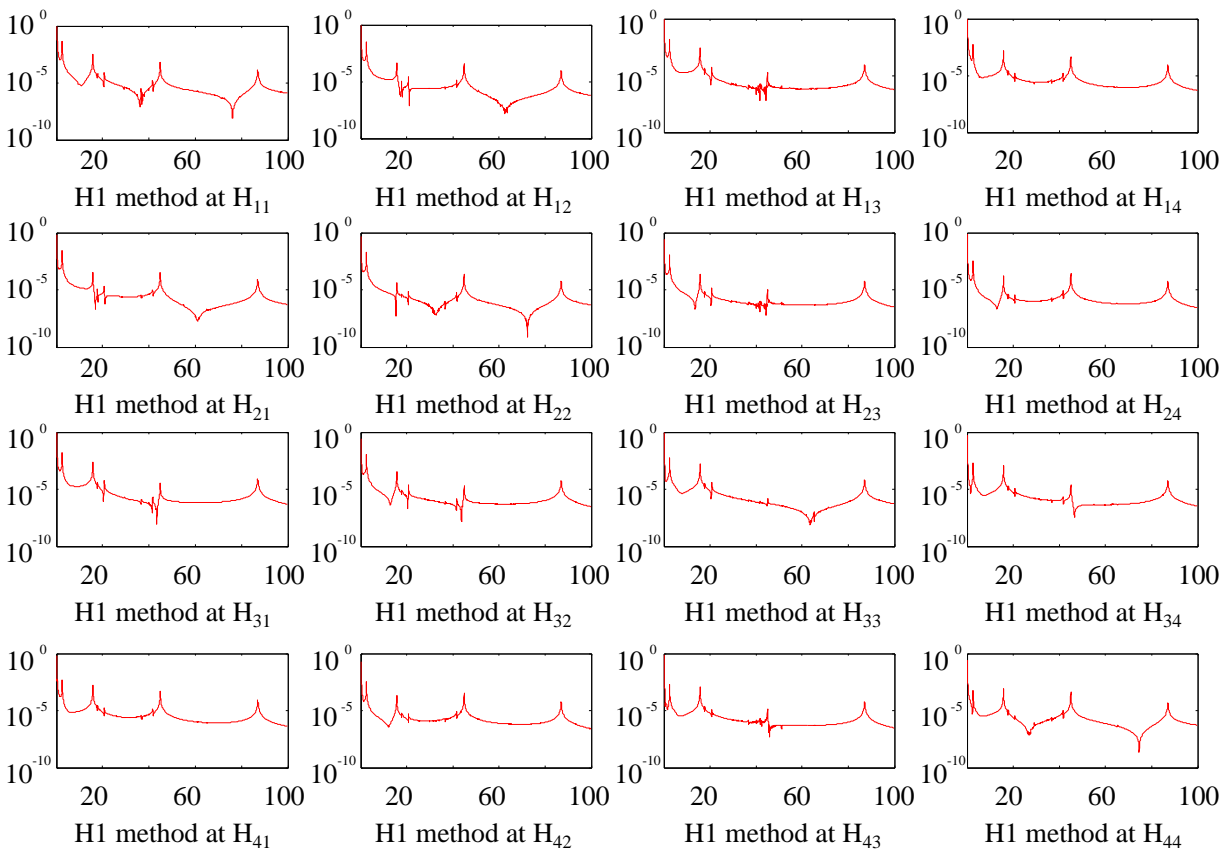

Figure 3.5: FRF matrix for the 4 DOF cantilever beam

Singular value decomposition (SVD) of the FRF matrix at each frequency line is performed to obtain the Complex Mode Indicator Function (CMIF) plot for the cantilever beam shown in Figure 3.1. In addition to the CMIF plot, which indicates the locations of potential natural frequencies for the structure, the SVD operation also provides the modal vectors (Table 3.10), and the participation values for each vibration mode. The singular values that are used produce the CMIF plot and are used to locate the poles of the system by peak picking. All of the peaks in the CMIF plot were found at the expected locations that had been determined from previous numerical calculations. The CMIF plot shown in Figure 3.6 has the locations of the first four bending modes highlighted. The information found at the locations of each of these four natural frequencies was subsequently used to calculate the modal flexibility matrix for the cantilever beam.
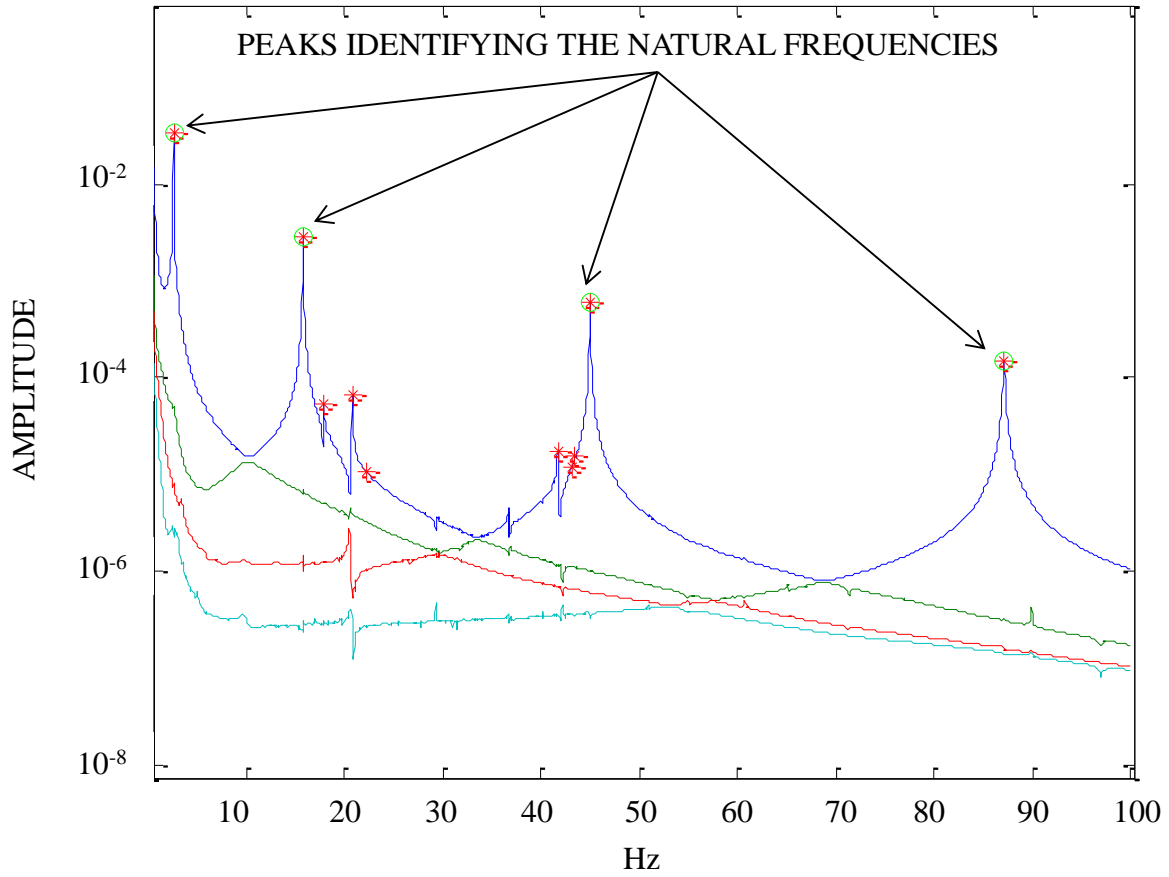
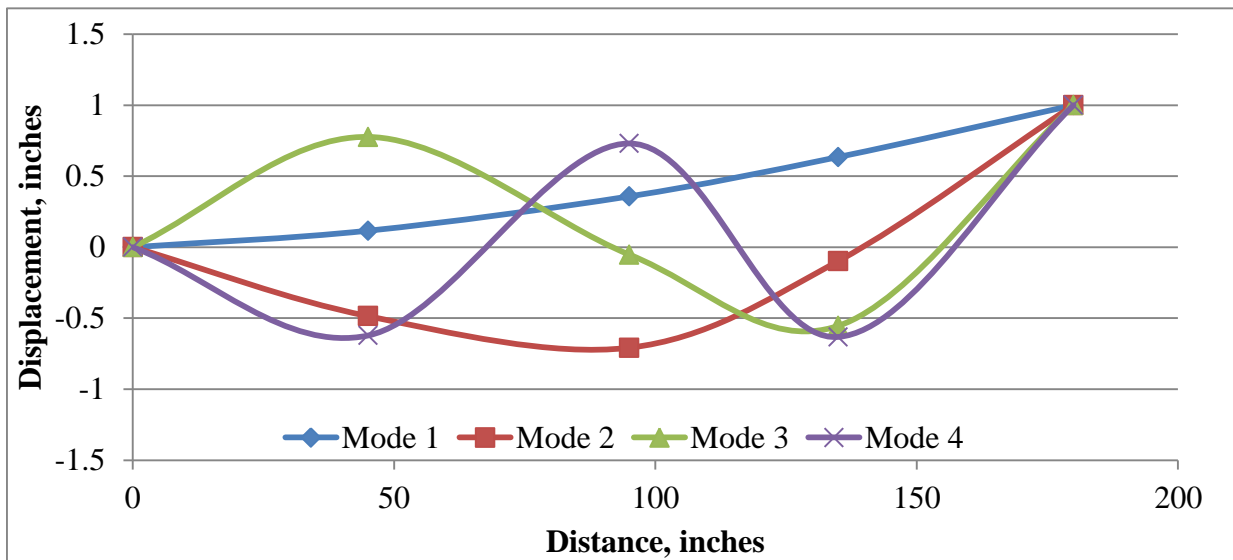Figure 3.6: CMIF plot for the cantilever beam

Figure 3.7: normalized mode shapes for the cantilever beam

Enhanced FRF (eFRF) functions are obtained for each mode by scaling the FRFs at the driving point locations. The eFRF takes advantage of the modal orthogonality relationship to suppress the contributions of other modes in the FRF for each mode. This modal filtering essentially reduces the MDOF FRF into a series of SDOF FRFs. These SDOF FRFs are used to estimate the damping ratio and damped natural frequencies for the system. Using the methods previously discussed, the modal parameters are calculated and the modal flexibility matrix coefficients for the cantilever beam are computed as shown in Table 3.9.

Table 3.9: Modal flexibility of HSS cantilever from impact testing

	DOF 1	DOF 2	DOF 3	DOF 4
DOF 1	0.06816	0.04154	0.02224	0.00682
DOF 2	0.04154	0.02670	0.01511	0.00489
DOF 3	0.02224	0.01511	0.00946	0.00338
DOF 4	0.00682	0.00489	0.00338	0.00149

Table 3.10: Modal Flexibility calculated using unit mass normalized modal vectors

	DOF 1	DOF 2	DOF 3	DOF 4
DOF 1	0.07516	0.04629	0.02511	0.00783
DOF 2	0.04629	0.02965	0.01677	0.00542
DOF 3	0.02511	0.01677	0.01023	0.00358
DOF 4	0.00783	0.00542	0.00358	0.00149

The modal flexibility was also calculated using unit mass normalized mode shape vectors based on numerical information. The natural frequencies and mode shapes taken directly from the information contained at the peaks of the CMIF plot were used with a calculated mass matrix to unit mass normalize the modal vectors.

The flexibility matrices obtained from the different numerical and experimental approaches were compared by virtually loading all of the DOFs with 100 lbs. and computing the resulting deflection profile for the cantilever beam. The deflection profiles obtained from the five different modal flexibility matrices are shown in Figure 3.8. The modal flexibility computed using only experimental data has a maximum difference of 6% (stiffer) in terms of the displacement computed at the free end from the other flexibility matrices. This confirms the approximate nature of the modal flexibility matrix and that the approximation is very reasonable using the first four bending modes identified for the cantilever beam.
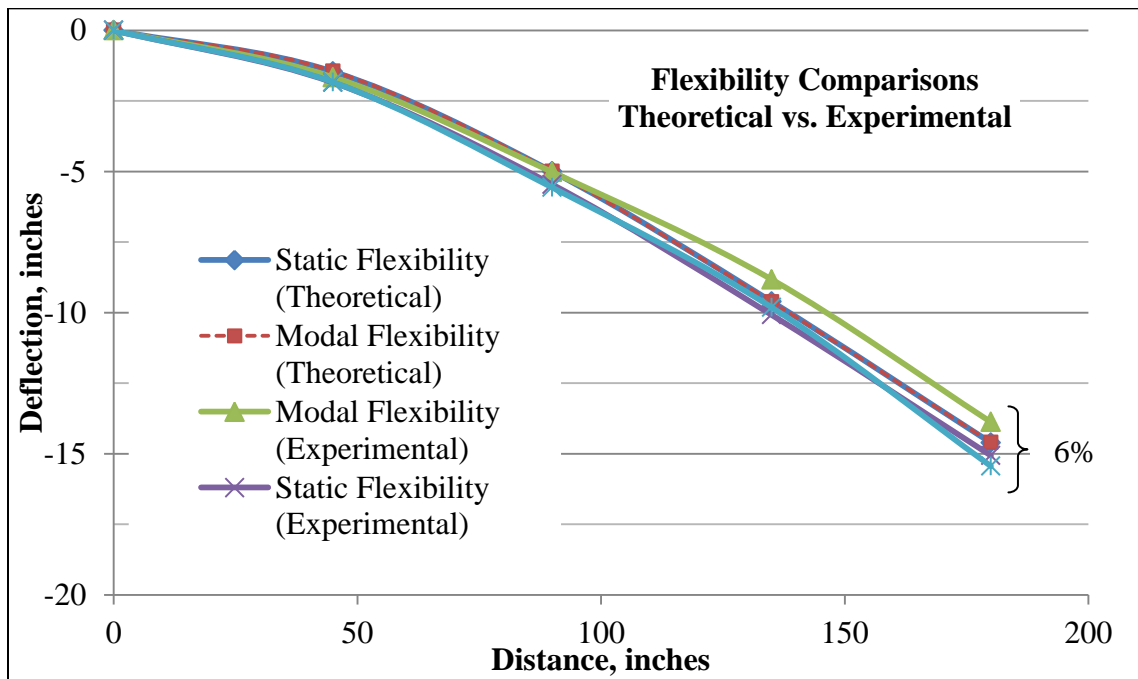

Figure 3.8: Comparison of deflection profiles for the HSS cantilever

3.4 DESCRIPTION OF THE GRID MODEL STRUCTURE

A large scale steel grid model structure was tested as part of this study to validate the experimental and analysis procedures that would be used for multi reference impact testing of an

in-service bridge. The grid structure is constructed of W8x10 structural steel members in the longitudinal and transverse directions. The grid has three longitudinal girder lines and seven transverse girder lines. The longitudinal girders consist of a single beam section that spans the entire length between the supports. The transverse girders span the 4.5 feet distance between the longitudinal girders. The grid structure is simply supported with an overall span length of 24 feet and a total width of 9 feet. The transverse girders are connected to the longitudinal girders by a combination of vertical clip angles and by top and bottom cover plates. The connections of the grid at the supports are designed to act as a roller and pin support. Several photographs of the grid structure before the sensors were installed on it are provided in Figure 3.9.
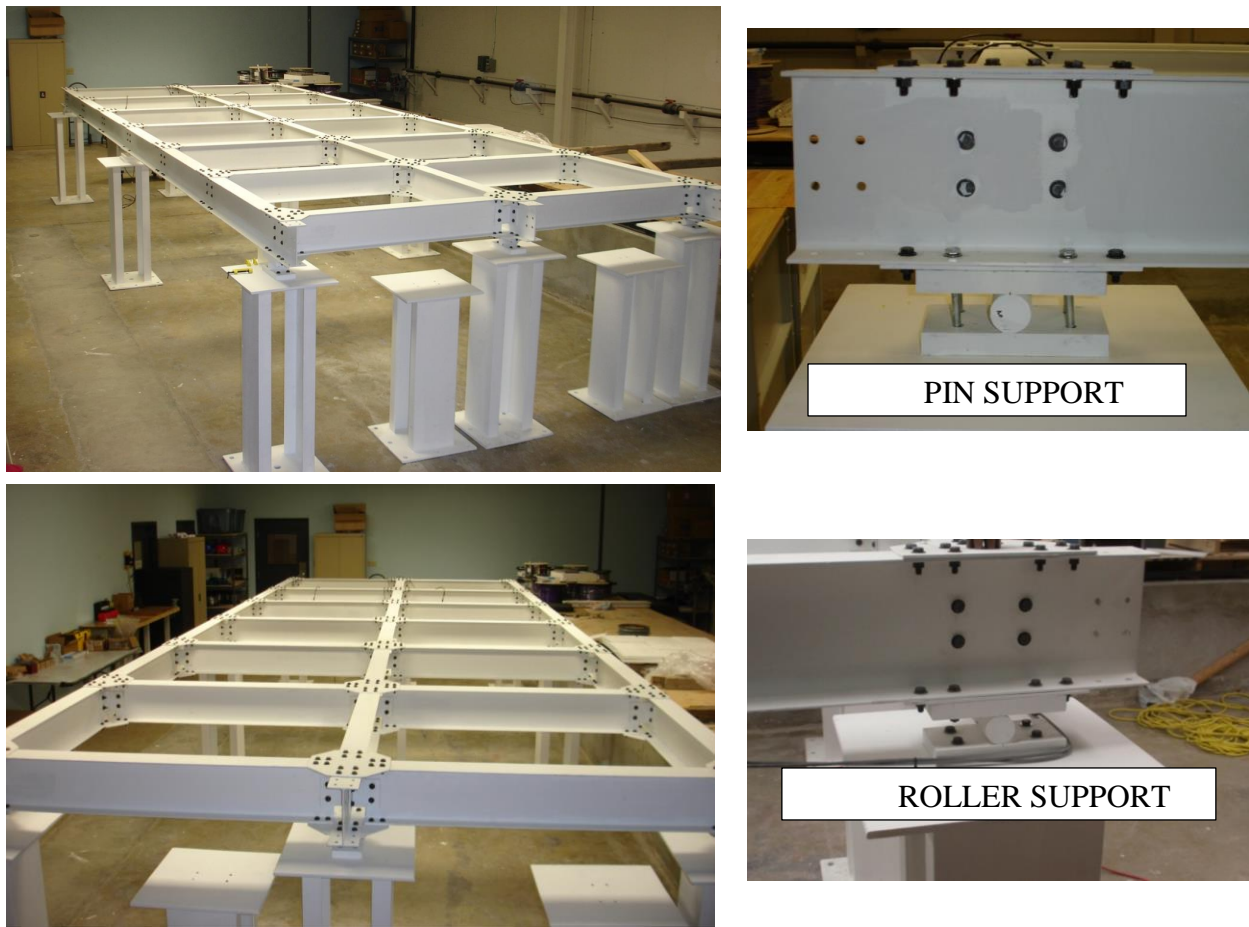

Figure 3.9: Photographs of the steel grid model structure in the laboratory.
Photo taken by Jason Herrman, Fall 2010 Engineering Research Center

3.5 INSTRUMENTATION OF THE GRID MODEL

The grid model structure was instrumented with a variety of different sensor types before it was tested. These sensors consisted of strain gages, displacement transducers and accelerometers. The sensor cables were routed to a central data acquisition cabinet that housed the data acquisition and control hardware. A total of 63 sensors were installed on the structure. The details of the sensors installed on the grid are provided in the following sections.

3.5.1 Accelerometers

The grid model was instrumented by a total of 21 accelerometers for measuring the vibration response during impact dynamic testing. The accelerometers were installed to measure the vertical vibration responses of the grid induced by the impact dynamic loadings. The accelerometers were placed at the intersections of the longitudinal and transverse girders. Model 393C accelerometers from PCB Piezotronics Inc. were used at all points on the grid structure except for the support locations. Model 393B05 accelerometers also from PCB Piezotronics Inc. were installed at the support locations since they are more sensitive than the other accelerometers. The 393C accelerometers were attached to the grid structure using magnets. The 393B05 accelerometers were installed at the support locations using hot glue. Photographs of the accelerometers installed on the grid structure are shown in Figure 3.10. The nominal specifications for the accelerometers installed on the grid structure are summarized in Table 3.11.

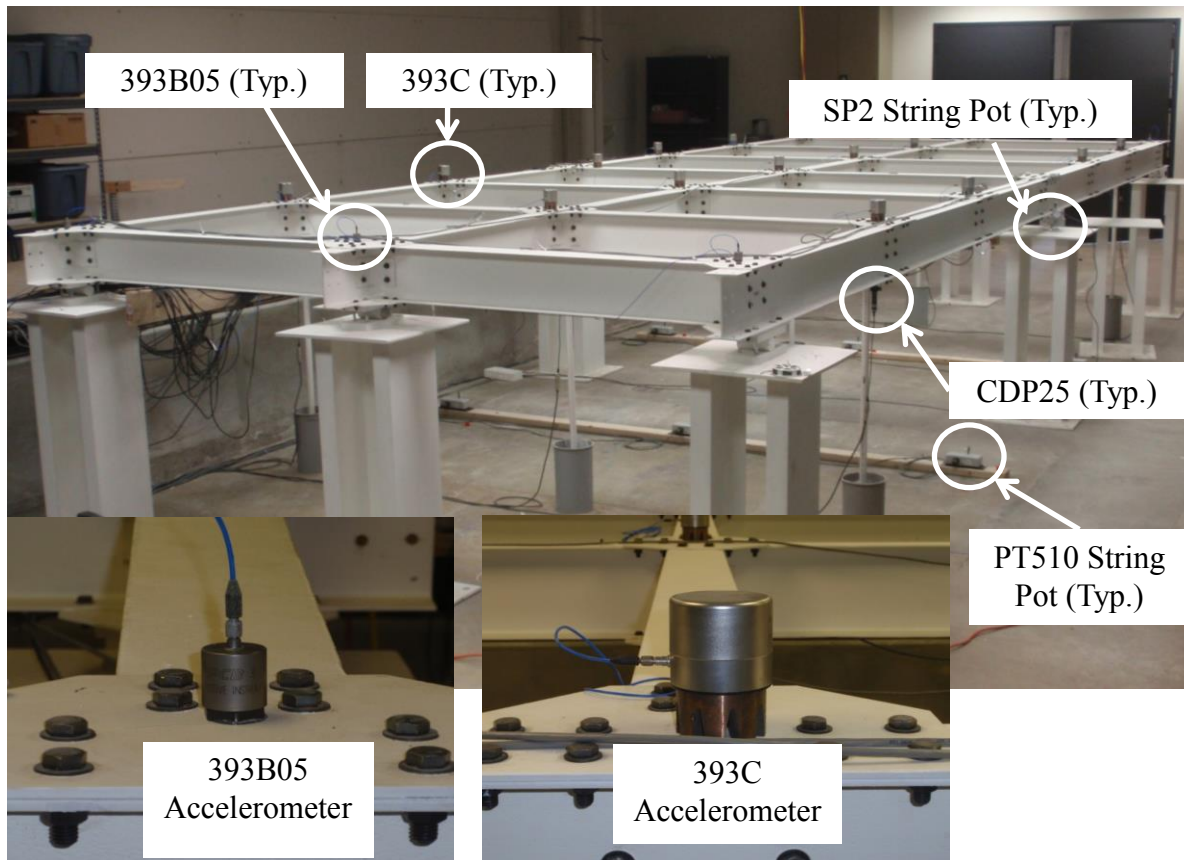Figure 3.10: Photographs of accelerometers installed on the grid model structure.
Photo taken by Jason Herrman Fall 2010, Engineering Research Center

Table 3.11: Sensor Specifications

Specification	393B05	393C
Sensitivity	10 V/g	1000 mV/g
Measurement Range	0.5 g pk	2.5 g pk
Frequency Range (+- 5%)	0.7 to 450 Hz	.025 to 800Hz
Broadband Resolution	0.000004 g rms	0.0001 g rms

3.5.2   Displacement Gages

A total of 15 displacement gages were installed on the grid model to measure the vertical displacements at various points during static load testing. These sensors were located below the intersections of all longitudinal and transverse girders except at the support locations. The specific locations of the displacement gages on the grid structure are shown in Figure 3.14. Three different types of displacement gages were used on the grid model structure. These included TML Model CDP-25 displacement transducers, Celesco Model PT-510 string pots and Celesco Model SP2-12 compact string pots. The CDP-25 transducers were installed at grid points B1, B2, B3, D2, F1, F2 and F3 as indicated in Figure 3.11. These transducers were attached to short PVC pipe sections that had been anchored in concrete that was placed in standard cylinder molds. The concrete cylinders were located under the grid model such that the transducer tips were located at the middle of the grid intersection points. The Celesco PT-510 gages were located under grid points C1, C2, C3, E1, E2, and E3. The Celesco SP2-12 gages were installed at grid points D1 D3 as shown in Figure 3.12. The Celesco PT-510 gages were attached to wooden 2x4 sections that were anchored to the concrete floor slab under the grid model structure (Figure 3.13). The gage wires were extended to the bottom side of the grid connections using piano wire. The Celesco SP2-12 gages were connected to attachment fixtures that were connected to pedestals located under the grid (Figure 3.12).

Figure 3.11: TML CDP-25 displacement transducer installed under the grid model structure.
Photo Taken by Jason Herrman, Fall 2010 Engineering Research Center

Figure 3.12: Photograph of SP2-12 string pot installed on grid structure.
Photo Taken by Jason Herrman, Fall 2010 Engineering Research Center

Figure 3.13: Photograph of PT-510 string pot installed under the grid model structure.
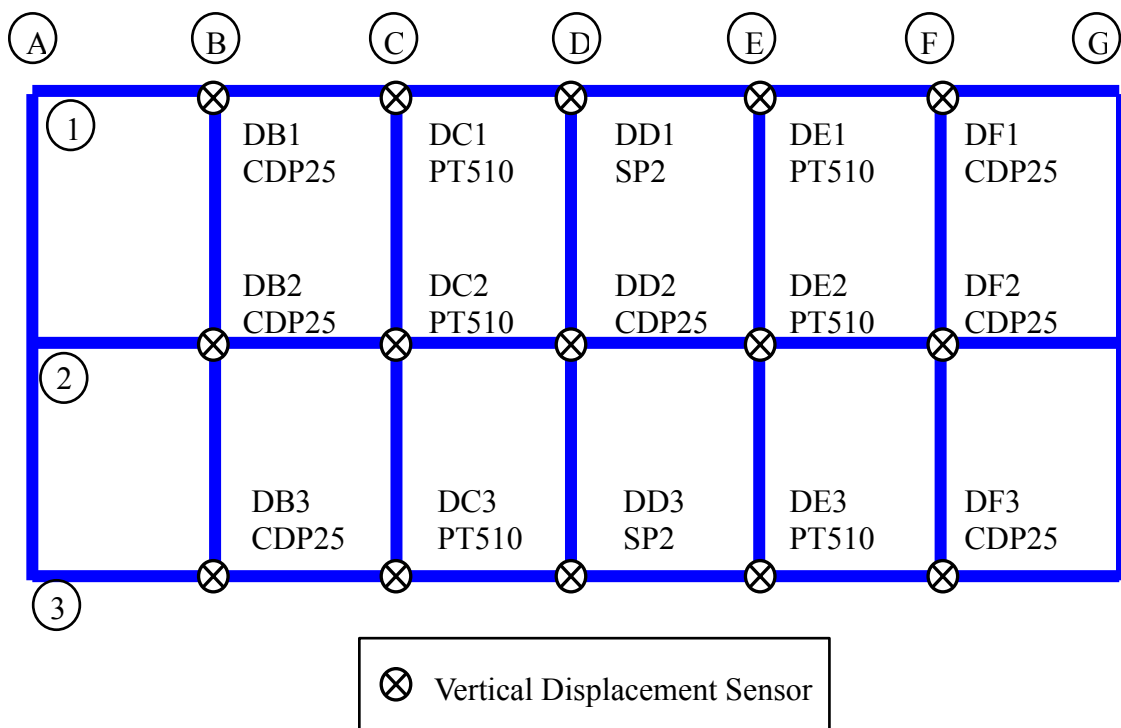Photo Taken by Jason Herrman, Fall 2010 Engineering Research Center

Figure 3.14: Displacement gage locations.

3.5.3   Strain Gages

A total of 26 strain gages were installed at various locations on the grid model structure. The locations of the strain gages are shown in Figure 3.15. A total of 15 strain gages were attached to the bottom flanges of the longitudinal girders, approximately 2 inches from the cover plates connecting the transverse and longitudinal girders. A total of five strain gages were installed on the top flanges of the longitudinal girders at 2 inches from the cover plates. The remaining six strain gages were attached to the bottom flanges of the transverse members at grid lines C, D, and E. The strain gages were all 350 Ohm weldable strain gages that were attached to the structure by microdot welding. Figure 3.16 shows a typical strain gage installed on the grid model structure. The strain gages were used to back-calculate bending moments at the sensor locations during static load tests using the basic mechanics relationships between strain, stress and bending moment.
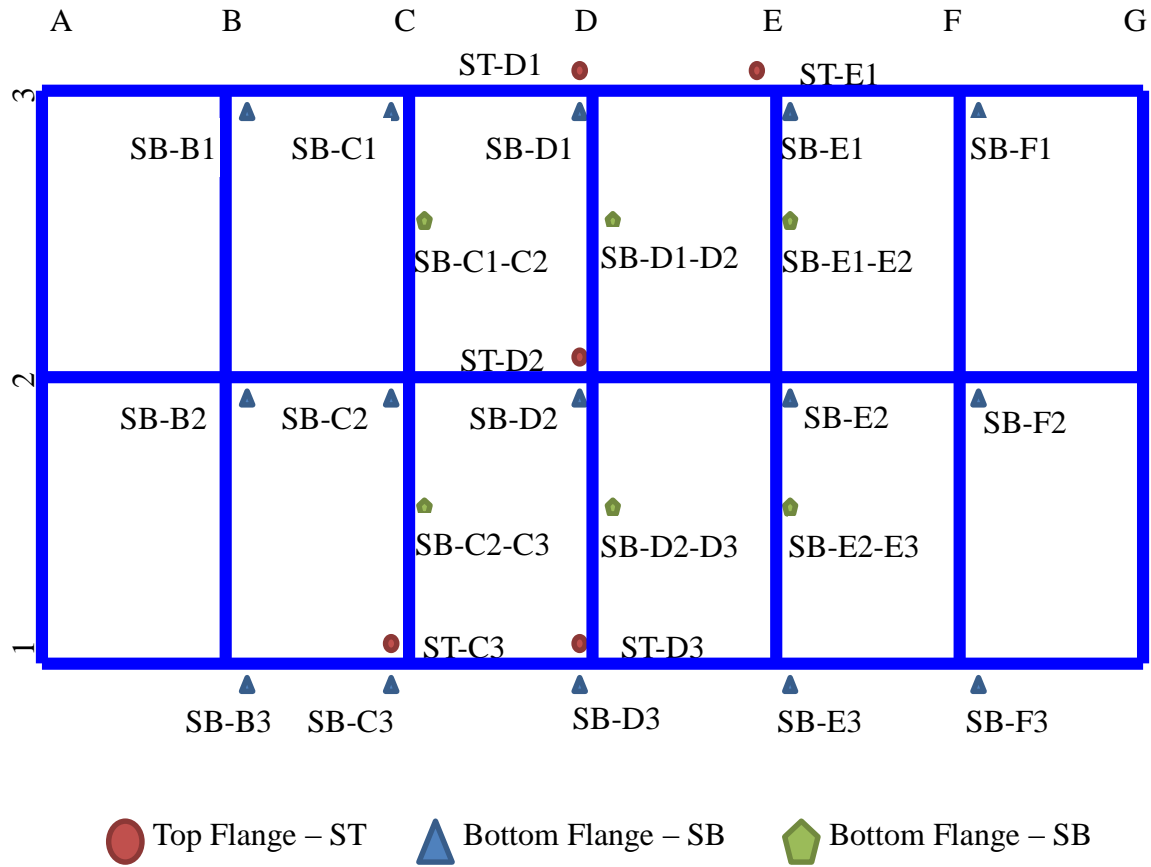
Figure 3.15: Grid model with the locations of the strain and displacement gages

Figure 3.16: 350 Ohm weldable strain gage installed on grid model structure.
Photo taken by Jason Herrman, Fall 2010 Engineering Research Center

3.6   STATIC LOAD TESTING

3.6.1   Testing Procedure

The static load testing of the grid structure included a total of seven different load cases. Multiple steel plates that measured 12 in x 12 in x ½ in and that weighed 20 pounds each were used to load the grid structure. The measurements recorded from the different static load test cases were used to construct a static flexibility matrix for the grid model and to calibrate a finite element model of the structure.

The first test case consisted of placing steel plates at each of the 15 grid points to measure the static flexibility matrix for the structure. The remaining test cases were used to evaluate the behavior of the model under different loading scenarios. The static flexibility matrix found from

the first test case was used as a baseline for comparison with the modal flexibility matrix found from the multi reference impact testing and to calibrate the finite element model.

The grid response measurements from each static load cases were recorded using a 10 Hz sampling rate and a total of 100 samples were recorded during each load case. The recorded measurement data were subsequently analyzed using MATLAB. Each load test case started with zero initial load applied to the grid structure.

3.6.2   Static Flexibility Matrix Test

The first load test was performed to acquire the static flexibility matrix for the grid structure. For this testing, the steel load plates were placed on the grid structure at the intersections of the longitudinal and transverse members. The support locations were not loaded, so a total of 15 locations were subject to the applied loading. The loading was applied to each point separately in a series of four increments of 100 pounds for a total load of 400 lbs. After the loading sequence for a given grid point was completed, the loading sequence was repeated at a different grid point until all 15 unsupported grid points were evaluated. Figure 3.17 illustrates the typical loading sequence that was applied to each of the 15 grid points that were evaluated. The strain and displacement sensors at all locations on the grid model were measured for each increment of the loading sequence at each of the 15 grid points.
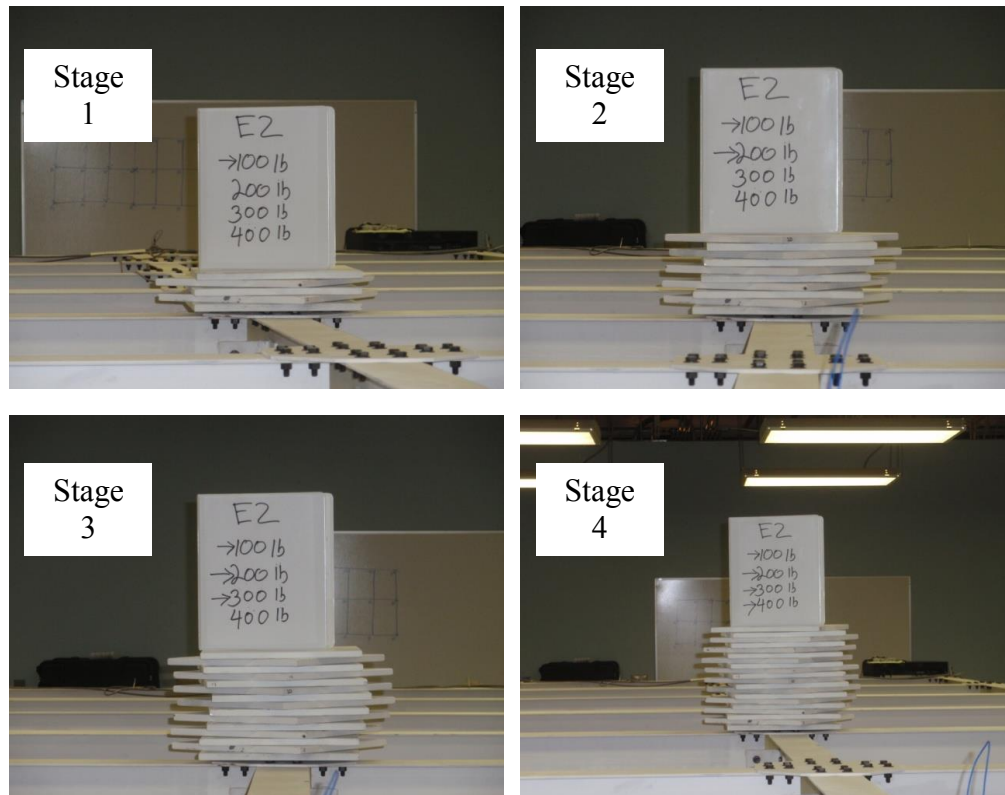
Figure 3.17: Load steps displayed at E2 of the grid model

Photo taken by Jeremy Rawn, Summer 2010 Engineering Research Center

3.6.3   Other Load Testing Scenarios

The grid structure was also evaluated for six additional load cases as described in the following:

1. Load every node of the grid, excluding the supports, with 40 pound loads.

2. Load every node on girders C, D, and E with 100 pound loads.

3. Load girder one at every node with 160 pounds.

4. Load girder two at every node with 160 pounds.

5. Load girder three at every node with 160 pounds.

6. Load girders one and three at nodes B, C, D, E, and F with 80 pounds.

Schematics of the load placement on the grid structure for each of these load cases are provided in Figure 3.18 through Figure 3.23.
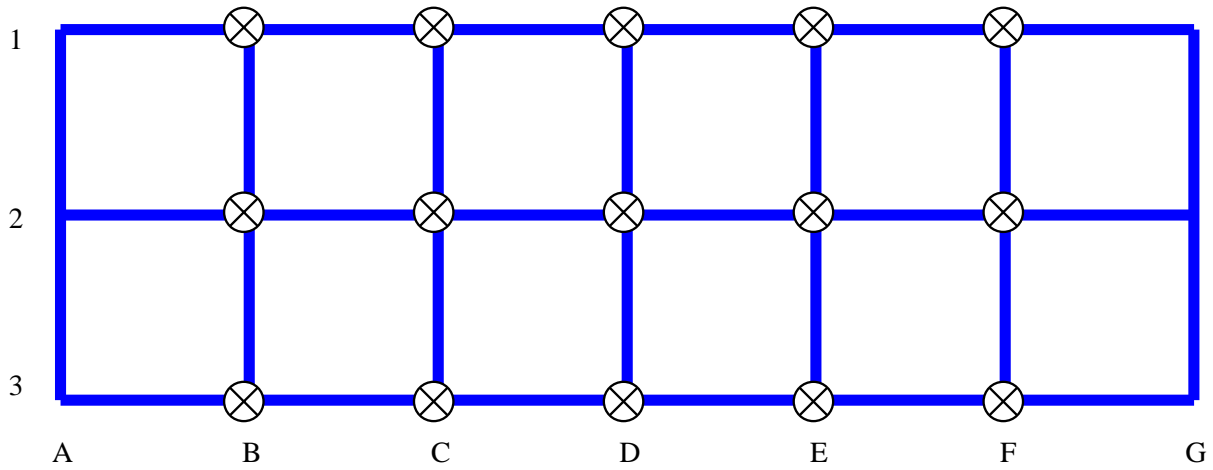

Figure 3.18: Case 1 - 40 lbs applied to each location noted.
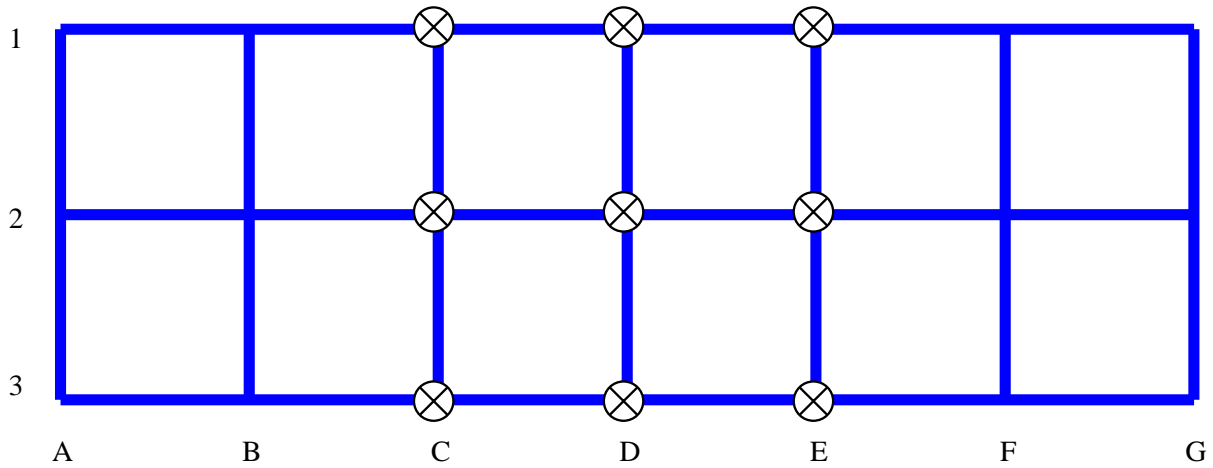
Figure 3.19: Case 2 - 100 lbs applied to each location noted.
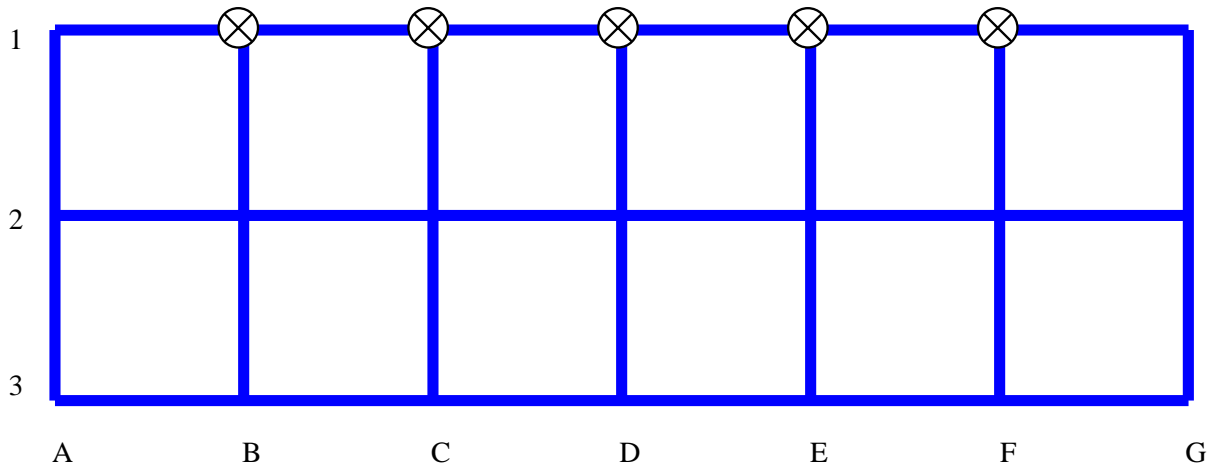
Figure 3.20: Case 3 - 160 lbs applied at each location noted.
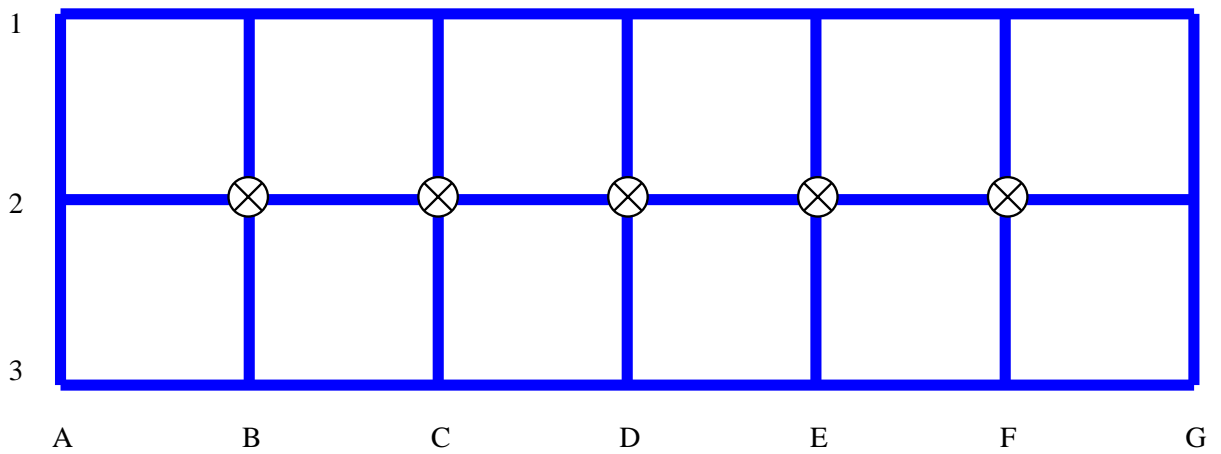
Figure 3.21: Case 4 - 160 lbs applied to each location noted.
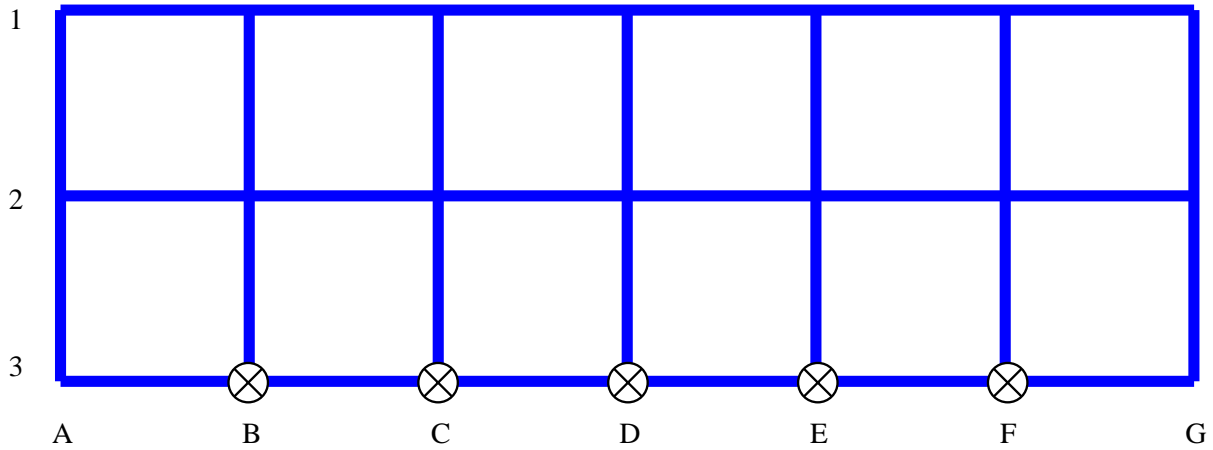
Figure 3.22: Load Case 5 – 160 lbs applied to each location noted.
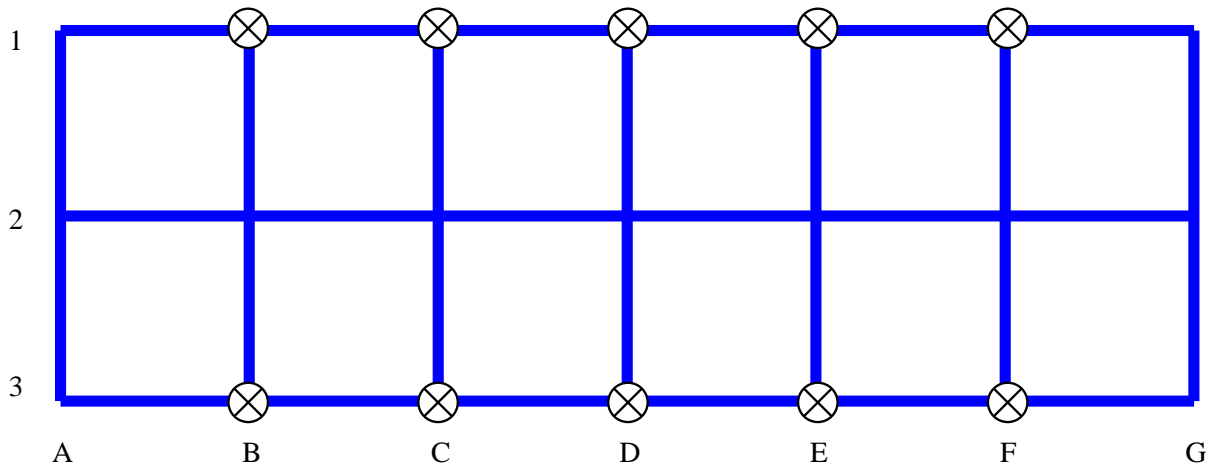
Figure 3.23: Load Case 6 – 80 lbs applied to each location noted

In each load case, 100 data points were recorded and averaged to obtain a single displacement and strain value that could be obtained for each sensor location. With an average value obtained for each point, each averaged load step would have the initial no load average subtracted from each load step. This value would be the actual displacement at each node for

each loading step. Once the actual displacement and strain is known for each point, the data can be compared with the output from a finite element model of the grid structure.

3.7   FINITE ELEMENT MODEL OF THE GRID STRUCTURE

The computer program SAP2000 (SAP2000, 2011) was used to construct a finite element model of the grid model structure. Each of the longitudinal and transverse members of the grid was represented by a three dimensional frame elements in the software. The support locations on the longitudinal girders were modeled as pins and rollers in the longitudinal direction of the span, and as pins in the transverse directions. The initial FE model modeled the connections between the longitudinal and transverse members as fully fixed, and the additional bending stiffness provided to the longitudinal and transverse members by the top and bottom cover plates at these locations was neglected. An extruded section view of the FE model of the grid is shown in Figure 3.24 and can be compared to the grid shown in Figure 3.25.

Each of the load cases executed in the static testing of the grid model was also simulated with the FE model. The FE model can be adjusted by comparing the output from the simulated load cases with the measured results until the two results show acceptable agreement. Once the FE model has been calibrated to reflect the measurements, modal analysis of the FE model can be performed to determine the natural frequencies and the modal order. This information is useful for validating the results of the subsequent impact dynamic testing of the grid structure.
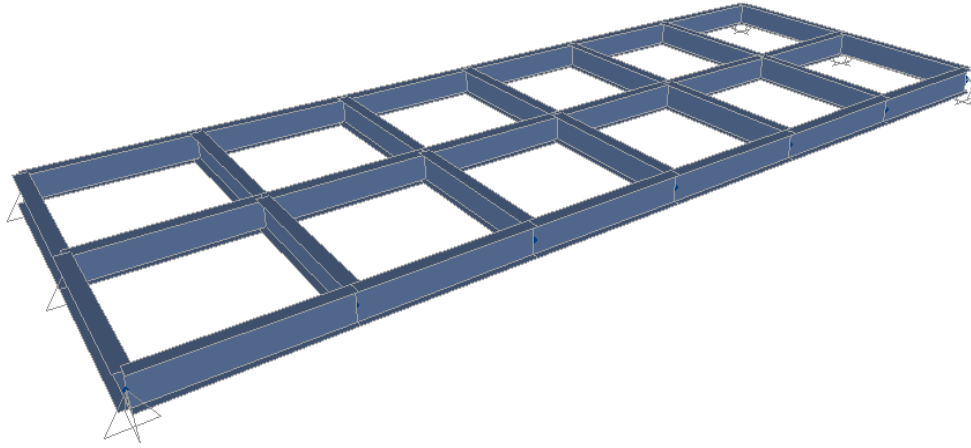
Figure 3.24: Extruded member view of the FE model of the grid structure.

Figure 3.25: Grid model without sensors.

Photo taken by Jeremy Rawn, Fall 2009 Engineering Research Center

3.8   STATIC LOAD TEST RESULTS

The experimental results did not compare particularly well with the initial FE model of the grid model structure. The initial FE model was modified to include the contribution to the girder stiffness of the cover plates at the longitudinal/transverse member connections. A second set of static load tests were then executed on the grid model structure. The load amount used for each load step was increased for the second set of static load tests. The original loading consisted of four 100 pound load steps with a maximum load of 400 pounds. The second load test used three load steps of 200 pounds each totaling a maximum load of 600 pounds.

3.8.1   Calculated bending moments from strains measured in static load cases

The strain gage measurements from the longitudinal girders were used to calculate bending moments at these sensor locations. These results are summarized for each load case in Table 3.12. In the table, the SB refers to strain gage locations that were on the bottom flange of the longitudinal girders and ST refers to the strain gages that were located on the top flange of the girders. The measured strain data from each load case were used to calculate bending moments at the strain gage locations using equation 3.9.

$$M = \varepsilon \ \text{x} \ E \ \text{x} \ S \hspace{4cm} [3.9]$$

Table 3.12: Bending moments calculated from measured strains from Cases 1- 6

Gage	Case 1	Case 2	Case 3	Case 4	Case 5	Case 6
Strain - SB-B1	3.86	4.55	12.42	4.69	-1.93	5.28
Strain - SB-B2	4.12	5.01	5.17	6.17	5.21	5.16
Strain - SB-B3	4.51	5.64	-2.18	5.68	14.70	6.07
Strain - SB-C1	5.62	8.08	18.13	7.04	-3.09	7.55
Strain - SB-C2	6.25	9.21	8.04	8.85	8.20	8.02
Strain - SB-C3	6.36	9.35	-3.41	8.17	20.75	8.50
Strain - SB-D1	7.51	11.67	24.21	9.76	-4.15	10.08
Strain - SB-D2	5.09	12.05	10.07	10.49	10.47	10.54
Strain - SB-D3	7.56	11.79	-4.19	10.03	24.43	10.02
Strain - SB-E1	6.71	9.82	21.60	8.56	-3.45	9.08
Strain - SB-E2	6.84	10.14	8.93	9.55	9.04	8.92
Strain - SB-E3	7.06	10.31	-3.75	9.20	22.47	9.41
Strain - SB-F1	3.78	4.41	11.98	4.54	-1.69	5.14
Strain - SB-F2	3.84	4.59	5.00	5.83	4.73	4.84
Strain - SB-F3	3.87	4.49	-1.81	4.77	12.15	5.18
Strain - ST-C3	-6.47	-9.55	3.64	-8.42	-21.19	-8.69
Strain - ST-D1	-7.64	-11.90	-24.95	-10.02	4.48	-10.29
Strain - ST-D2	-8.01	-12.40	-10.33	-10.87	-10.87	-10.56
Strain - ST-D3	-8.25	-12.85	4.53	-11.08	-26.72	-10.94
Strain - ST-E1	-6.77	-10.11	-22.19	-8.83	3.58	-9.08
*All values given in kip-in						

3.9   MULTI REFERENCE IMPACT TESTING OF THE GRID MODEL

3.9.1   Methods of Testing

Once the static load testing of the grid model was completed, a multiple-reference impact test (MRIT) of the grid was performed using an instrumented hammer and accelerometers. The execution and analysis of the MRIT for the grid model structure served as an effective practice run for the procedures that were to be implemented in the field testing using the FWD as an impact device. Because the grid model structure was located in the laboratory, its system identification would be subject to less uncertainty than would be expected with a full-scale bridge test in the field. The grid model structure is also slightly more representative of an actual bridge in terms of its structural complexity than the very simple cantilever beam model, so this testing served as a more realistic baseline for evaluating and validating the testing and data analysis procedures that would be employed in the field for the full-scale bridge testing.

The MRIT dynamic testing procedure employed for the grid model was very similar to that which was used to evaluate the cantilever beam structure. Each unsupported node of the grid structure was struck by the impact hammer (Figure 3.26) and the corresponding structural vibration responses were recorded from all of the measurement degrees of freedom on the grid structure. The vibration responses of the grid structure were measured by vertically oriented accelerometers that were placed at the connections between the longitudinal and transverse grid members. The measured accelerations and input forces from each impact of the instrumented hammer were processed to determine the natural frequencies, mode shapes, damping ratios and

modal scaling factors. These modal parameters were used to form the modal flexibility matrix for the grid according to Equation [3.10].

$$H_{pq}(\omega=0)= \sum_{r=1}^{m} \left[\frac{\psi_{pr}\psi_{qr}}{M_{A_r}(-\lambda_r)} + \frac{\psi_{pr}^*\psi_{qr}^*}{M_{A_r}^*(-\lambda_r)} \right]$$

[3.10]

3.9.2 Testing Procedure

The MRIT program was executed for the grid model using the Smart Office (SO) Analyzer software from M+P International. This particular software package is purpose built for executing dynamic tests and for processing and analyzing the resulting measurements. The measured vibration responses of the grid and the impact force records could be viewed on the fly with this software to verify that clean data was being recorded. The impact force time record was inspected after each hit to verify that the impact was a pure impulse force. The measured vibration responses were viewed to ensure that none of the sensors responses exceeded their input range. Ordinary coherence functions computed between the input and each output locations were generated from each hit and were inspected after each hit along with the generated frequency response functions (FRFs) that were computed from each input-output measurement. The peaks of the FRF are indications of the locations of the natural frequencies of the structure. The ordinary coherence function plot is evaluated to verify that a measured response is due to the input and not uncorrelated noise. The ordinary coherence function plot should ideally be a flat line with a value of one at the locations each peak in the FRF. Multiple input-output records were recorded for each impact location and the FRFs obtained were averaged to minimize any variances in the measurements. The natural frequencies and mode shapes for the grid model

structure determined from the MRIT data using the SO software were compared to the modal

parameters identified from the calibrated FE model of the grid structure.

Figure 3.26: Impact testing with instrumented hammer at node B1 of the grid model structure.
Photo taken by Dr. Kirk Grimmelsman

3.9.3   MRIT Results for the Grid

3.9.3.1   Modal parameter identification method

The natural frequencies and mode shapes were extracted from the MRIT data for the grid

model using the Complex Mode Indicator Function (CMIF) and enhanced FRF (eFRF) approach.

The vibration responses measured from each input location generated one column of the FRF

matrix. The diagonal elements of the FRF matrix correspond to the output measurements recorded at the hammer input location, or the so called driving point locations. The driving point measurements are particularly important as they are later used for scaling the mode shapes to the modal mass of the structure (e.g. mass normalized mode shape vectors). The driving point measurements are also used in developing the eFRFs. The number of eFRF functions is limited to the number of driving point measurements (or the number of columns in the FRF matrix).

The CMIF algorithm is performed once the FRF matrix from the input-output measurements on the structure has been constructed. The FRF matrix is a three dimensional matrix with the number of rows equal to the number of output locations, the number of columns equal to the number of input locations, and the final dimension (into the page) equal to the number of frequency lines from DC to the Nyquist frequency (one half of the sampling frequency) in the frequency domain. The elements of the FRF matrix represent the displacement at each measurement node divided by the input force and these values are defined at each frequency line. Singular Value Decomposition (SVD) of the FRF matrix is performed at each frequency line yielding a set of left and right singular vectors and a diagonal matrix of singular values sorted in descending order. The singular values at each frequency line are plotted versus frequency to obtain the CMIF plot. The largest peaks on this plot are usually where the natural frequencies of the structure are located, but all peaks are investigated. The CMIF plot for the grid with selected peaks is shown in Figure 3.27. The peaks identified in the CMIF plot are denoted in the figure by an asterisk. This CMIF plot covers the frequency band from DC to 120 Hz, but the modes used to develop the modal flexibility matrix for the structure are all located in the DC to 100 Hz frequency range. The left singular vector associated with each peak singular value in the CMIF plot is an estimate of the mode shape for that corresponding frequency.
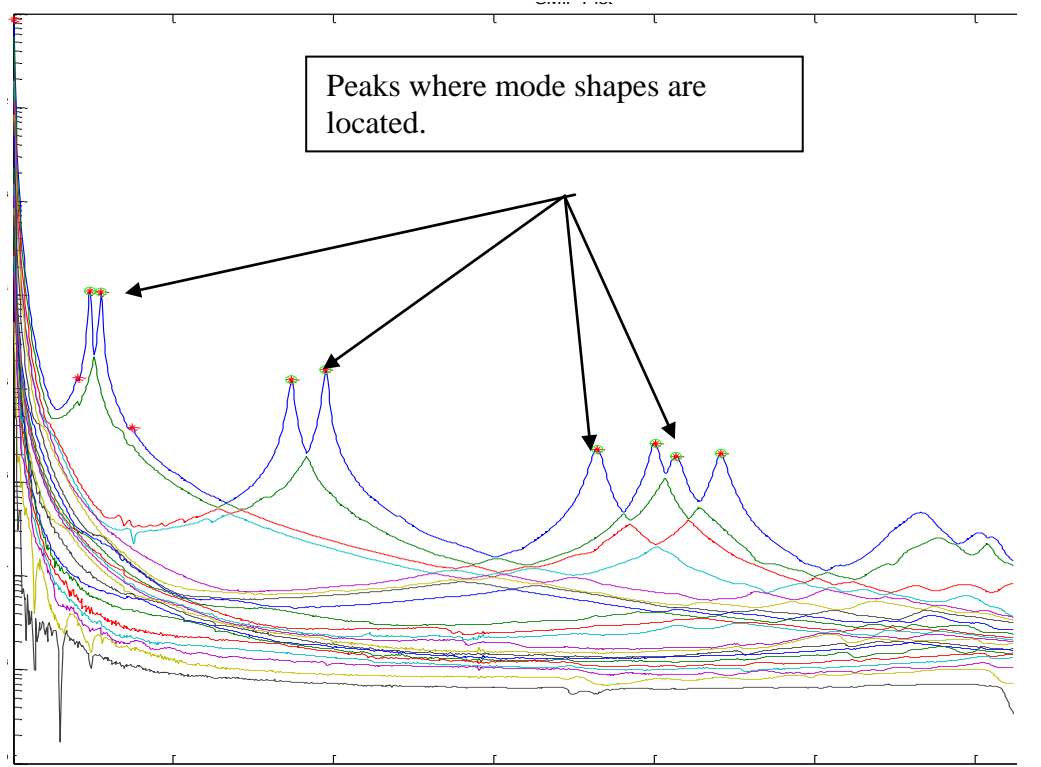
Figure 3.27: CMIF plot developed from MRIT data from grid model structure.

3.9.3.2 Frequencies and Mode Shapes

The natural frequencies and mode shapes for the grid model were identified from the MRIT data and were found to be close to those predicted by the FE model. The results from the CMIF also compare closely to the results obtained from the M+P SO software results. The results from the three methods used to find the frequencies and mode shapes are summarized in Table 3.13. The mode shapes for each method are displayed in Figure 3.28 through Figure 3.30. The percent differences between the frequencies calculated using M+P SO software and the CMIF algorithm are all less than 1%.

Table 3.13: Natural frequencies of identified mode shapes for the grid using SAP 2000, M+P, and CMIF

Mode Description	Frequency, Hz		
	SAP2000	M+P	CMIF
1st Bending	9.179	9.45	9.625
1st Torsion	10.014	10.968	11
2nd Bending	36.14	34.068	34.75
2nd Torsion	39.526	38.973	39.125
3rd Bending	78.74	66.937	72.75
1st Butterfly	83.542	79.808	80
3rd Torsion	87.26	82.672	82.875
2nd Butterfly	90.827	88.547	88.25

$f_1 = 9.1709$ Hz $\qquad$ $f_2 = 10.014$ Hz $\qquad$ $f_3 = 36.140$ Hz

$f_4 = 39.526$ Hz $\qquad$ $f_5 = 78.740$ Hz $\qquad$ $f_6 = 83.542$ Hz

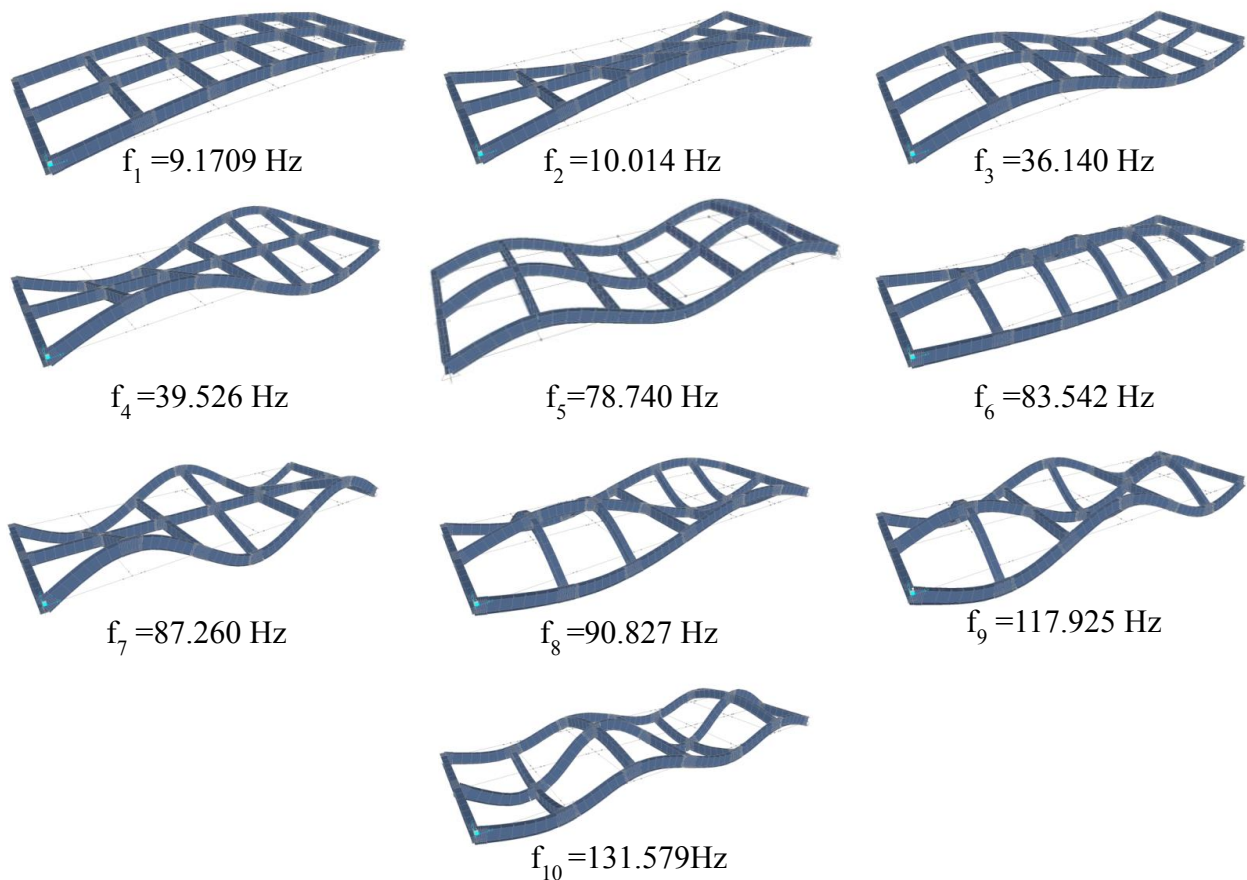$f_7 = 87.260$ Hz $\qquad$ $f_8 = 90.827$ Hz $\qquad$ $f_9 = 117.925$ Hz
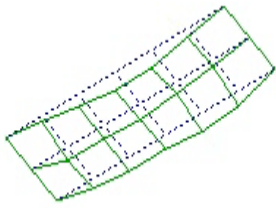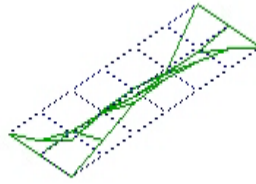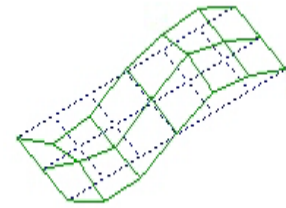
$f_{10} = 131.579$ Hz

Figure 3.28:Natural frequencies and mode shapes from FE model of the grid model (SAP2000).

Bending Mode 1
$f_1 = 9.450$ Hz

Torsion Mode 1
$f_2 = 10.968$ Hz

Bending Mode 2
$f_3 = 34.068$ Hz

Torsion Mode 2
$f_4 = 38.973$ Hz

Bending Mode 3
$f_5 = 66.937$ Hz

Butterfly Mode 1
$f_6 = 79.808$ Hz
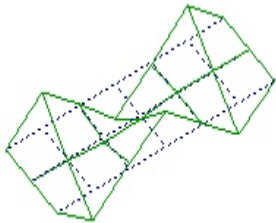
Torsion Mode 3
$f_7 = 82.672$ Hz
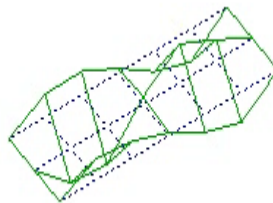
Butterfly Mode 2
$f_8 = 88.547$ Hz
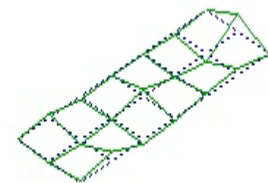
Combination
Bending
$f_9 = 112.407$ Hz

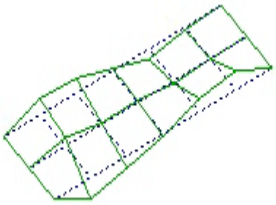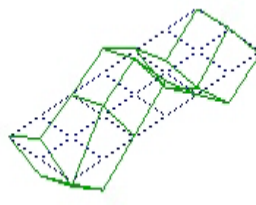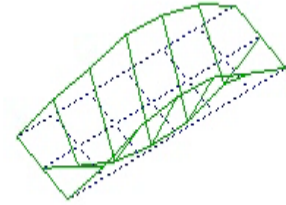Figure 3.29: Natural frequencies and mode shapes identified for the grid model structure from M+P SO software.
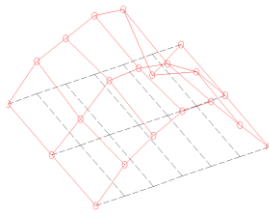
Bending Mode 1
f_1 =9. 500 Hz
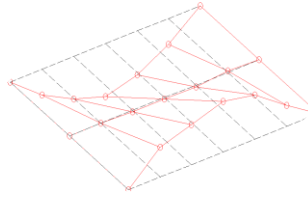
Torsion Mode 1
f_2 =10.875 Hz
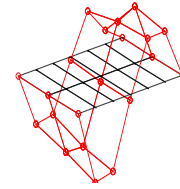
Bending Mode 2
f_3 =34.000 Hz
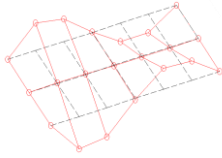
Torsion Mode 2
f_4 =39.000 Hz
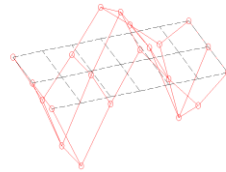
Bending Mode 3
f_5 =67.000 Hz
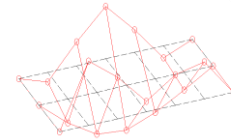
Butterfly Mode 1
f_6 =79.808 Hz
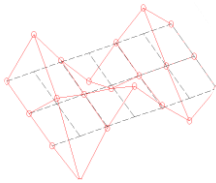
Torsion Mode 3
f_7 =82.750 Hz
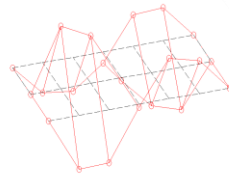
Butterfly Mode 2
f_8 =87.875 Hz

Figure 3.30: Natural frequencies and mode shapes for grid model identified from CMIF algorithm.

3.9.3.3 Modal Flexibility Matrix Computation

The modal parameters of the grid were calculated and analyzed from the CMIF algorithm. As discussed previously for the cantilever beam testing, modal parameters consist of the poles (frequencies and damping), mode shapes, and modal scaling. Modal A (M_{A_r}) is the modal scaling factor that estimates the modal mass. Using equation [3.10] the modal flexibility is

calculated using only the modal parameters identified from the MRIT data. The eight modes used to calculate the modal flexibility matrix are evaluated to verify if they provide an accurate estimation of the static flexibility matrix. To compare the static and modal flexibility matrices for the grid model in a physically meaningful manner, both matrices are multiplied by a uniform load vector of unit magnitude and the resulting girder displacements are obtained at each measurement node for the grid. The resulting displacement is referred to as the Uniform Load Surface (ULS). Figure 3.31 through Figure 3.33 show the three longitudinal girder line deflection profiles obtained by applying a uniform load vector to the flexibility matrices obtained from the FE model (analytical), the static load test, and the MRIT data. The two dynamic profiles shown and listed as Dynamic 1 and Dynamic 2 represent the multiple tests performed on the grid model that display the consistency in the testing method.
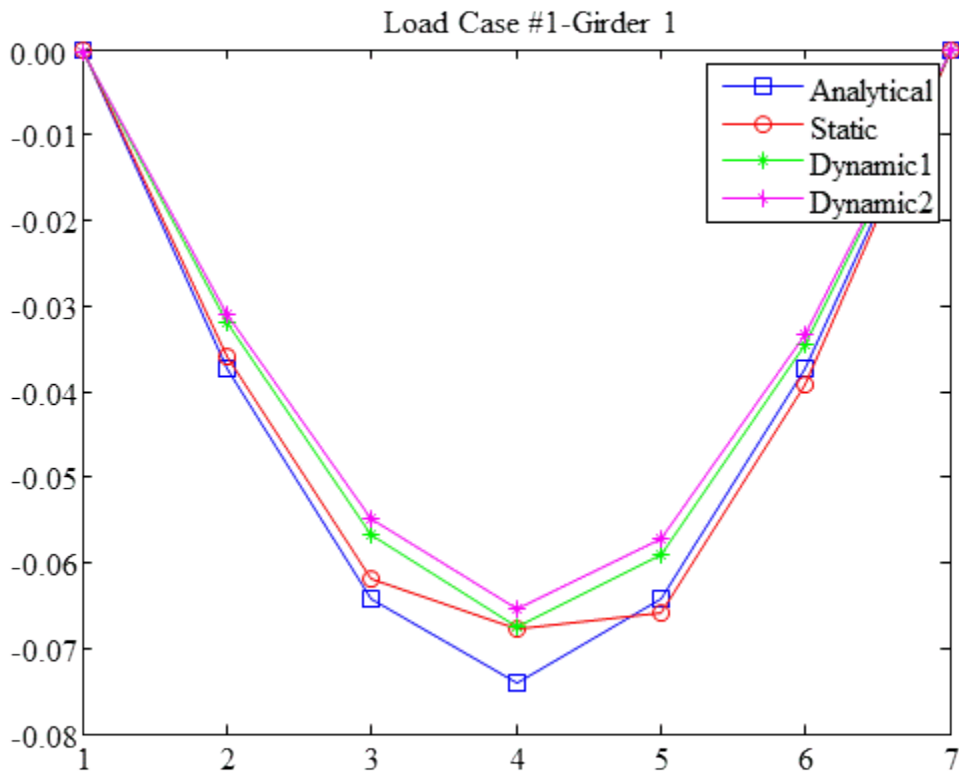
Figure 3.31: Displacement profiles for Girder 1 from analysis and experiments.
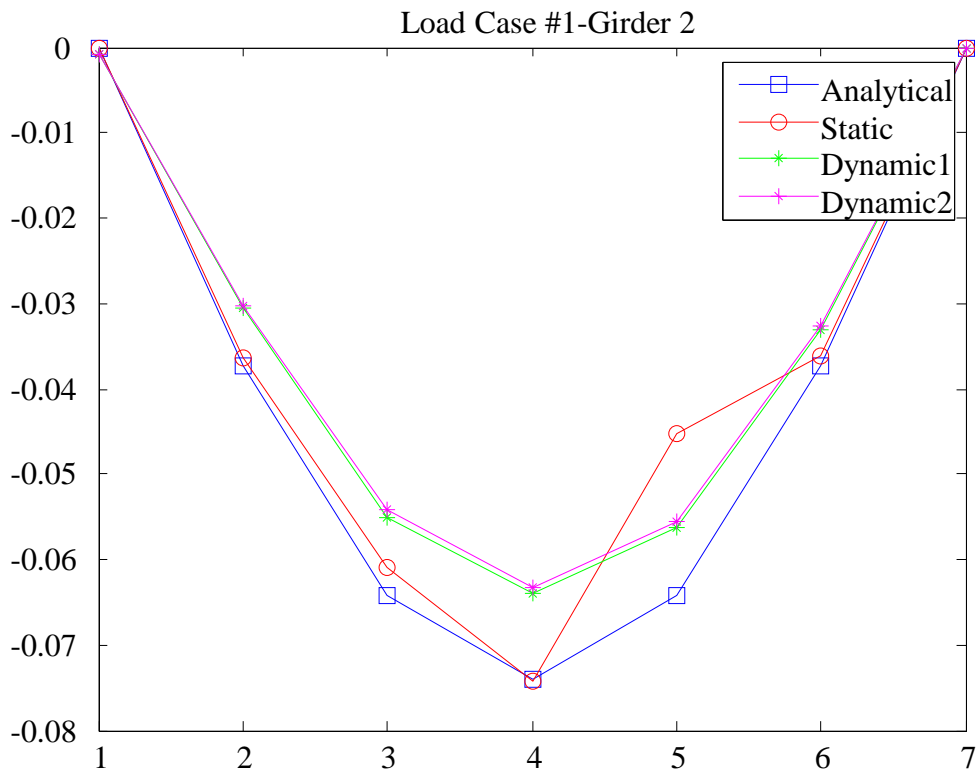
Figure 3.32: Displacement profiles for Girder 2 from analysis and experiments.
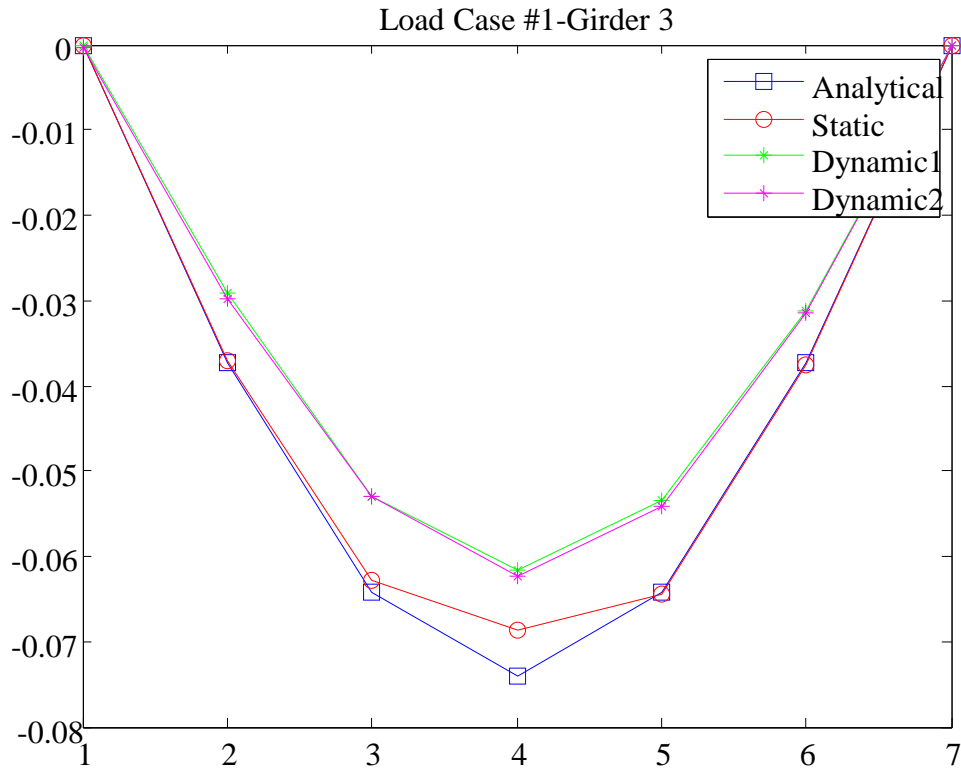
Figure 3.33: Displacement profiles for Girder 3 from analysis and experiments.

3.9.3.4 Discussion

The displacement profiles for the three longitudinal girder lines permit a physical comparison of the static and modal flexibility matrices. Both of the impact tests performed had very similar results and the displacement profiles obtained from the ULS plot directly on top of each other. This result is positive because the two impact tests were performed on separate occasions and produced results that were similar. The displacement lines for the static test and the analytical model are also close. This should be the case because the FE model had been adjusted using the strain and displacements measured from the static load test. The displacement profile for Girder 2 shown in Figure 3.32 has a sensor error at node E2. The difference between

the results of the static test and the impact tests vary between 15% and 20% on the three girders. This range is larger than what is desirable to draw an accurate estimation for the modal flexibility. In all cases, the girder displacement profiles obtained from the modal flexibility matrices were smaller than the static flexibility matrices (static load test and FE model). One possible reason for this difference is truncation error that occurs from using only eight modes to identify the modal flexibility matrix. The higher vibration modes of the grid were not successfully captured because of the spatial resolution of the instrumentation layout. Due to a limited amount of space for sensor placement, the number of sensors used did not allow for the higher mode shapes to be properly viewed. Having more modes will allow for a better approximation of the static flexibility. A more likely reason for the difference is probably due to the calibration of the force transducer in the impact hammer used for the MRIT program. Several attempts were made to calibrate the dynamic force output from the hammer by striking it against a reference load cell. This testing showed a consistent difference in the force measured by the two devices. The differences between the static and modal flexibility matrices could be reduced by a better calibration of the force transducer on the impact hammer used for the testing. Although there are differences in the displacements predicted by the static and modal flexibility matrices obtained from the grid model, the results were close enough to warrant confidence in the experimental and analytical approaches that were used in evaluating the grid structure.

4 FIELD TESTING PROGRAM

4.1 INTRODUCTION

The purpose of the field testing program was to evaluate the feasibility of using a falling weight deflectometer (FWD) as a dynamic excitation device for impact testing of bridges. Impact testing offers a rational and quantitative approach for globally characterizing in-service bridges. Such quantitative characterizations have broad and consistent meaning to structural engineers and can be used to reliably assess the current performance of the structure and future changes in the structure's condition. The most important advantages of being able to use a FWD for impact dynamic testing of bridges are that it can be easily deployed to many structures, it can provide large and consistent impacts to the structure, and most state departments of transportation already own FWD devices and are very familiar with their operation. In order to evaluate the merits of the proposed impact testing approach, a MRIT program was performed on two in-service bridges using both a conventional modal impact hammer (instrumented sledge) and a FWD device. The modal parameters for each structure were identified from each test approach and compared with each other to evaluate the effectiveness of the FWD as a dynamic impact device. Modal flexibility matrices were also estimated for the bridges tested from the identified modal parameters and compared.

4.2   IDENTIFICATION AND SELECTION OF THE TEST BRIDGES

A field inspection survey was undertaken prior to the execution of the field testing program to identify full-scale bridges that would be suitable for testing. The focus of the inspection survey was on bridges that were located within a 20 mile radius of the University of Arkansas campus. This proximity criterion was selected to keep travel costs associated with the field testing to a minimum. Numerous bridges were located within this range, and field visits to each structure were performed to evaluate the suitability of each candidate to serve as a test specimen. Eleven bridge structures were identified as possible candidates. After visiting and assessing the attributes of these eleven bridges, two final candidates were identified for the field testing program. These two structures were selected on the basis of their ease of access for installing the instrumentation, the level of traffic demand on the structure, and the representative nature of their structural systems. The two bridges selected for the field testing program included a modern concrete deck on rolled steel beam bridge (Hancil "Tiny" Hartbarger Bridge) and an older Parker pony truss bridge (Baptist Ford Bridge, AHTD Bridge No. 18802). Both of these structures were located very near to the University of Arkansas campus (within 10 miles), provided easy access for instrumentation and testing, and did not service significant levels of daily traffic. The structural designs of these two bridges were considered to be representative of many bridges within the US National Bridge Inventory. It should also be noted that the design and construction plans could not be located for either bridge. Field measurements of the member and structure geometries were performed on both bridges to identify their geometric configurations.

4.3   DESCRIPTION OF THE MULTI-BEAM BRIDGE STRUCTURE

The Hartbarger bridge (Figure 4.1) is a ten span, concrete deck on rolled steel beam bridge structure that was constructed in 1987. The bridge carries two lanes of traffic and is located on S. Black Oak road (County Road 57) just east of Fayetteville, AR. The bridge crossing consists of 10 simply supported spans each having a span length of 50 feet and a width of 27 feet. The lanes on the bridge are twelve feet wide and there is an 18 inch wide barrier on each side of the bridge. The framing plans for each span are identical and consist of four rolled steel beams (W27x94) that support the 8 in. thick reinforced concrete deck (Figure 4.2). The framing plan for the bridge also includes five transverse lines of channel diaphragms that are bolted to connection plates which are welded to the beam webs. The impact testing program for this bridge was executed exclusively on the second span located at the west end of the bridge.

Figure 4.1: Hancil "Tiny" Hartbarger Bridge - concrete deck on multi-beam bridge.
Photo taken by Jeremy Rawn, Fall 2010 Fayetteville, Arkansas

Figure 4.2: Hartbarger Bridge – view of framing plan from underside of bridge.
Photo taken by Jeremy Rawn, Fall 2010 Fayetteville, Arkansas

4.4 DESCRIPTION OF THE BAPTIST FORD BRIDGE

This bridge crossing consists of three 100 ft. long, simply supported truss spans and carries two lanes of traffic across the West Fork of the White River and is located just south of Fayetteville, AR. The bridge was constructed in 1930, and is located on County Road 1194. The bridge carries very little traffic (less than 20 vehicles per day), and therefore was an ideal candidate for the field testing program. The superstructure details of each truss span are identical, and each truss span consists of 10 panels spaced at 10 ft. The width of the bridge measured from

center to center of the trusses is 22.3 ft. The truss depth varies along the span length and has a maximum value of 14 ft at the midpoint of the span. The 8 in. thick reinforced concrete deck is supported directly on I-shaped rolled steel floorbeams that span between the bottom panel points of the upstream and downstream trusses. The truss members consist of rolled and riveted built-up sections as follows:

- Top Chords: two channels, a top cover plate, and lacing;

- Bottom chords: two channels with batten plates;

- Verticals: I-beams; and

- Diagonals: I-beams and two angles with batten plates.

Photographs showing various views of the truss spans are provided in Figure 4.3 – Figure 4.5. No plans could be located for the bridge, and field measurements were used to determine the geometric characteristics of the truss and its members. The impact dynamic testing was performed on the middle span of the bridge crossing.

Figure 4.3: Baptist Ford Bridge – Elevation View of Typical Span
Photo taken by Jeremy Rawn, Fall 2010 Fayetteville, Arkansas

Figure 4.4: Baptist Ford Bridge – View of Bridge Deck
Photo taken by Jeremy Rawn, Fall 2010 Fayetteville, Arkansas

Figure 4.5: Baptist Ford Bridge - View from Underside
Photo taken by Jeremy Rawn, Fall 2010 Fayetteville, Arkansas

4.5   METHODS OF TESTING

A separate instrumentation and testing plan was developed for each of the bridges that were tested. The instrumentation plans for each bridge were devised such that the modal parameters of each structure could be identified from the dynamic testing program. Particular attention was paid to ensuring that adequate spatial resolution would be provided by the instrumentation layout to identify enough vibration modes to achieve a good estimate of each structure's modal flexibility matrix. Multiple Reference Impact Testing (MRIT) methods were used to evaluate each bridge.

4.6   IMPACT TESTING DEVICES

A Dynatest falling weight deflectometer (FWD) and a Model 086D50 portable impact hammer from PCB Piezotronics Inc. (Figure 4.6) were both used to provide impact dynamic excitation of the two bridges. The impact hammer testing data was used as a baseline for evaluating the performance of the FWD as an impact source. The impact hammer is easier to deploy on a bridge structure than the FWD device, but is labor intensive and subject to operator induced variations and experimental uncertainty (e.g. signal to noise ratio in the measurements) that could be mitigated by the FWD device.

Figure 4.6: Falling Weight Deflectometer with Bumpers below Load Plate and Modal Impact
Hammer
Photo taken by Jason Herrman, Fall 2010 Fayetteville, Arkansas

FWD devices are more typically used to evaluate pavement/subgrade conditions by measuring the deflection profiles that result due to the impact force provided by the system. The FWD operates by lowering an 11 inch diameter circular strike plate onto a flat surface, generally a pavement. A predetermined amount of weight is dropped is dropped on top of a steel rod that is

connected to the strike plate which transfers the impact force to the pavement surface. A series of geophones that are lowered on the pavement surface are used to measure the resulting deflection profile due to the impact force. The onboard geophones were not used for this research and a separate array of accelerometers was installed on the bridges to measure the global vibration responses of each structure due to the dynamic impact force.

A measurement of the dynamic impact force generated at each input location by the FWD device was required in order to develop the frequency response functions (FRFs) during MRIT testing of each bridge. The FWD's onboard instrumentation was not suitable for such measurements due to synchronization requirements with the external accelerometer array, and a dedicated dynamic force transducer was used for this purpose. This represented a significant challenge for the research program. Prior experience with FWD devices had shown that multiple impacts are produced during operation of the FWD due to rebound of the drop weights. Since multiple impacts are not desirable in MRIT applications, the development of the device used to measure the impact forces produced by the FWD needed to minimize the potential for rebound (and multiple impacts) of the drop weights. A further constraint to this design was that the FWD device itself could not be physically modified to achieve this objective. As a result, a dynamic force plate design was developed that incorporated viscoelastic absorbers, also referred to as "bumpers," in an attempt to minimize the potential for multiple impacts from rebound of the drop weights during the FWD operation.

4.7   BUMPER SYSTEM USED FOR TESTING

Various methods for reducing of the potential for multiple impacts due to rebound of the FWD drop weight were considered prior to the implementation of the field testing program. Given that the FWD could not be internally or permanently modified to meet this objective, the two primary approaches considered included the use of pressurized gas type shock absorbers and the use of calibrated rubber shock absorbers (bumpers) that could be implemented in the design of the external force plate that would be used to measure the dynamic impact force produced by the FWD device. The pressurized gas type shock absorbers were subsequently ruled out as an option due to their considerable cost and their much larger size relative to the calibrated rubber shock absorber alternative.

A number of calibrated rubber shock absorbers were purchased for evaluation with the FWD device from EFDyn Inc. in Tulsa, Oklahoma. The specific devices investigated are referred to as elastomer bumpers and are normally used in industrial automation applications for absorbing dynamic forces induced by production processes. These devices are relatively inexpensive, small in size, and easy to install. Since the level of the dynamic impact force that would be produced by the FWD device on the two bridges that had very different stiffness characteristics was uncertain, a total three different sizes of elastomer bumpers were purchased for use with the instrumented force plate. The manufacturer specifications for the TecsPak series bumpers that were purchased are given in Table 4.1.

A basic force plate design that incorporated the different sizes of elastomer bumpers was developed for the field testing program. Separate force plates were constructed for each of the three different models of elastomer bumpers. Each force plate consisted of two 12 in. x 12 in. x

¾ in. thick aluminum plates. A Model 200C50 Dynamic Impact Force sensor from PCB Piezotronics Inc. with a 50,000 lbf force capacity was placed at the center of the bottom aluminum plate. The bumpers were placed at the four corners of the bottom aluminum plate. The second aluminum plate was installed on top of the bumpers. The basic idea was that the force plate would be centered under the circular loading plate of the FWD device on top of the bridge deck. As the FWD load plate was loaded by the drop weights, the bumpers would deform allowing the dynamic force to be transferred through the force sensor and into the bridge deck. It was hypothesized that the deformation of the elastomer bumpers would enable the full dynamic impact force to be transferred through the force sensor while also absorbing some of the impact force and reducing the potential for rebound of the drop weights and the corresponding multiple impacts that would result. Representative photographs of the force plate assemblies developed for use with the FWD device are shown in Figure 4.7 through Figure 4.8. It should be noted that although the initial configuration of each force plate utilized four elastomer bumpers located at the corners of the plate, provisions were also incorporated into the design of each plate to permit a tripod configuration of the bumpers around the central force transducer. This was done to allow the vertical stiffness of the force plate to be reduced if warranted during the actual field testing with the FWD device.

Table 4.1: TecsPak Bumper Specifications

Specification	GBA-107S	GBA-113S	GBA-119S
Peak Dynamic Force	1300 LBS	3000 LBS	5300 LBS
Rated Energy Capacity	550 IN-LBS	1700 IN-LBS	5000 IN-LBS
Free Height	1.77	2.58	3.62
Solid Height	0.86	1.25	1.78

Figure 4.7: Bottom of force plate assembly with TecsPak GBA 119S bumpers at corners (impact force sensor not shown)

Photo taken by Jeremy Rawn, Fall 2010 Engineering Research Center

Figure 4.8:Bottom of force plate assembly with TecsPak GBA 113S bumpers (corners) and Model 200C50 impact force sensor (center).

Photo taken by Jeremy Rawn, Fall 2010 Engineering Research Center

Figure 4.9: Bottom of force plate assembly with TecsPak GBA 107S bumpers (corners) and Model 200C50 impact force sensor (center).
Photo taken by Jeremy Rawn, Fall 2010 Engineering Research Center

Figure 4.10:Force plate assembly (TecsPak GBA 107s bumpers) with top aluminum plate installed.
Photo taken by Jeremy Rawn, Fall 2010 Engineering Research Center

4.8   HARTBARGER BRIDGE INSTRUMENTATION PLAN

The instrumentation plan devised for the Hartbarger bridge included a total of 24 uniaxial accelerometers to measure the vertical vibrations of the bridge induced by the dynamic impact forces. A total of 16 Model 393C accelerometers from PCB Piezotronics, Inc. were installed on the underside of the top flanges of the 4 longitudinal beams using magnets. The remaining 8 accelerometers used for the bridge were Model 393B05 accelerometers also from PCB Piezotronics. The 393B05 accelerometers have a higher sensitivity but smaller input range than the 393C accelerometers, and as a result, these accelerometers were installed at the ends of each longitudinal beam directly above the bearings. The vertical beam vibrations at the bearing locations were expected to be essentially zero, and these sensors were deployed to verify this assumption during the impact testing. The nominal manufacturer specifications for each type of accelerometer are summarized in. The layout of the accelerometers on the bridge is shown schematically in Figure 4.11.
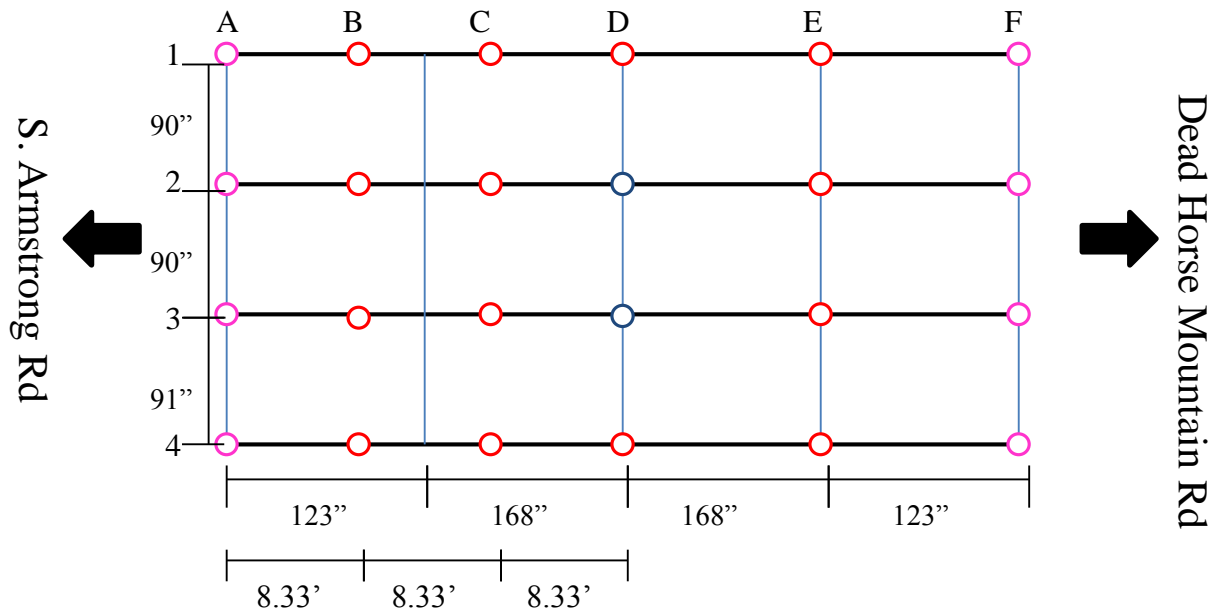
Figure 4.11: Accelerometer locations on the Hartbarger bridge

The accelerometers were all connected to a National Instruments PXI data acquisition mainframe (DAQ) with National Instruments Model 4472B dynamic input modules that was located underneath the bridge. The accelerometers were connected to the DAQ system via 50 Ohm coaxial cables that were routed to each sensor location on the underside of the bridge. The bridge was pre-wired for testing before the impact testing of the bridge, and the connectivity and proper functioning of each accelerometer was validated just before the impact testing was performed.

Since the impact forces were to be applied to the bridge through the top surface of the concrete deck, the corresponding locations of the accelerometers on the longitudinal beams were also marked with chalk marks made on the deck surface. This ensured that all impact locations coincided with accelerometer locations.

Table 4.2:Accelerometer Specifications Nominal Specification

	PCB 393 B05	PCB 393C
Sensitivity	10 V/g	1000 mV/g
Measurement Range	0.5 g pk	2.5 g pk
Frequency Range(+- 5%)	0.7 to 450 Hz	.025 to 800Hz
Broadband Resolution (1 to 10000 Hz)	0.000004 g rms	0.0001 g rms

4.9   IMPACT TESTING OF THE HARTBARGER BRIDGE

The MRIT testing of the Hartbarger Bridge was performed on November 15, 2010. The bridge was tested on the same day using the FWD and a portable instrumented sledge hammer as impact devices. The FWD used for the testing was provided by the Arkansas Highway and Transportation Department (AHTD) and arrived at the bridge for testing at 10:00 a.m. Personnel from the AHTD operated the FWD and provided traffic control at the site during the execution of the field tests. The bridge was completely closed to traffic during each impact of the structure, and subsequently reopened after the measurements at each input location on the bridge were completed. November 15th was also the first day that the FWD was available for evaluating how the testing procedure would be implemented with the bridge.

Before the actual impact testing of the bridge was started, several trial impacts were performed using the FWD to test the performance of the force plates with the elastomer bumpers. Several impacts were performed using the FWD and the force plate without the load cell connected to inspect how the elastomer bumpers behaved under actual loading. The first force plate evaluated had the smallest sized bumpers. All four of the bumpers were attached to the plate and increasing loads of 6,000, 9,000, and 12,000 pounds were dropped by the FWD. It was not possible to visually determine if the bumpers were deflecting adequately under these loads to fully engage the force transducer. The force transducer was then connected to the DAQ system to

measure the generated impact forces. The same three load steps were again applied to the force plate except they occurred in reverse order. Using the four small bumpers, the load cell did not draw contact. The force plate configuration tested used only three of the small bumpers in a tripod arrangement. A double impact was recorded by the force plate for each of the three load steps.

A third trial was performed using the force plate with the medium sized bumpers. In this trial, the force sensor was place on top of the aluminum plate and the bumpers were in contact with the deck surface. The other aluminum plate was placed on top of the force sensor since direct impacts FWD load plate to the force transducer were not permitted by the AHTD. A full 17,000 lb load was manually dropped and the result was a multiple impact response.

An error was noticed in the definition of the sensitivity of the force sensor in the DAQ software during the first force plate trial was detected and corrected. The original force plate configuration with the four small bumpers was evaluated again. The configuration of the force plate was slightly modified from the original configuration for this test based on the observations with the other force plate trials. In this trial, the force sensor was attached to the underside of the aluminum plate that was in direct contact with the FWD strike plate. The first FWD impact used 6,000 lb force, and a double impact was registered. Next, a 9,000 lb force was dropped onto the load cell. The first impact using a 9,000 lbf of weights was successful and did not register a double impact. A second impact was attempted using the same parameters and a double impact was recorded by the force sensor. It was observed that the plate on which the force sensor was attached had moved off center after the first impact and caused the double impact to be recorded. The plate was moved back to its original position of being square with the base plate and 9,000 lbf was dropped again. From this drop, another good hit was recorded. Having successfully

recorded a series of good impacts with this setup, the impact testing of the bridge with the FWD was initiated. The force plate configuration used the 4 smallest bumpers and the force transducer was located on the underside of the top aluminum plate of the assembly. The FWD impacts were produced using 9,000 lbf of drop weights.

Following the initial debugging of the experimental setup for the FWD device, impact testing of the bridge was initiated. Some researchers have recommended that five impacts be performed at each input location for MRIT of steel stringer bridges (Lennett et al, 1997) however only three impacts were recorded at each input location with the FWD to minimize the disruption to traffic on the bridge. Eight impact (input) locations on the bridge were selected for use with the FWD device. These locations were designated as A1, B1, B2, C2, D2, D3, E3, and F4 as indicated in Figure 4.12. Most of the input locations were selected on the basis of adequately exciting the desired vibration modes of the structure. Two support locations were also selected as input locations to be able to activate any mechanisms in the bearings and substructure that might influence the global dynamic response of the superstructure. The FWD impact testing began at location A1 would progress in increasing alphabetical and numbered order through the remaining input locations. The deck geometry, the presence of the concrete barriers along the edges of the deck, and the dimensions of the FWD would not permit the impact locations to be directly above the output (accelerometer) locations on the exterior beam lines. The FWD was moved as close as possible to the curb line of the bridge for these points, but a small offset in the distance between the input and output locations was unavoidable.
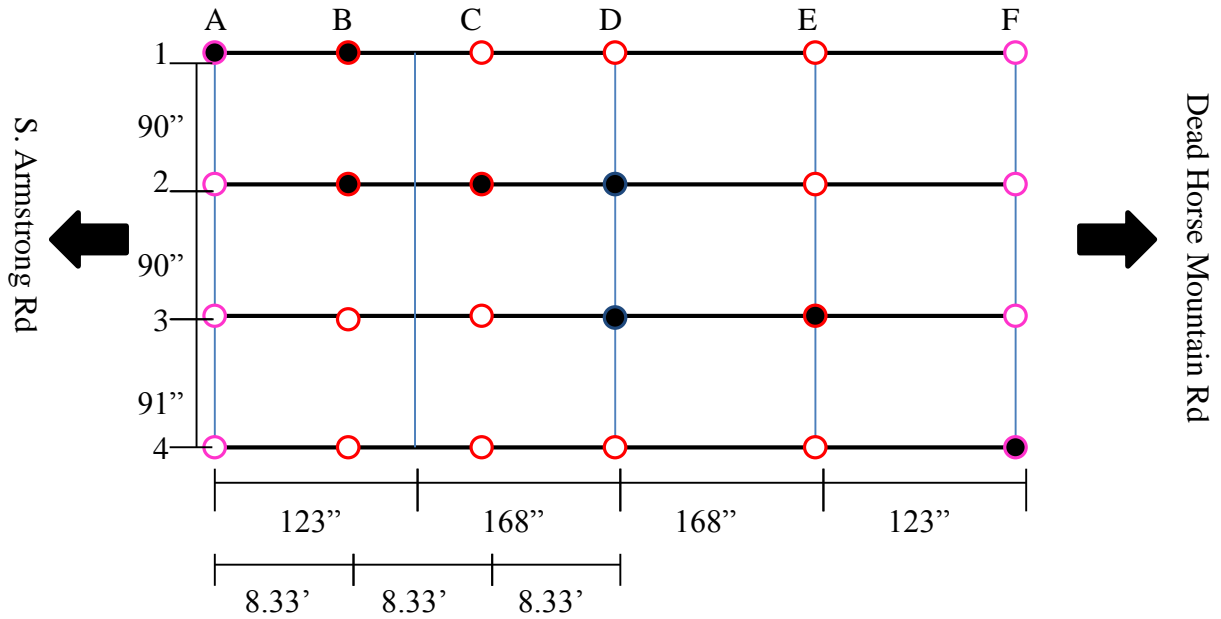
Figure 4.12: Pre-Determined Impact Locations on the Hancil "Tiny" Hartbarger Bridge

The force records obtained from location A1 were inspected after all hits at this point had been completed. There appeared to be a double impact in the measured forces. The rebound and secondary impact that resulted from it occurred in such a short time frame it was not automatically detected and rejected by the SO Analyzer software that was being used for the data collection process. Despite the double impact, the force measurements collected from this input location were among the best that had been obtained using the FWD device and the setup was moved to the next input location. At input location B1, the recorded impact force had no secondary impacts. This would be the only such impulse that would be recorded from the FWD testing. The impacts at locations C2 and D2 produced force measurements with double peaks that were similar to those obtained from input location A1. The test personnel were unable to characterize the reasons for the double hits due to the fast speed of the falling weight during impact testing. The double impact may have occurred because the elastomer bumpers were not able to absorb the initial impact from produced by the initial drop of the weights completely, by

the load cell bouncing against the bottom plate of the load plate assembly, or the mechanics of the force transducer within the force plate. Representative plots of the force versus time measurements that were recorded from input locations A1, B1, C2, and D2 are shown in the Figure 4.13.

Upon completion of the FWD impact testing, the bridge was also tested using a Model 0896D50 portable impulse hammer from PCB Piezotronics Inc. For this testing, all 24 accelerometer locations were subject to impact forces using this hammer. A total of three measurement runs were recorded at each of the 24 output (accelerometer) locations on the bridge. Traffic control was not available after the FWD was removed from the site, so the impulse hammer measurements were taken in between vehicle crossings of the bridge. These were spaced far enough apart for the bridge to be able to complete the testing at all 24 input locations in just about 1.5 hours.
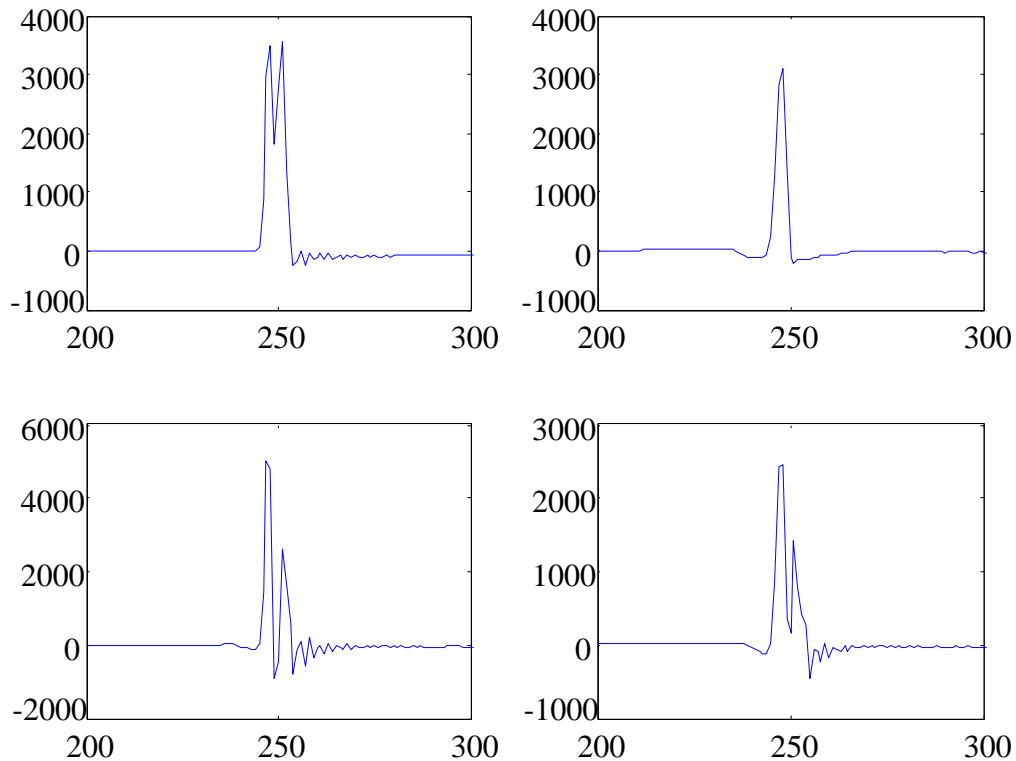
Figure 4.13: Measured impact forces produced by FWD at input locations A1, B1, C2, and D2 (all plots are lbf versus time in seconds).

4.10   IMPACT TESTING OF THE BAPTIST FORD BRIDGE

The Baptist Ford Bridge was tested on November 16th, 2010. The procedure used for testing this bridge was similar to that used for the Hartbarger Bridge. Impact testing was first completed using the FWD device and then by a portable impact hammer. An issue that needed to be resolved from previous day of testing was the force sensor that stopped functioning during the FWD testing. The force transducer was evaluated in the laboratory on the night before to determine if it could be used again. The researchers were able to get the force transducer working again, and the FWD testing of the Baptist Ford Bridge was possible the next day.

The weather on the morning of the test day was rainy, so setup of the equipment took longer than what was expected. The heavier rain in the morning became a light drizzle around 11:00 a.m. After 11:00 a.m., the remainder of the day was sunny. Testing of the Baptist Ford Bridge did not have the traffic complications experienced the previous day at the Hartbarger Bridge because the normal traffic usage of this bridge is very low. The Baptist Ford Bridge is located just upstream of the main north-south highway in the area and any traffic crossing the bridge must go out of their way to do so. Such traffic was simply kept on the main route during the field testing.

The cables for the accelerometers to be installed on the Baptist Ford Bridge during the impact testing were installed the week before the test to permit the test setup to be performed more quickly. A total of 25 accelerometers were used to record the vertical vibration responses of the bridge due to each impact force. The accelerometers were placed on the bottom chords of the trusses at the truss joint locations. Additional accelerometers were installed on the underside of the deck at the center of the transverse floodbeams that spanned between the two trusses. Due to a limited number of sensors, the north half of the span had a higher spatial resolution than the southern half. Still, enough sensors were used to acquire accurate mode shapes. The locations of the accelerometers on the bridge structure and the impact locations used are shown in Figure 4.14 and Figure 4.15. All of the accelerometers were installed on the steel members of the truss bridge using magnets.

The cables from each accelerometer were routed to the National Instruments DAQ, which was located on the first span of the bridge. The proper operation of each accelerometer was verified after all of the sensors were connected to the DAQ. The SO analyzer software from

M+P International was used to acquire the measurements from the force sensor and the accelerometers during the impact testing.

A series of initial impact trials was performed with the FWD device and the force plate assemblies to identify the optimal testing configuration for the bridge. The force plate with the four smallest elastomer bumpers and a 9,000 lbf drop weight was tried initially as this approach had shown some success during the previous day of testing. This setup proved unsuccessful for the Baptist Ford Bridge. The drop weight for the FWD was subsequently increased to a 12,000 lbf and again no impact was detected. To resolve this issue, a three bumper configuration was attempted. The three bumper system with a 12,000 lbf drop weight yielded a successful impact record and this setup was selected for the testing. The impact was successful in that it was able to trigger the data acquisition system; however, the time record of the measured impact force was very similar to the impact forces recorded from the Hartbarger Bridge and appeared to still contain double impacts. In an effort to resolve this issue, a number of other modifications to the force plate assembly were attempted to try to minimize the rebound of the FWD drop weight and the resulting occurrence of double impacts.

One modification attempted with the force plate assembly was to use a stiff modeling class between the top and bottom plates of the assembly instead of the elastomer bumpers. The impacts recorded using the clay instead of the bumpers led to multiple impact records that could not be used in post processing. A number of different placements of the clay were also attempted with the force plate but none of these proved successful and the force plate with only three elastomer bumpers was utilized for the FWD impact testing.

As was the case for the FWD impact forces measured from the other bridge, a quick double impact could also be observed in the force time records measured for this bridge. The

record of the actual impacts would remain constant so that there was consistency in the test. Impact locations were predetermined for the bridge based on reciprocity and locations that would excite certain mode shapes. Nine locations were selected for impacts including: C1, E2, E3, F2, G1, G2, H1, H2, and J3. The locations of these points are shown on Figure 4.14. Because of a small curb that ran along either side of the bridge deck, the FWD was unable to reach the edges of the bridge. To counter this issue, the sensors were place further in on the transverse girders. Impacts were performed at the nine picked locations. The time data from the impacts contained the same double peak at all of the impacted locations. In post analysis, which will be discussed in the conclusions, the time data would be altered to match that of the true impact felt on the bridge from the FWD. Testing of the bridge lasted for 1 hour from the first impact of the FWD until the last impact.
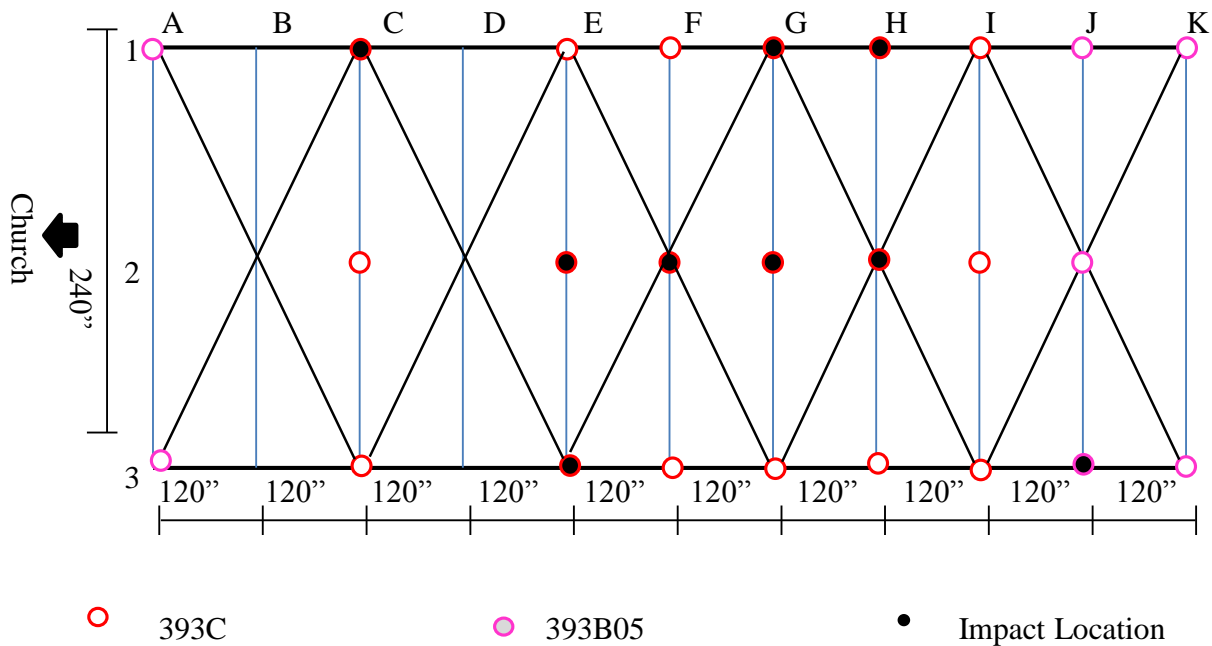
Figure 4.14: FWD Impact Locations for the Baptist Ford Bridge (Plan View of Deck)
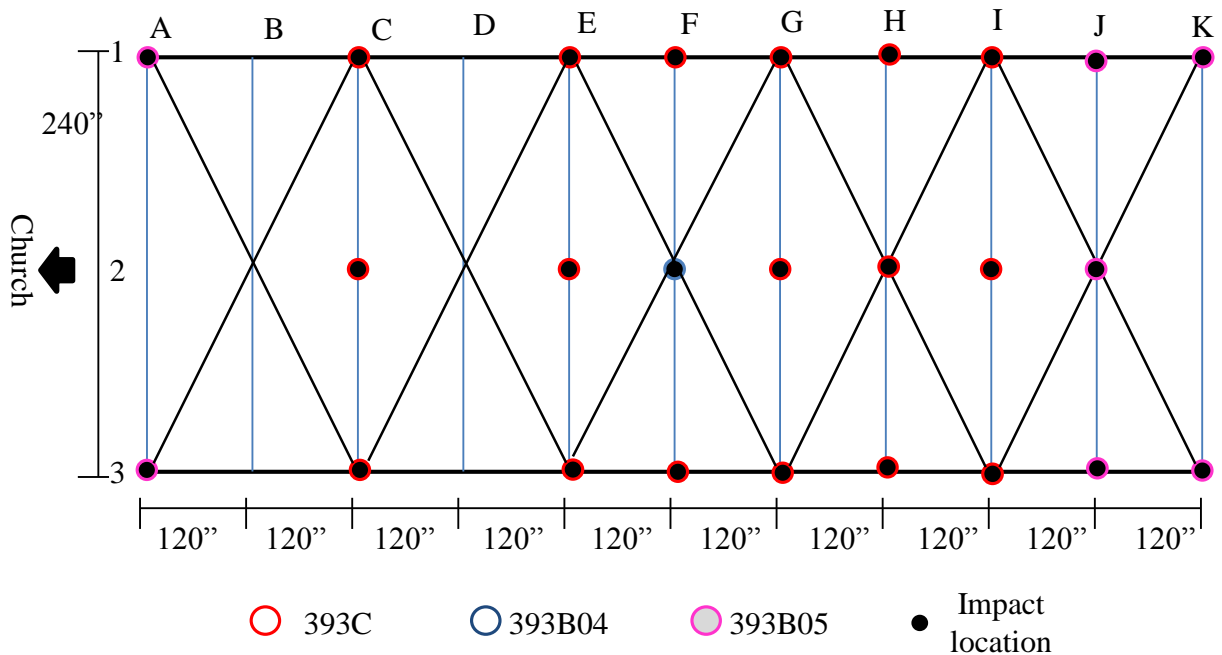
Figure 4.15: Portable Hammer Impact Locations for the Baptist Ford Bridge
(Plan View of Deck)

The hammer testing took place on the bridge after the completion of the FWD testing. Again, the hammer testing is important so that there is a method of comparison for the FWD data. Using the hammer, the bridge was impacted at every location that an accelerometer was located, 25 locations total. The impact locations from the hammer are shown on Figure 4.15. A three impact average was used at each location to stay consistent with the FWD.

4.11   RESULTS

Post-processing of the measured data was completed using two different methods, the complex mode indicator function (CMIF) and multivariate mode indicator functions (MvMIF). The MvMIF, "indicates the existence of real normal modes, CMIF indicates the existence of real

normal or complex modes and the relative magnitude of each mode. Furthermore, MvMIF yields a set of force patterns that can best excite the real normal mode, while CMIF yields the corresponding mode shape and modal participation vector" (Allemang, 1999). The MvMIF is the modal parameter identification algorithm that is used by the SO Analyzer software from M+P International. The SO Analyzer software can also identify natural frequencies, mode shapes, and damping ratios from the measurement data using a finite difference estimation algorithm or a quadrature estimation algorithm. The data is collected from the FRF's which are calculated by the H1 method. Because of its quick usability to locate natural frequencies and mode shapes in the single degree of freedom estimator, M+P was used to get the initial modes. This process was used while processing both the FWD data and the data collected using the impact hammer.

4.11.1 Hartbarger Bridge

The data acquired from the portable impact hammer on this bridge were analyzed first. Using the modal parameter identification methods described above, the first seven vertical modes for the bridge were located using the finite difference estimation. These results (natural frequencies and mode shapes) are shown in Figure 4.16.

1st bending 5.845 Hz   1st torsion 7.712 Hz   1st butterfly 12.50 Hz

2nd bending 21.85 Hz   2nd torsion 22.77 Hz   2nd butterfly 26.04 Hz

3rd bending 40.94 Hz
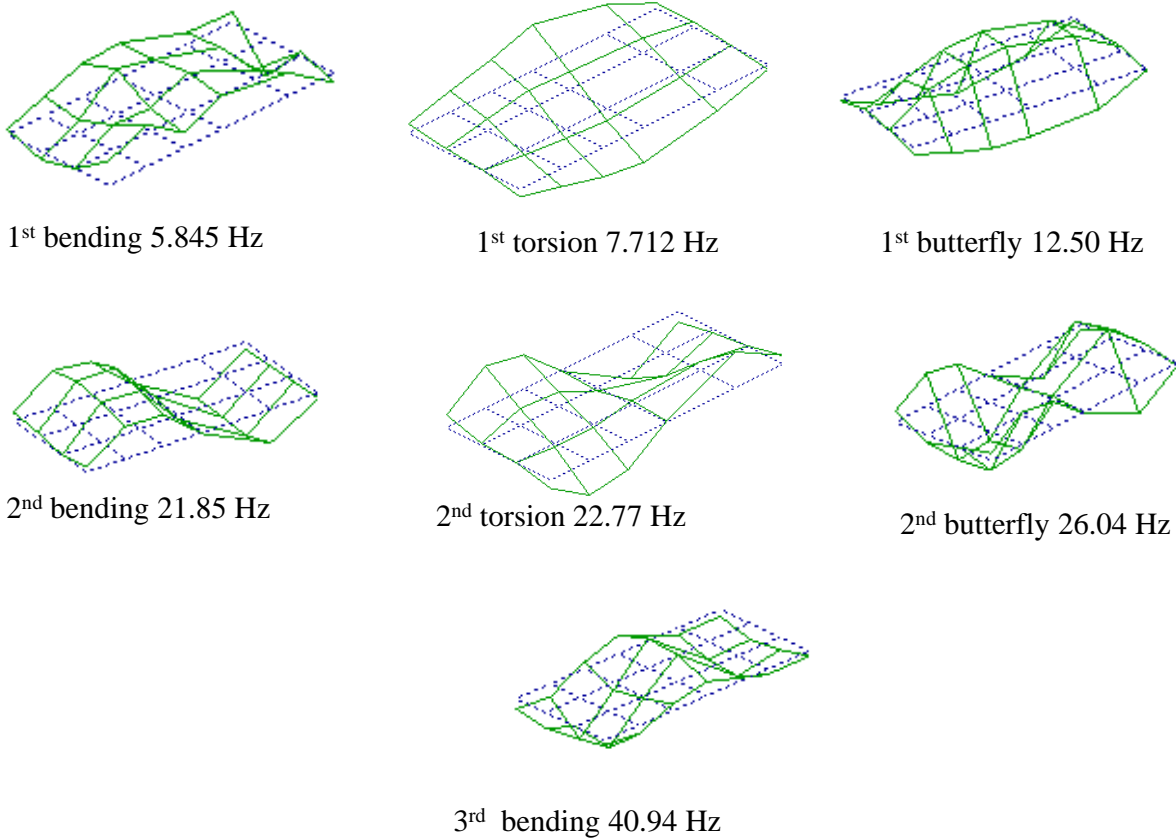
Figure 4.16: Natural frequencies and mode shapes identified for from the portable impact
hammer measurements using a finite difference estimation algorithm.

The natural frequencies and mode shapes were also identified using the CMIF algorithm to provide a second basis for comparison of the modal identification parameters. The CMIF algorithm was coded in MATLAB. The natural frequencies mode shapes and found using the CMIF algorithm correlate well to those identified using the finite difference estimation. A total of 7 modes were identified and are displayed in Figure 4.17. The natural frequencies of the mode shapes show good correlation between the two methods of analysis used. The differences between the two are listed in Table 4.3.

1st bending 6.1440 Hz   1st torsion 7.021 Hz   1st butterfly 12.5074 Hz

2nd bending 21.7234 Hz   2nd torsion 22.7474 Hz   2nd butterfly 26.1120 Hz
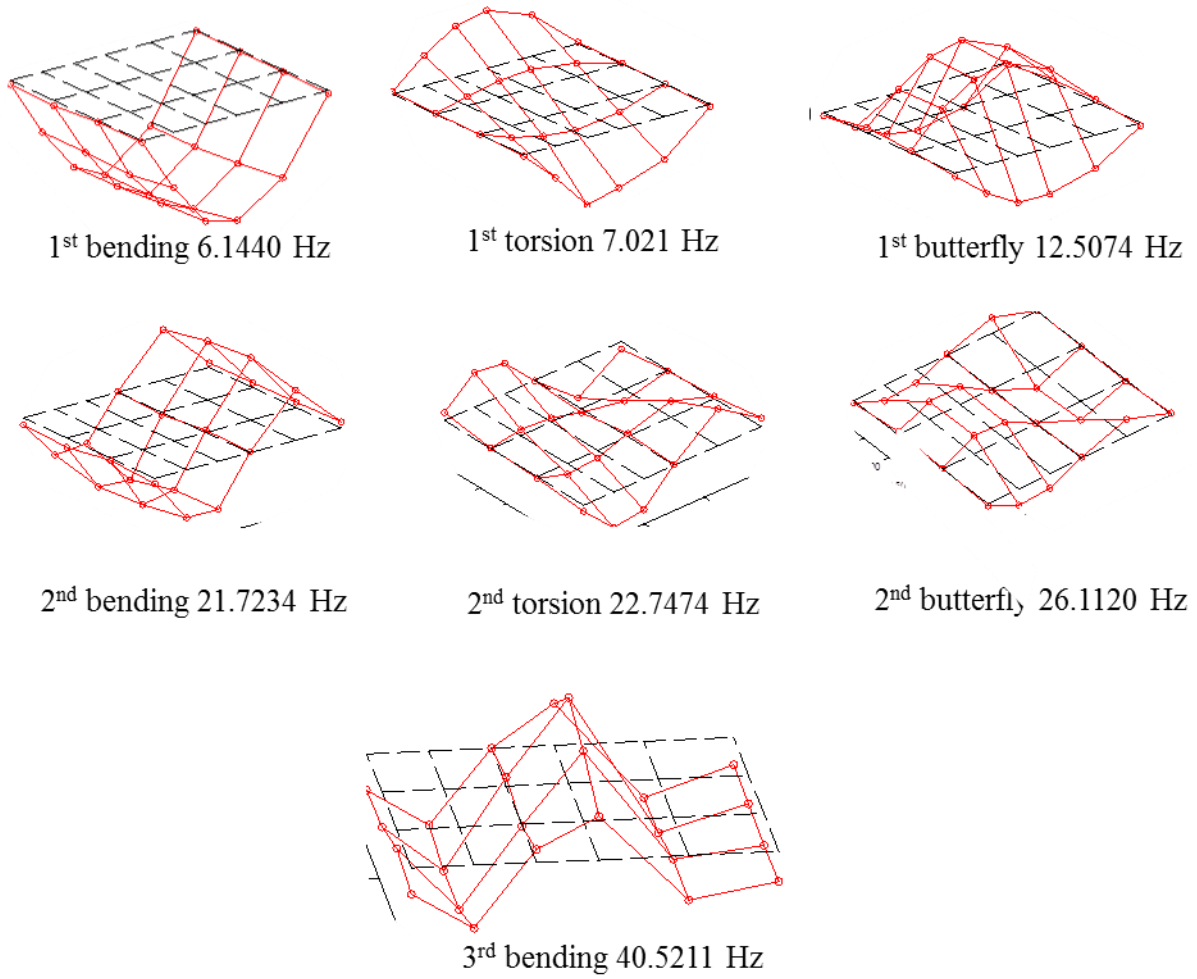
3rd bending 40.5211 Hz

Figure 4.17: Natural Frequencies and mode shapes identified from the portable impact hammer measurements by CMIF algorithm

Table 4.3: Comparison Between the Natural Frequencies of the Selected Modes

| | CMIF | Finite Difference | |
Mode	Hartbarger Hammer Frequency (Hz)	Hartbarger Hammer Frequency (Hz)	% difference
1st bending	6.144	5.845	4.87%
1st torsion	7.021	7.087	-0.94%
1st butterfly	12.5074	12.49	0.14%
2nd bending	21.7234	21.85	-0.58%
2nd torsion	22.7474	22.66	0.38%
2nd butterfly	26.112	26.04	0.28%
3rd bending	40.5211	40.94	-1.03%

One observation that may be made from this data processing is that the 1st bending mode of the structure was not identified as clearly from the finite difference approach as it was using the CMIF algorithm. As shown in Table 4.3, the natural frequency of the 1st bending mode found from the finite difference identification was most different (almost 5%) of any of the frequencies identified using the 2 algorithms. The coherence plot generated from the input and output measurements between 0 Hz and 8 Hz also dips below 1.0, indicating that the measured vibration response is not exclusively the result of the measured input in that frequency band. This uncertainty could be the reason for the poor quality of the mode shape identified for the first bending mode shown in Figure 4.16. The CMIF algorithm had no difficulty dealing with this uncertainty and the mode shape obtained by this approach for the first bending mode (Figure 4.17) appears quite reasonable.

Having identified the natural frequencies and mode shapes of the bridge from the portable impact hammer measurements, the vibration measurements collected using the FWD impacts were evaluated next. The results obtained from the measurements obtained with the

FWD impacts were not as clear in comparison to the results from the portable impact hammer. There are a number of possible reasons for this result.

The issues that arose with operating the FWD and the modifications to the force plate that were encountered during the impact testing of this bridge are likely the main cause of these differences. All of the accelerometer locations were impacted using the portable impact hammer whereas only four of these locations could be tested using the FWD device. The vibration measurements recorded from the FWD also showed much less consistency between the input and output measurements than what was obtained from the portable hammer as the impact source. An examination of the time history plots of the measured vibrations indicated that only the measured impact and response from input location B1 appeared reasonable. The impact force measurements recorded from the FWD at locations C2 and D2 were not very clean. Although the measured vibrations outputs from the bridge from these locations were mostly clear data, the coherence between the input and output measurements were not as good. An analysis of the measurements also revealed that the accelerometer at location G3 exceeded the input range for the FWD impact at location C2. The accelerometers at G2, G3 and G4 all exceeded their permissible measurement range for the FWD impact at location D2.

Because of the issues mentioned above, the finite difference algorithm in the SO Analyzer software was unable to identify reasonable natural frequencies and mode shapes using the FWD impact data. As a result, the FWD impact data was only analyzed using the CMIF algorithm that was implemented in MATLAB. The CMIF analysis of this data identified a total of six natural frequencies and their mode shapes. A comparison of the six natural frequencies identified by the CMIF algorithm for the portable impact hammer and the FWD device is provided in Table 4.4. These results are relatively consistent between the two approaches. It

should also be noted that the data acquired from the portable impact hammer had a significantly better spatial resolution (in terms of the distribution of the impact forces on the bridge) than did the FWD data

Table 4.4: Natural frequencies identified by CMIF from FWD and portable hammer.

Mode	Hartbarger FWD Frequency (Hz)	Hartbarger Hammer Frequency (Hz)	% difference
1st bending	6	6.144	-2.40%
1st torsion	7	7.021	-0.30%
1st butterfly	12.5	12.5074	-0.06%
2nd bending	21.75	21.7234	0.12%
2nd torsion	-	22.7474	NA
2nd butterfly	26.1875	26.112	0.29%
3rd bending	40.8125	40.5211	0.71%

After the natural frequencies and mode shapes for the FWD impact data were identified, the subsequent analysis of this data considered three different approaches for dealing with the double impacts present in the force measurements. These approaches included (1) keeping the data as is for subsequent analysis, (2) modifying the measured force record to smooth/remove the double impact, and (3) and using the second approach but also scaling the measured force to match the known drop weight used with the FWD. Ideally, more than six mode shapes would be desirable for the subsequent analyses; however, this number was all that could be identified from the FWD impacts on this bridge.

The locations of the natural frequencies and the mode shapes associated with them did not change as the peaks were altered as described above. The frequencies of the peaks identified in the in the CMIF plot did show some variation from the frequencies located using unaltered CMIF, but it was slight. Because the peaks in the CMIF plot are used locate the natural

frequencies of the structure, it is preferable that the peaks in the CMIF plot can be clearly identified. Poor measurement data can lead to spurious and noise related peaks, and these peaks may be located very close to the peaks associated with the normal modes of vibration of the system. This will add uncertainty to the modal parameter identification results. Figure 4.18 through illustrate the nature of the effects of the using the unmodified and the modified force measurement data from the FWD impacts on the resulting CMIF plots generated from the input and output measurements. Figure 4.21 shows the CMIF plot generated for the bridge using the input from the portable impact hammer with the measured acceleration outputs.
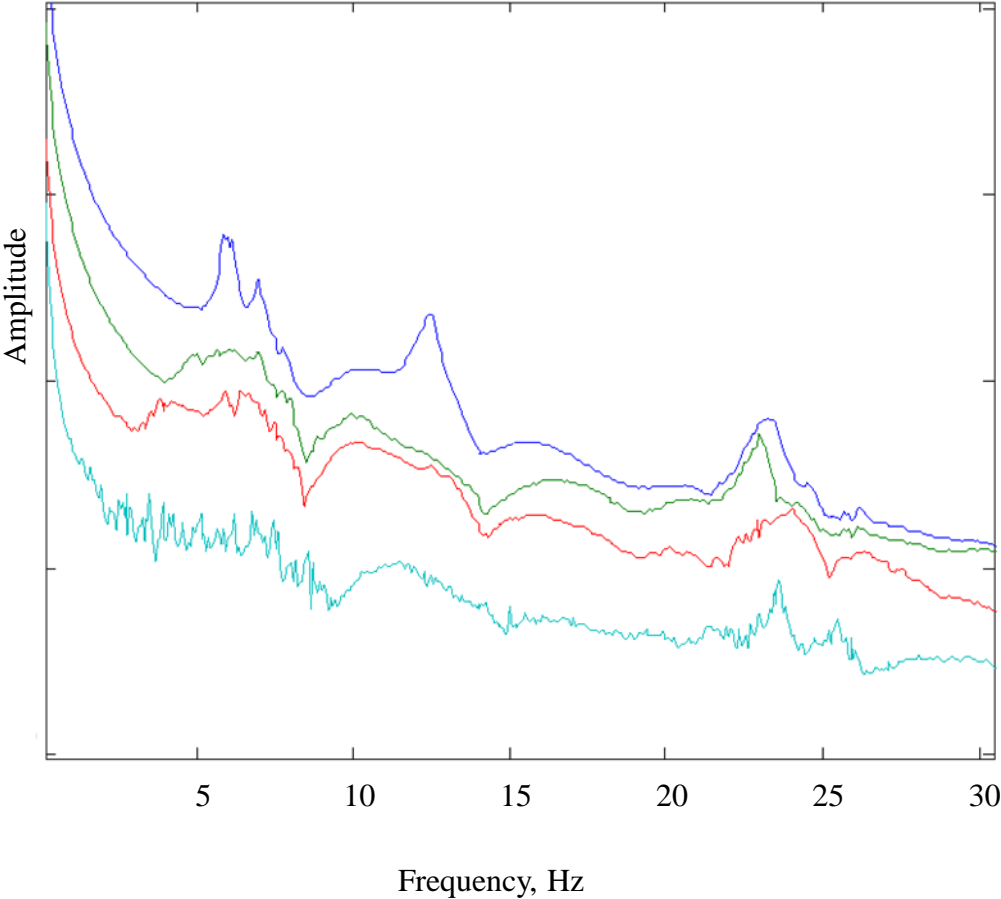
CMIF Plot, Actual Impact

Figure 4.18: CMIF plot for the Hartbarger Bridge using FWD impacts
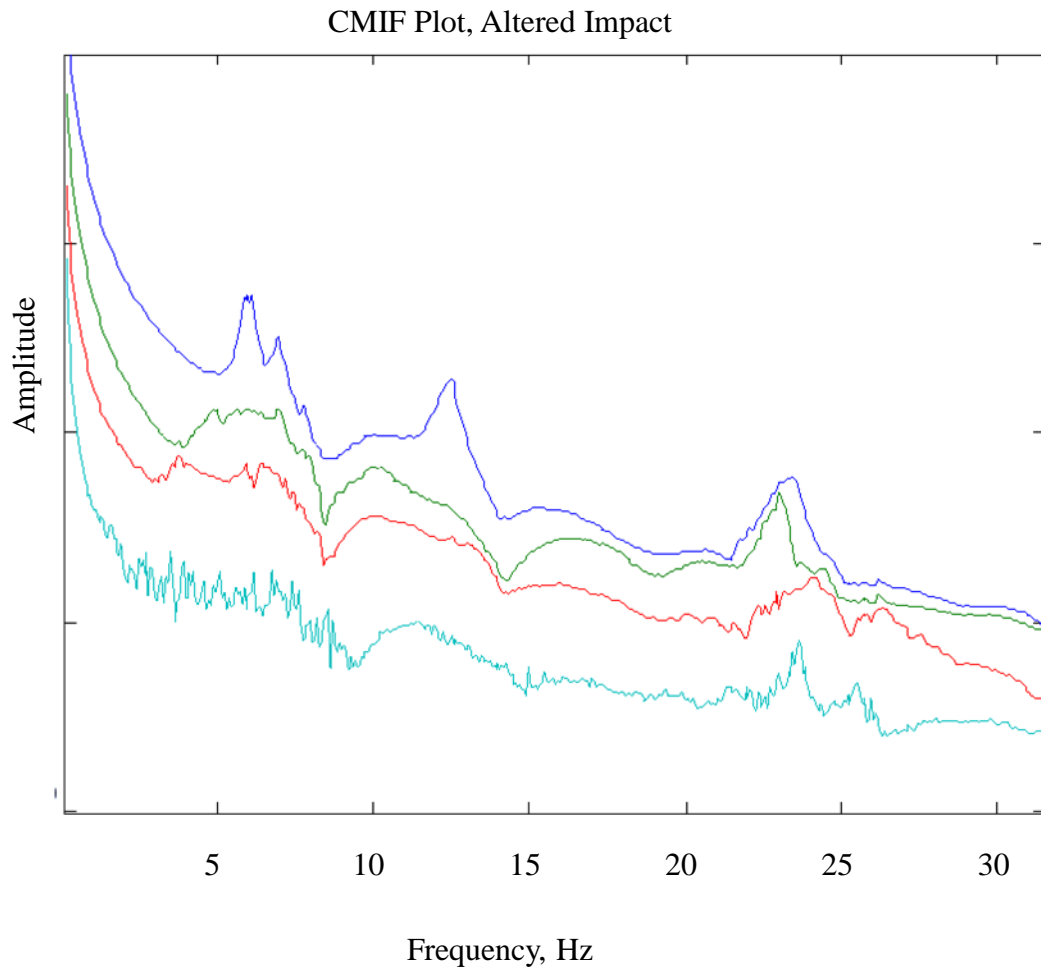
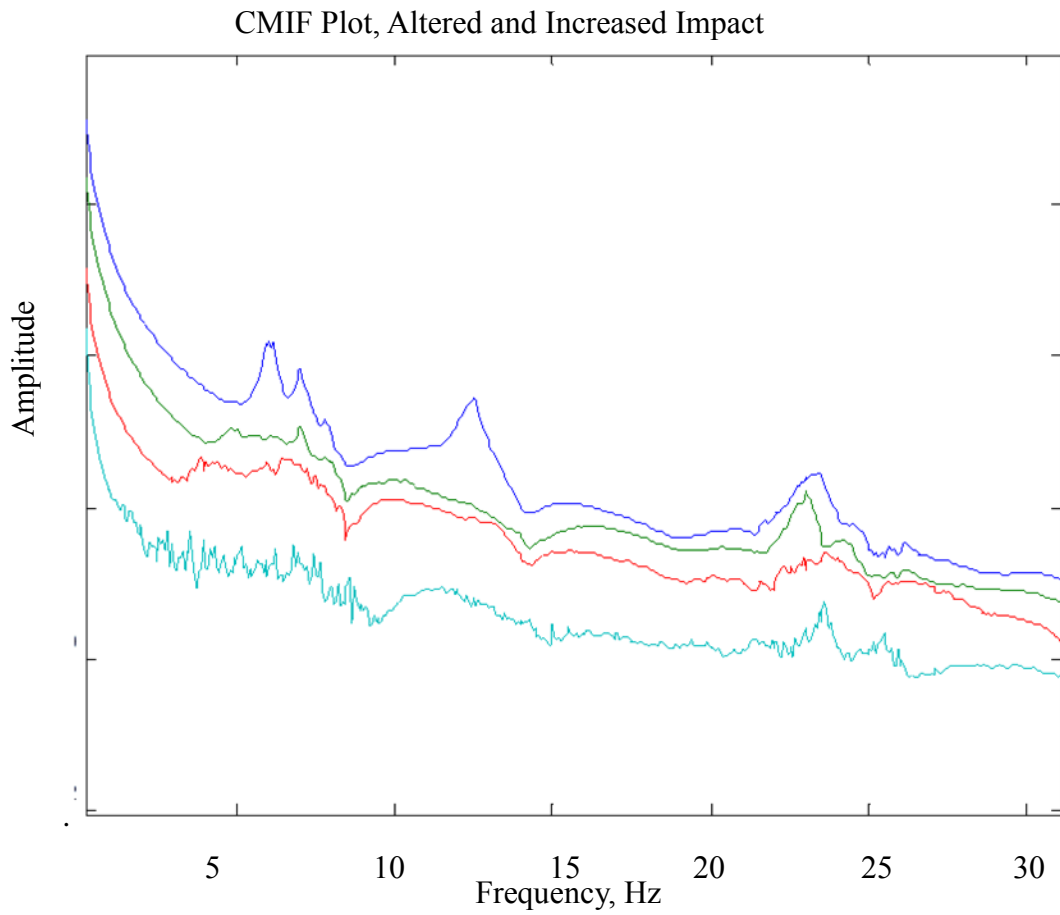Figure 4.19:CMIF for the FWD impact with curve fit to measured force.

Figure 4.20: CMIF plot of the Hartbarger Bridge using the FWD with the impact curve fit and increased to drop weight
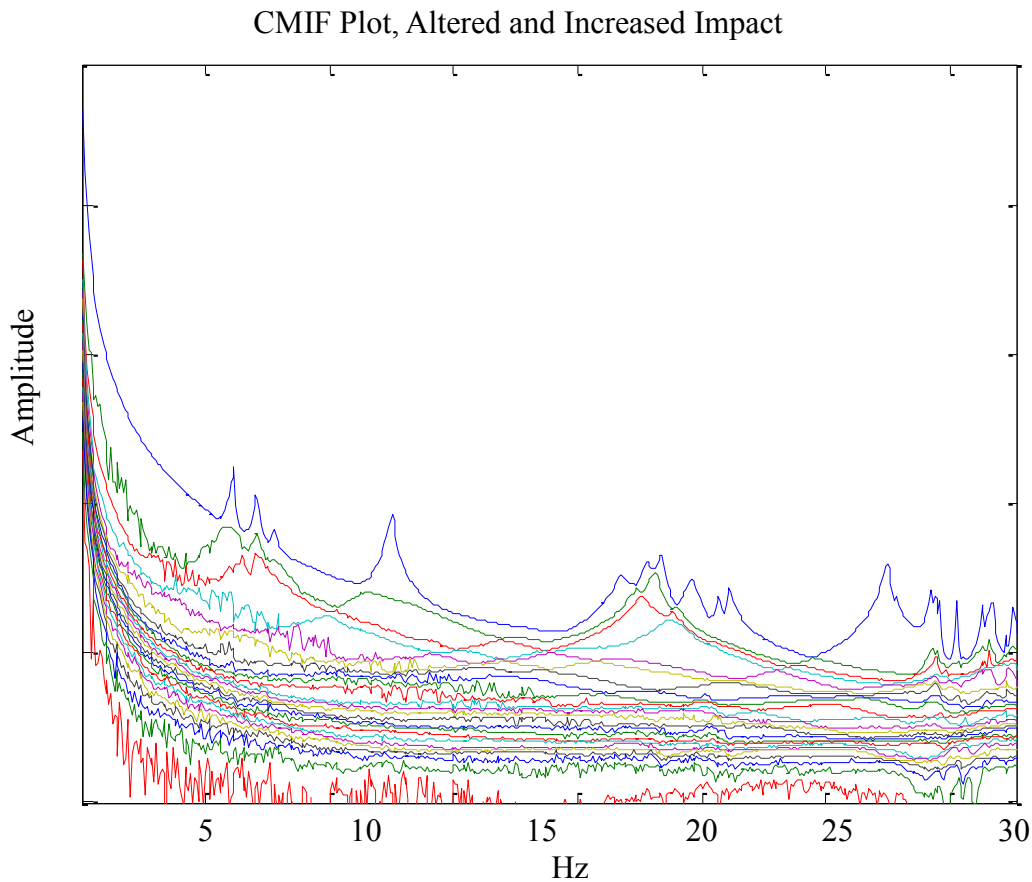
CMIF Plot, Altered and Increased Impact

Figure 4.21: CMIF plot for Hartbarger Bridge using portable impact hammer.

An evaluation of Figure 4.18 through Figure 4.21 reveals that the measurement data from the hammer impacts leads to a CMIF plot that has peaks that are much better defined than for the CMIF plots obtained using the FWD impacts. The peak at 12.5 Hz is dominant in all of the plots, but the peaks around 6 Hz and 23 Hz show a definite discrepancy. The data was processed and analyzed for the DC to 100 Hz frequency band to capture as many modes as possible for the bridge structure. To identify the modal parameters of the structure a peak picking process is used to identify the locations of the natural frequencies. "The peaks detected in the CMIF plot indicate the existence of modes, and the corresponding located frequencies of these peaks give the damped natural frequencies for each mode in the application of the CMIF for traditional modal parameter estimation algorithms" (Shih, 1989). Using the mode shape vectors and the modal

participation vectors associated with the peaks in the CMIF as weighting factors on the FRF, the peaks and the points around the selected peak can be turned into what is called the enhanced Frequency Response Function (eFRF). The eFRF is used to identify the modal parameters necessary for calculating modal flexibility.

Modal flexibility is determined from identified modal parameters including modal A (a parameter used to estimate modal mass), natural frequencies and mode shape vectors. The mode shape vectors and the damped natural frequencies associated with each mode. Modal flexibility is an approximation of the true static flexibility matrix due to truncation from the limited number of modes that can be identified from the experimental data (Catbas F.B., 2006) (Catbas, et al. 2006). "The deflected shape of a girder under virtual uniformly distributed load is termed as 'bridge girder condition indicator (BCGI),'" (Catbas & Aktan, 2002). Essentially, these researchers are stating that by plotting the deflection profiles of the individual beam lines is useful for locating damage or stiffness changes by monitoring if the deflection plots change over time. For the purposes of this research, the results provide a baseline measure of the bridge condition at the time of testing. These results can be compared results from future tests to detect changes in condition due to damage or deterioration.

The modal flexibility matrice for the Hartbarger bridge obtained using the portable impact hammer and the FWD were virtually loaded with a 1 kip load at each degree of freedom and the resulting deflections obtained (BGCI) for each beam line are shown in Figure 4.22 through Figure 4.24. The hammer and FWD impact data were inconsistent for the Hartbarger Bridge, and this inconsistency is reflected in the differences between the resulting displacement profiles.
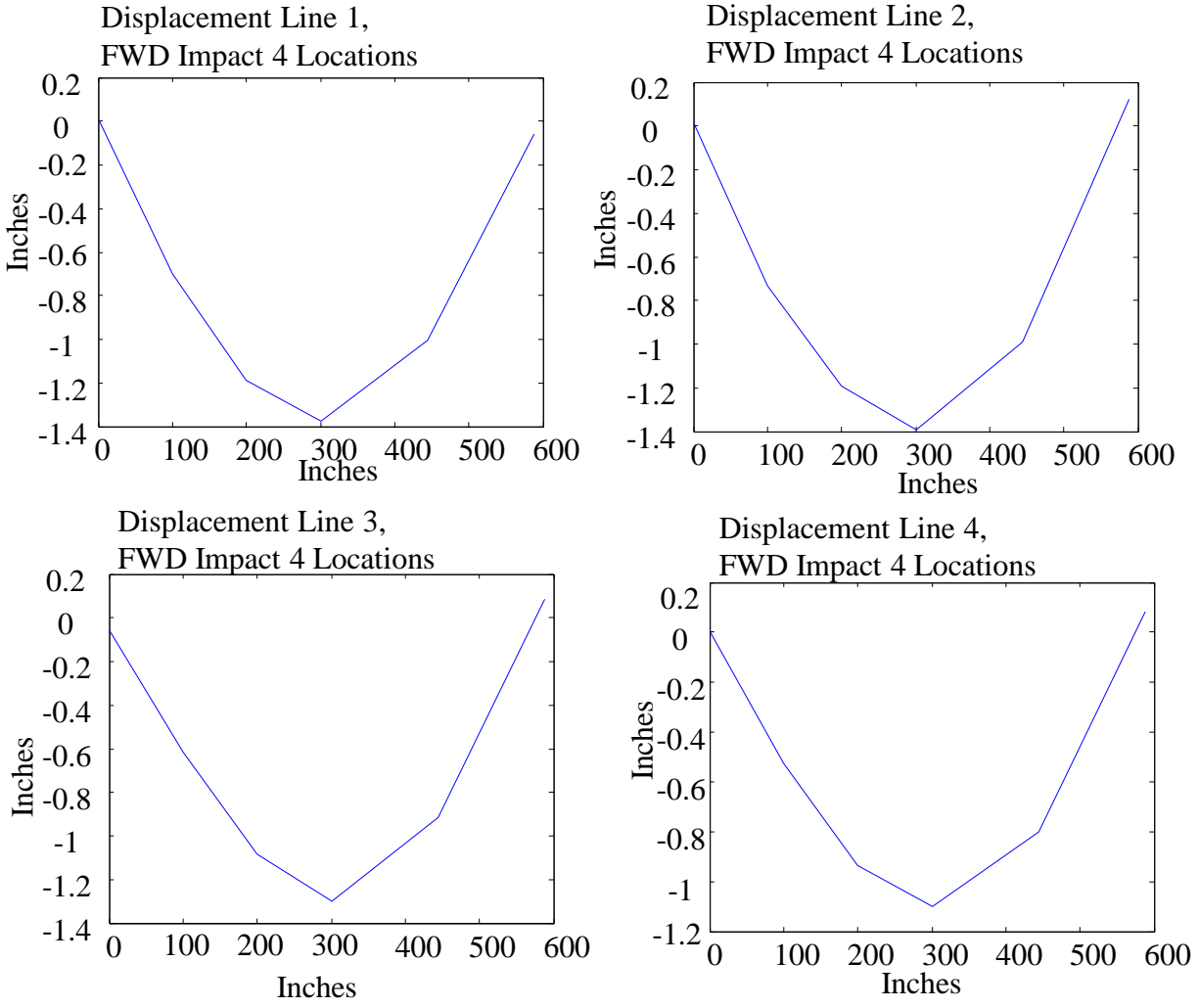
Figure 4.22: Deflection profiles from FWD derived modal flexibility with unaltered impact force measurements.
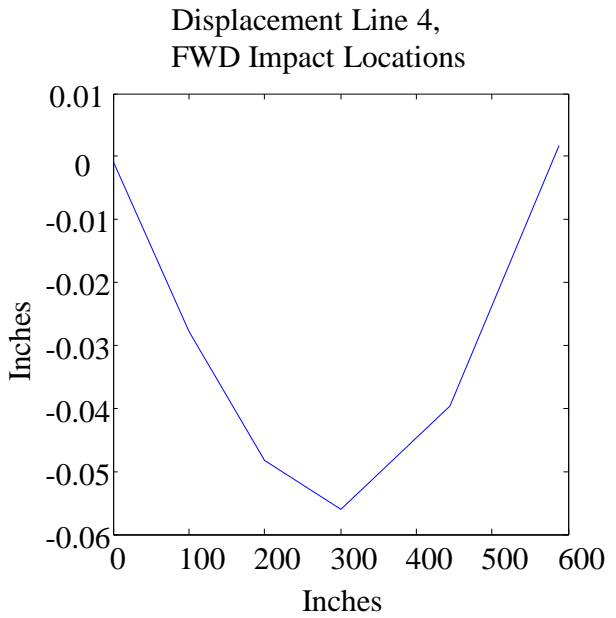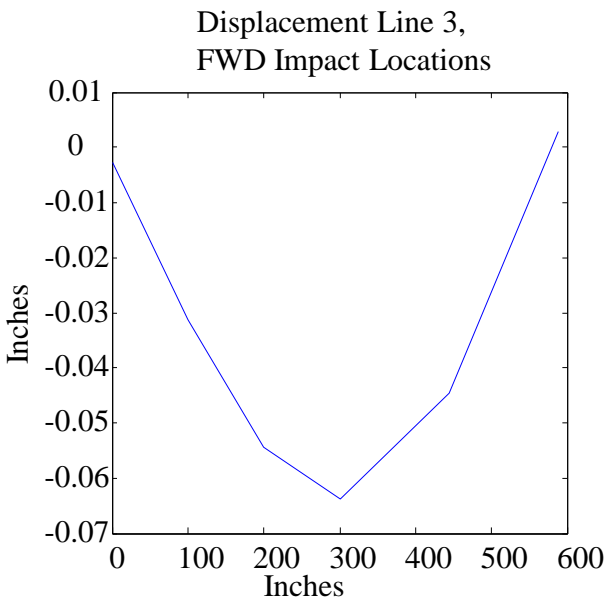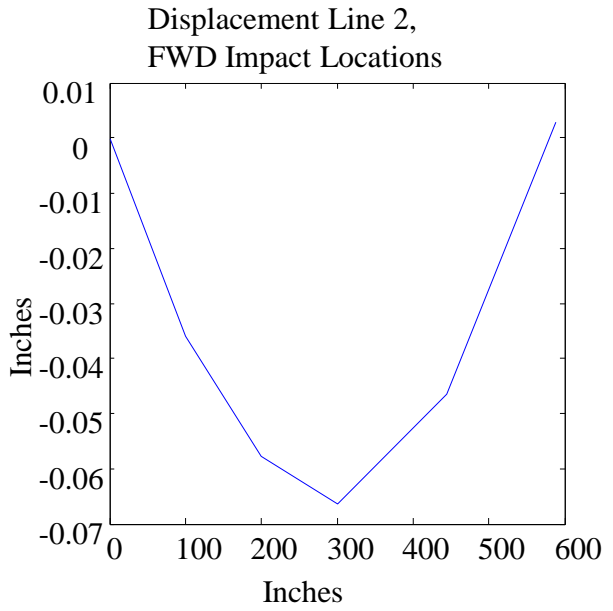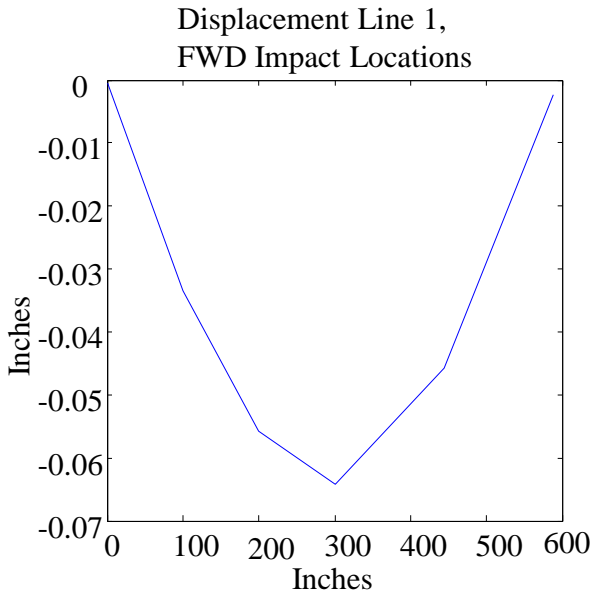
Figure 4.23: Deflection profiles from FWD derived modal flexibility with impact force measurements scaled to known drop weight magnitude.
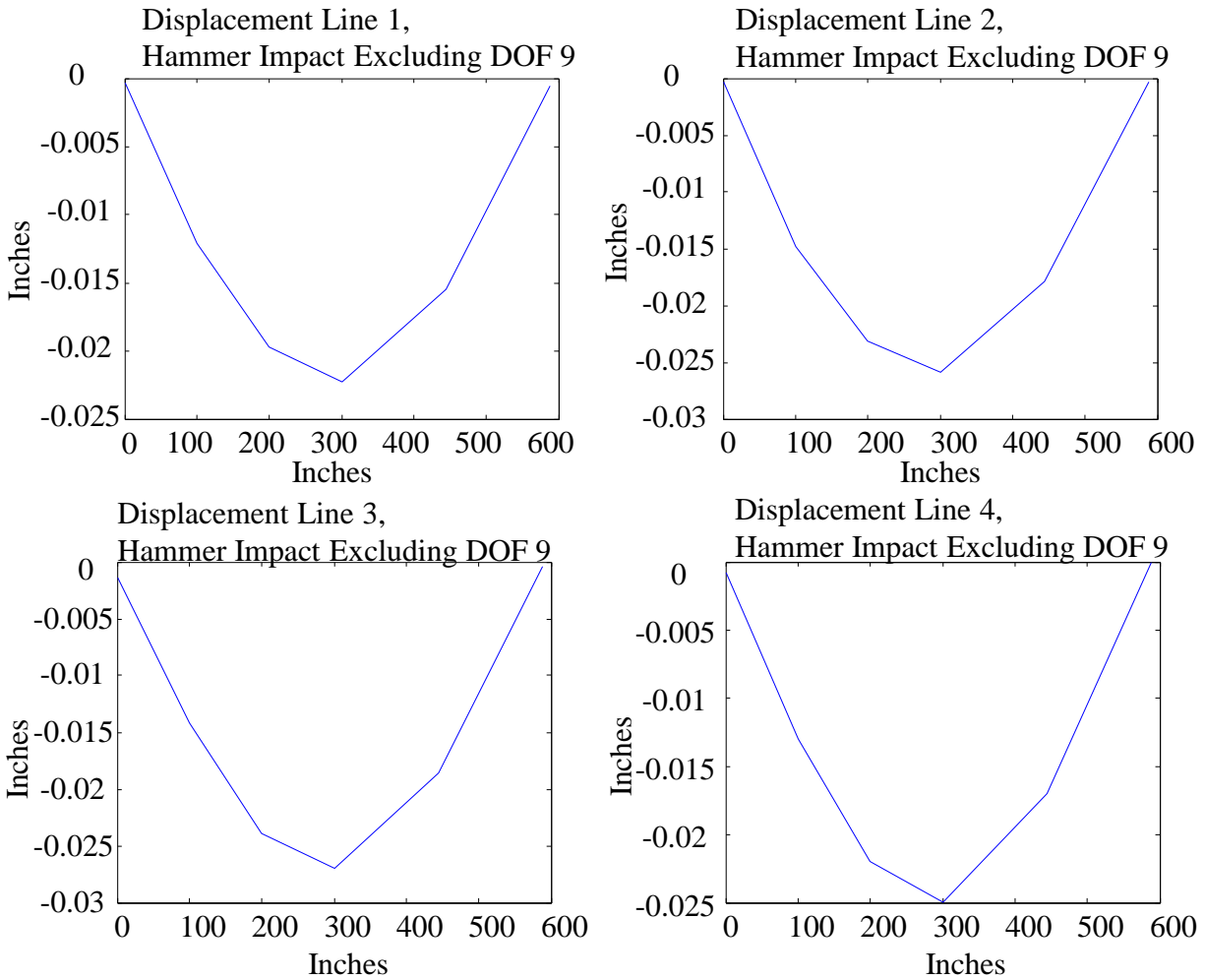
Figure 4.24: Deflection profiles from portable hammer derived modal flexibility.

The deflection profiles clearly illustrate the differences between the modal flexibility obtained by the portable impact hammer and FWD methods. The maximum deflections for each beam line obtained using the hammer impacts ranged from 0.023 inches to 0.028 inches. The maximum deflection from the unaltered FWD impacts was 1.2 inches. When the measured FWD impact is scaled to the actual drop weight value and a curve is fit over the double impacts, the resulting deflections are reduced to 0.06 inches. Altering the measured FWD impact forces to

correct for the force plate and double impact issues improves the results relative to the portable hammer results, but the differences remain large. The more consistent input-output measurements and the fact that more columns of the FRF matrix could be obtained from the portable impact hammer testing led to a more accurate and reliable modal flexibility matrix for this bridge. The results indicate that great care must be taken to ensure that good quality measurement data is obtained if the FWD device is to be used to identify modal flexibility for a bridge. The natural frequencies and mode shapes identified from the FWD device are less sensitive to the quality of the impacts since these parameters are properties of the structure and are not as significantly affected by the impact force, provided that it is broadbanded and the input locations that are not all at node points (zero displacement points) for the identified modes.

4.11.2 Baptist Ford Bridge

The results from the testing of this bridge were far more successful than the results obtained from the Hartbarger Bridge. The impact measurements from this bridge were analyzed using both the CMIF algorithm coded in MATLAB and the finite difference estimation algorithm available in the SO Analyzer software. As was the case for the Hartbarger Bridge, the FWD impact data could not be analyzed reliably using the finite difference method or the MvMIF. Because of this, only the CMIF algorithm was used to analyze the measurements obtained using the FWD impacts.

The portable impact hammer measurements were evaluated first to obtain a set of baseline results to compare with the FWD results. Initially, the processing began by finding the frequencies and mode shapes using the finite difference estimation. Using this method, the

structures first eight modes were located. The eight modes consisted of three bending and torsion modes and two of the butterfly modes. These eight modes are shown in the figure below in the order of the frequencies at which they were identified.

| 1st bending 4.185 Hz | 1st torsion 6.755 Hz | 2nd bending 9.6225 Hz |

| 3rd bending 13.195 Hz | 2nd torsion 17.205 Hz | 3rd torsion 23.83 Hz |

| 1st butterfly 35.6 Hz | 2nd butterfly 39.71 Hz |
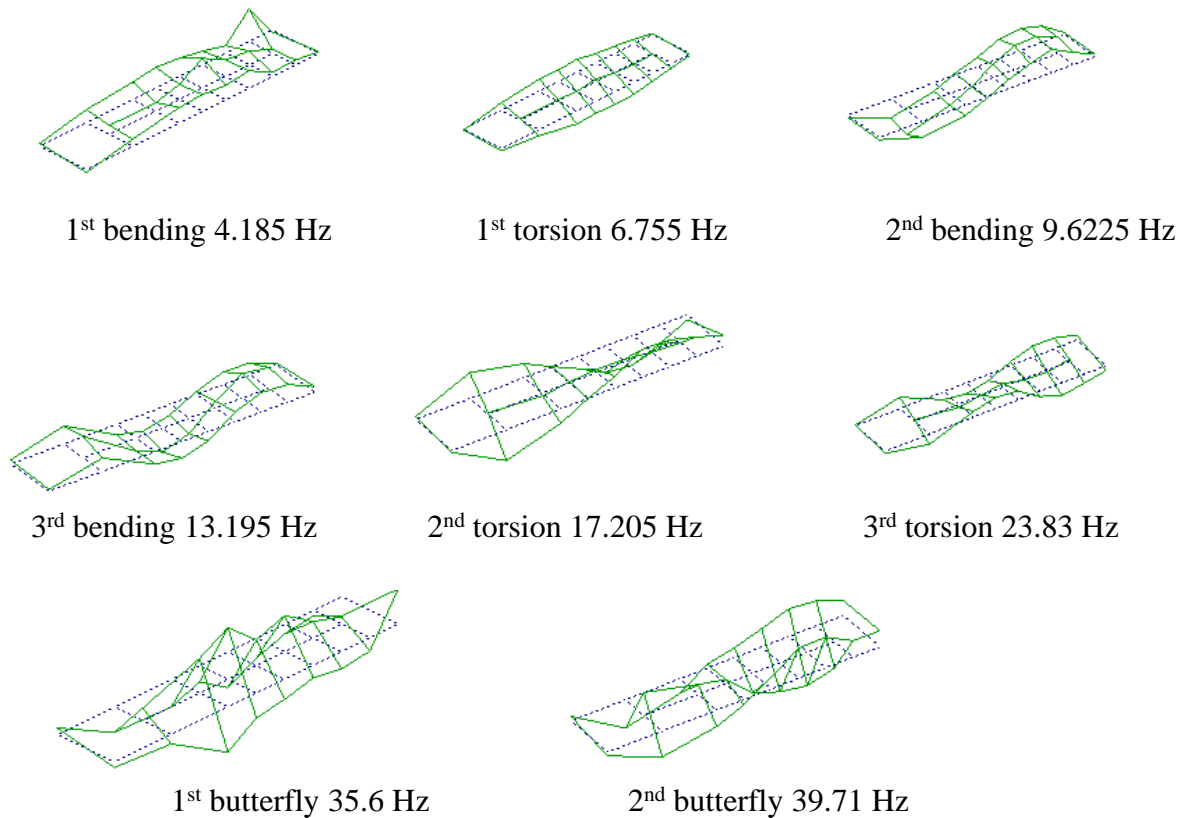
Figure 4.25: Mode shapes of the Baptist Ford Bridge using the portable impact hammer and finite difference estimation.

The eight mode shapes identified using the finite difference approach provided a good idea of where the natural frequencies would be located when the measurements were analyzed with by the CMIF algorithm. The portable impact hammer data was evaluated by CMIF to identify the natural frequencies, mode shapes, and modal A. The modal flexibility matrix was then computed using these identified modal parameters. The data collected from the hammer test gave very good results that compared closely to those found from the FWD impacts. Using the

CMIF plot and analyzing each peak within the plot, a total of twelve mode shapes were found that were able to be used in formulating the modal flexibility. These mode shapes and frequencies are listed in Table 4.5 along with those found from the FWD impacts processed with both the CMIF and the finite difference estimation. Finding twelve mode shapes within the first 25 Hz was very promising as the modal parameter estimation process was to begin. The five bending modes that are listed in the table are the only ones that can be reported with confidence. More shapes could be located, but because of the spatial resolution of the sensors on the bridge, the bending modes above 20.1874 Hz could not be used with confidence.

The data collected from the FWD impacts gave results that were much more consistent with that of the hammer for this bridge. The FWD test was more successful in part, because more input locations were impacted yielding more columns of the FRF matrix. The mode shapes that are associated with the natural frequencies summarized in Table 4.5 are shown in Figure 4.25 and Figure 4.26. The measurements from both the portable hammer and the FWD impacts were used to find the mode shapes that are shown in the figures.

Table 4.5: Natural frequencies and mode shapes identified for the Baptist Ford Bridge

	MATLAB (CMIF)			Finite Difference Estimation	
Mode	Baptist Ford Hammer Frequency (Hz)	Baptist Ford FWD Frequency (Hz)	% Difference	Baptist Ford Hammer Frequency (Hz)	Baptist Ford FWD Frequency (Hz)
1st bending	4.169	4.3154	3.39%	4.185	N\A
1st torsion	6.583	6.8023	3.22%	6.755	N\A
1st butterfly	37.96	37.9611	0.00%	35.6	N\A
2nd bending	9.581	9.6549	0.77%	9.623	N\A
2nd torsion	17.115	17.1154	0.00%	17.2	N\A
2nd butterfly	39.8629	39.7166	-0.37%	39.71	N\A
3rd bending	13.24	13.1657	-0.56%	13.19	N\A
3rd torsion	23.845	23.7714	-0.31%	23.83	N\A
3rd butterfly	44.47	44.3977	-0.16%	-	N\A
4th bending	17.554	17.4811	-0.42%	-	N\A
4th torsion	32.768	32.6949	-0.22%	-	N\A
5th bending	20.1874	20.1143	-0.36%	-	N\A

Figure 4.26: Mode shapes identified by CMIF algorithm for portable impact hammer measurements.

1st bending 4.3154 Hz   1st torsion 6.8023 Hz   2nd bending 9.6549 Hz
•Another torsion at 11.7 Hz

3rd bending 13.1657 Hz   2nd torsion 17.1154 Hz   4th bending 17.4811 Hz

5th bending 20.1143hz   3rd torsion 23.7714 Hz   4th torsion 32.6949 Hz

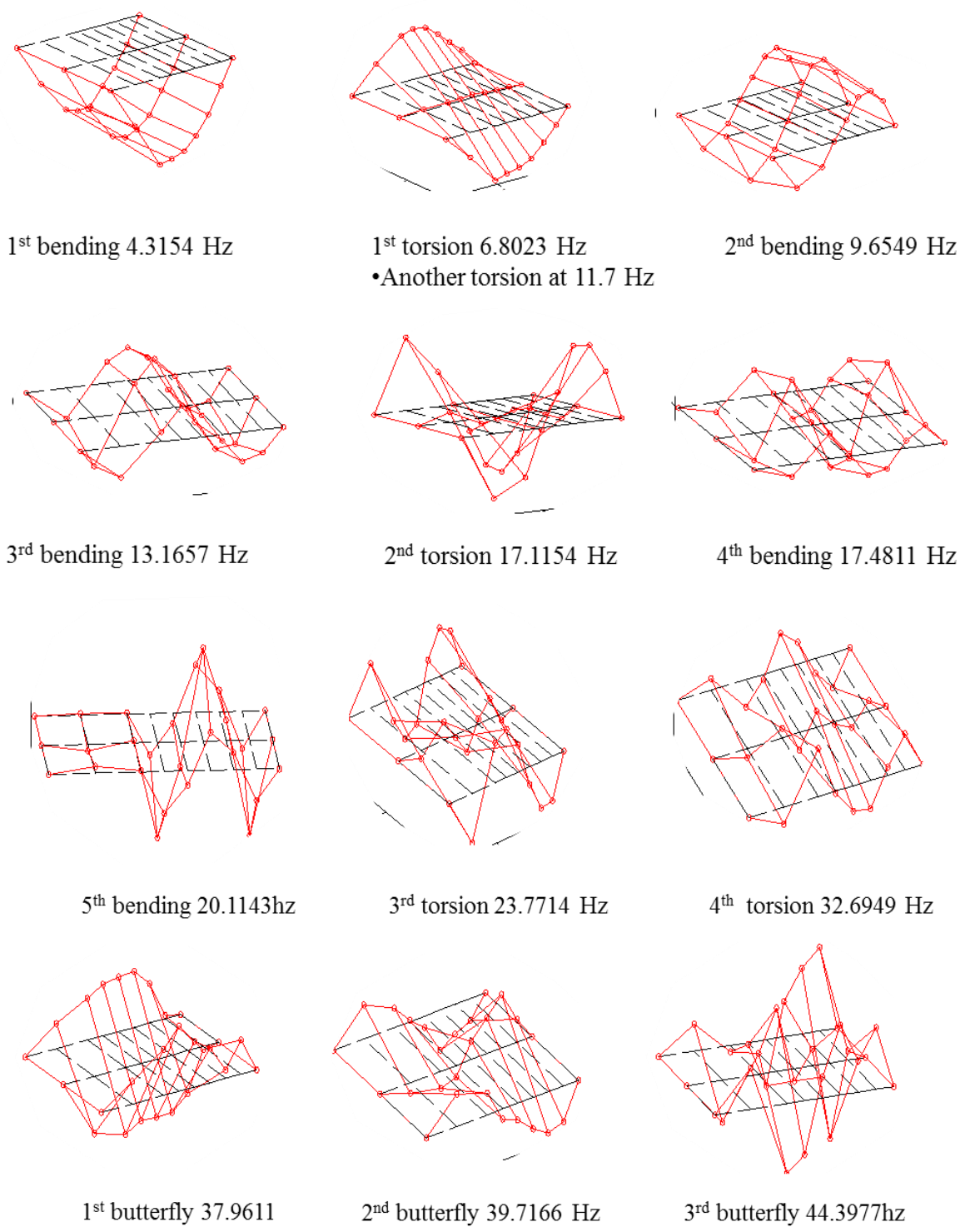1st butterfly 37.9611   2nd butterfly 39.7166 Hz   3rd butterfly 44.3977hz

Figure 4.27: Mode shapes identified by CMIF algorithm for FWD impact measurements.

It is clear from the mode shapes that this bridge is more flexible in the vertical direction than the Hartbarger Bridge because the mode shapes are far better defined. The torsion and butterfly modes show up very clearly for the Baptist Ford Bridge. The modes that are used to formulate the modal flexibility matrix correlate very well between the FWD and the hammer measurements.

The force and vibration measurements recorded for the FWD impacts were analyzed in three different ways: (1) with the measured impact force in its original state, (2) a curve was fit to the peaks in the force measurement to remove the double impact, and (3) the peak force was scaled up to match the known drop weight force. The measurements were analyzed as described for the Hartbarger Bridge and modal flexibility was computed for each approach. The modal flexibility matrices for the FWD and hammer impact data were virtually loaded by a 1 kip force at each DOF to obtain displacement profiles along the two truss lines and along the longitudinal centerline of the deck. The displacement profiles obtained from the FWD derived modal flexibility matrix that was developed using the unaltered FWD impact force measurements are shown in Figure 4.28 (upstream truss), Figure 4.29 (longitudinal centerline of bridge) and Figure 4.30 (downstream truss).
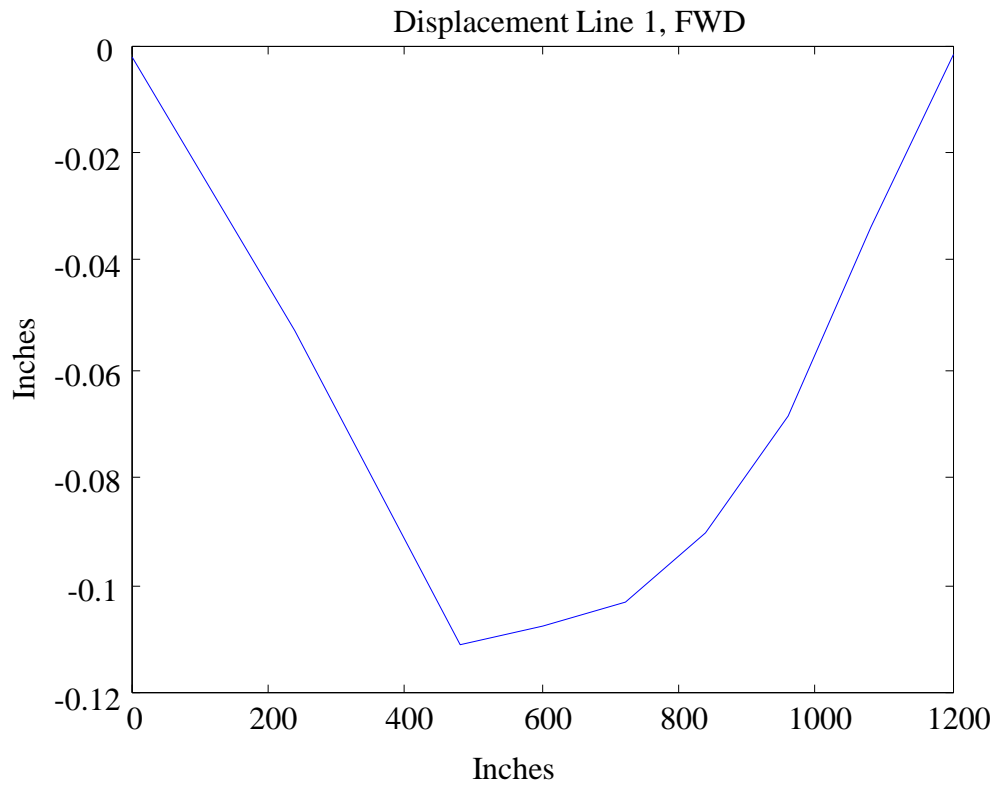
Figure 4.28: Displacement profile along upstream truss from FWD derived modal flexibility matrix.
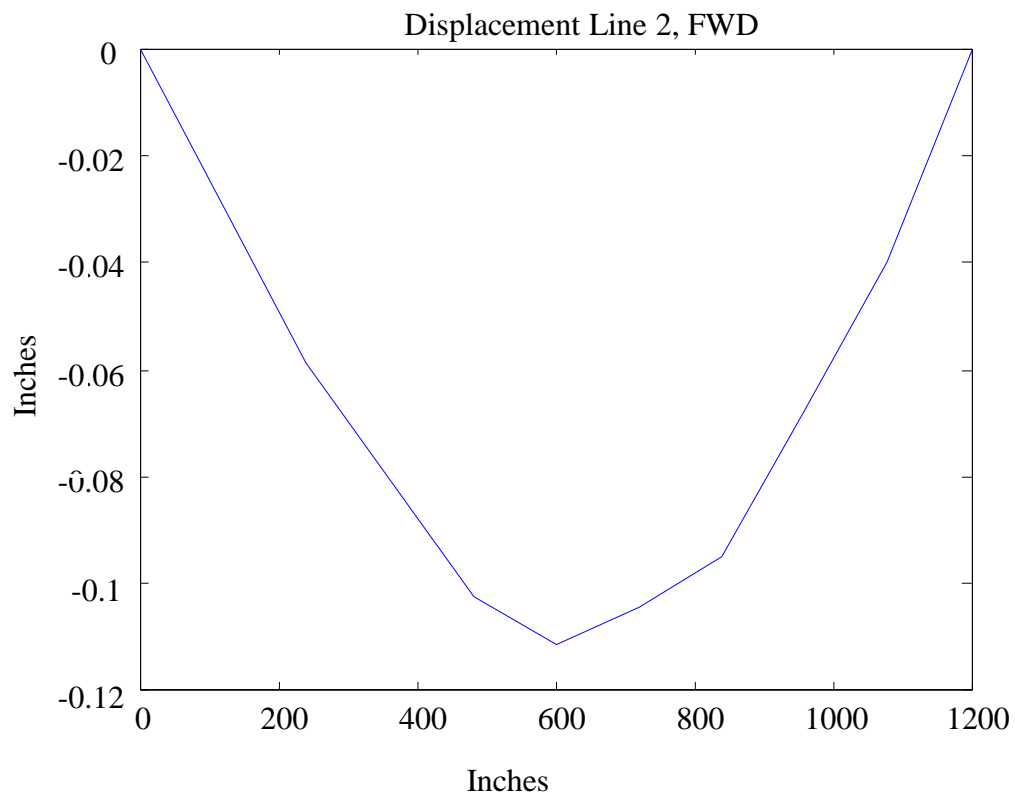
Figure 4.29: Displacement profile along longitudinal centerline of deck from FWD derived modal flexibility matrix.
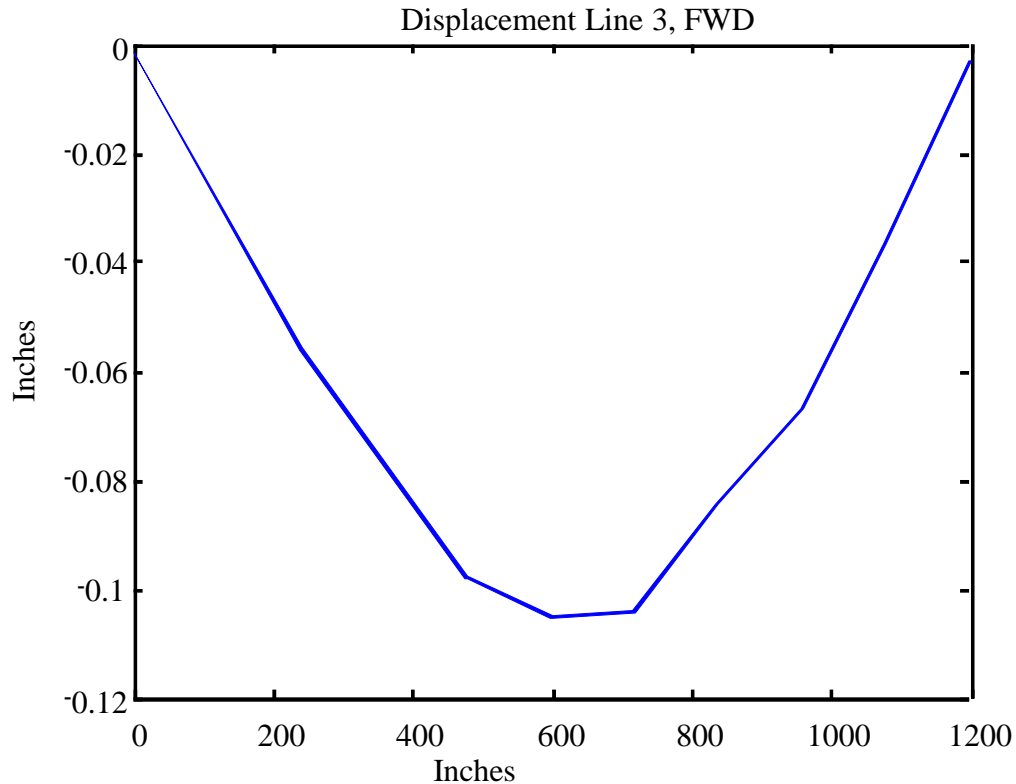
Figure 4.30: Displacement profile along downstream truss from FWD derived modal flexibility matrix.

The displacement profiles illustrate that when the modal flexibility matrix developed from the FWD impacts with unaltered impact force measurements is virtually loaded with 1 kip at each sensor location (measurement DOF), the maximum displacement of the bridge varies between 0.1 and 0.12 inches. Applying the same loading to the modal flexibility matrices obtained with the measured impact force from the FWD was modified by a curve fit over the double impacts, the maximum displacements of the bridge along the three longitudinal lines considered decreases to a range of 0.08 inches to 0.09 inches. In the case where the measured FWD impact forces were subject to a curve fit and were scaled according to the known drop weight value, the same analysis produces displacement profiles with maximum values between 0.06 inches and 0.07 inches.

The displacement profiles obtained from the modal flexibility matrices computed from the FWD impacts are compared to displacement profiles obtained in the same manner from the portable impact hammer measurements. The hammer impacts were performed at every sensor location (DOF) on the bridge. The results obtained from input sensor location G1 (see Figure 4.14) were excluded from the analysis due to a measurement error from the impact at F2. The displacement profiles for the three sensor lines obtained from the modal flexibility matrix determined from the portable impact hammer measurements are shown in Figure 4.31, Figure 4.32 and Figure 4.33.

Figure 4.31: Displacement profile along upstream truss from modal flexibility derived from portable impact hammer.
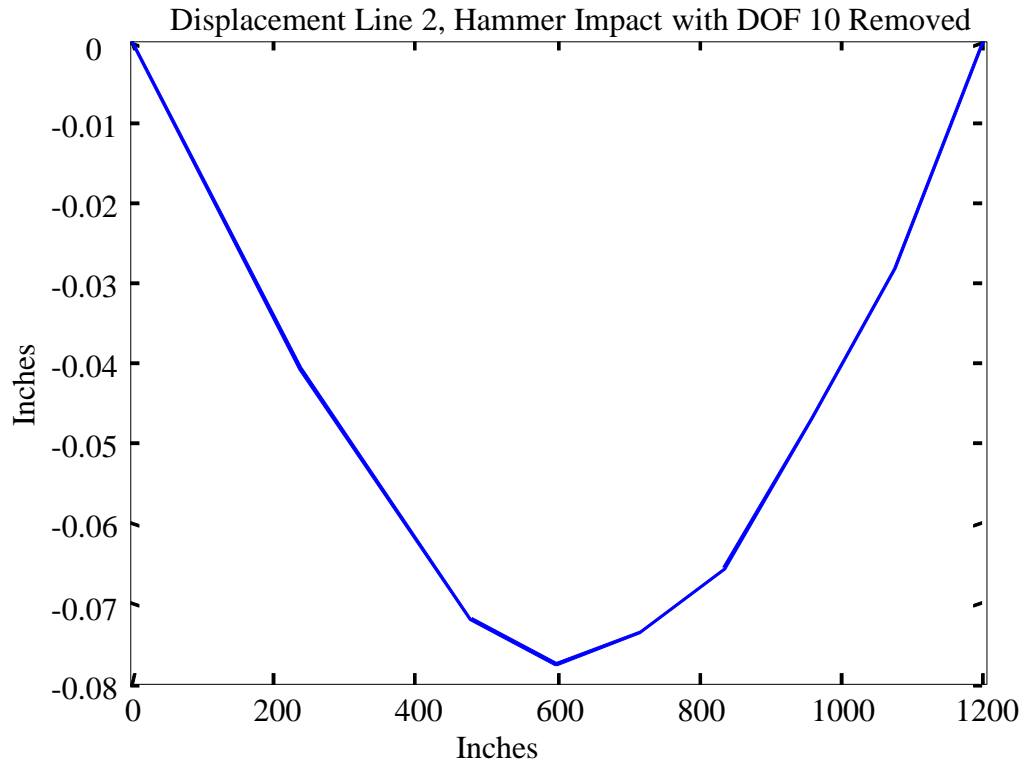
Figure 4.32: Displacement profile along longitudinal deck centerline from modal flexibility derived from portable impact hammer.
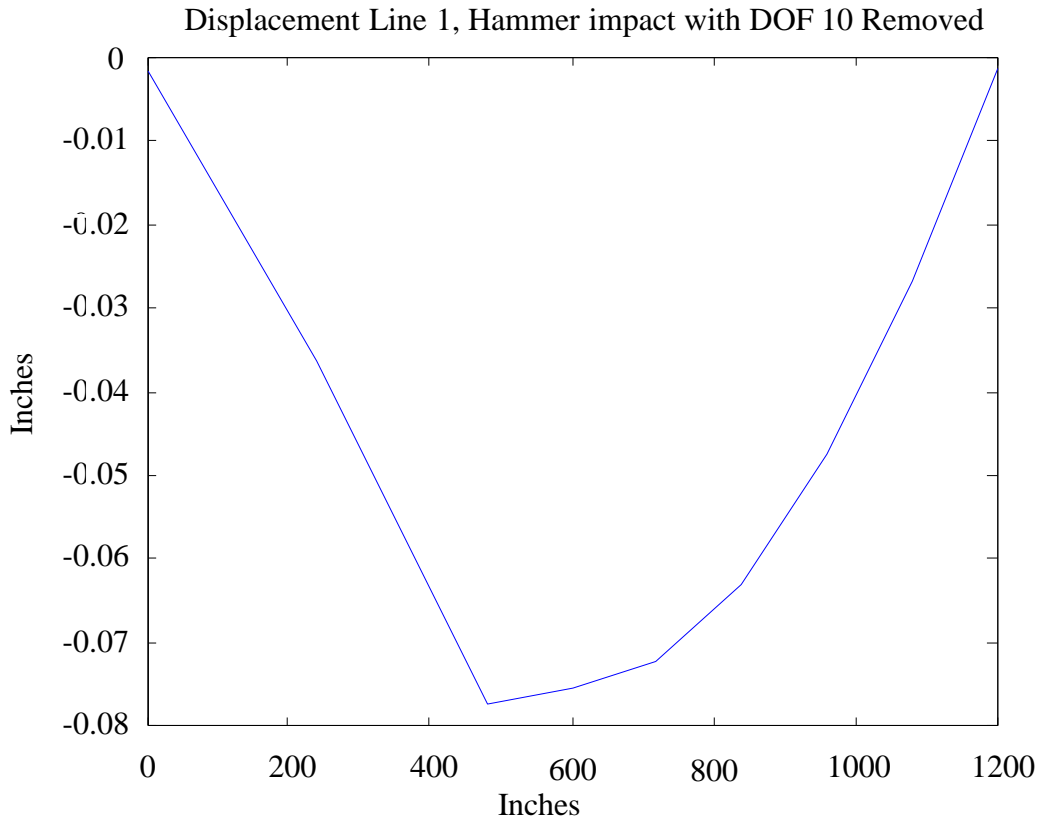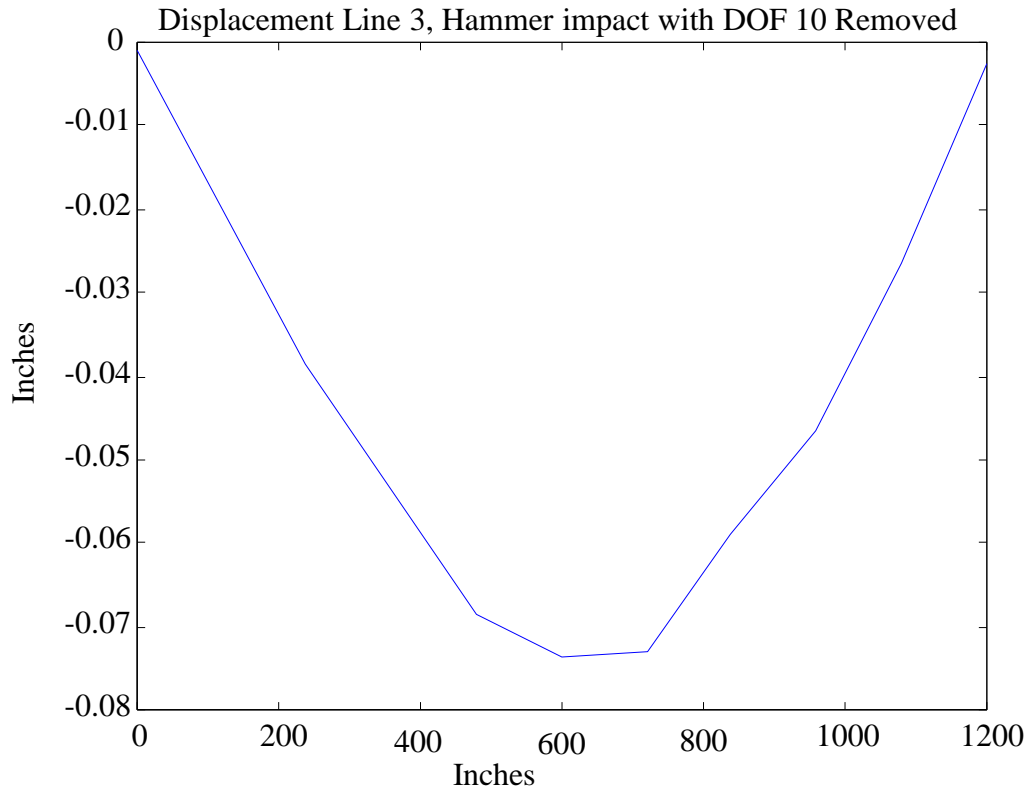
Figure 4.33: Displacement profile along downstream truss from modal flexibility derived from portable impact hammer.

The displacement profiles for the bridge obtained using the portable impact hammer measurements do show some level of correlation with the displacement profiles obtained from the FWD impact measurements. The maximum vertical displacements of the bridge computed using the portable impact hammer measurements range between 0.06 inches and 0.07 inches. These displacement results are shown and compared for the three longitudinal sensor lines for the bridge along with same profiles obtained from the FWD impacts that were curve fit and scaled to the actual drop weight magnitudes in Figure 4.34 and Figure 4.35. The FWD impact results are all within 10% of the values determined from the portable impact hammer measurements. These are very good results considering the global nature of the vibration response, that more sensor locations were impacted by the portable impact hammer than the

FWD, and that the double impacts from the FWD and force plate issues that limited the ability to directly measure the FWD impact forces in a reliable and consistent fashion. The FWD results could certainly be improved relative to the portable impact hammer if more time and money were available to develop and validate a better force plate system to be used with the FWD device.
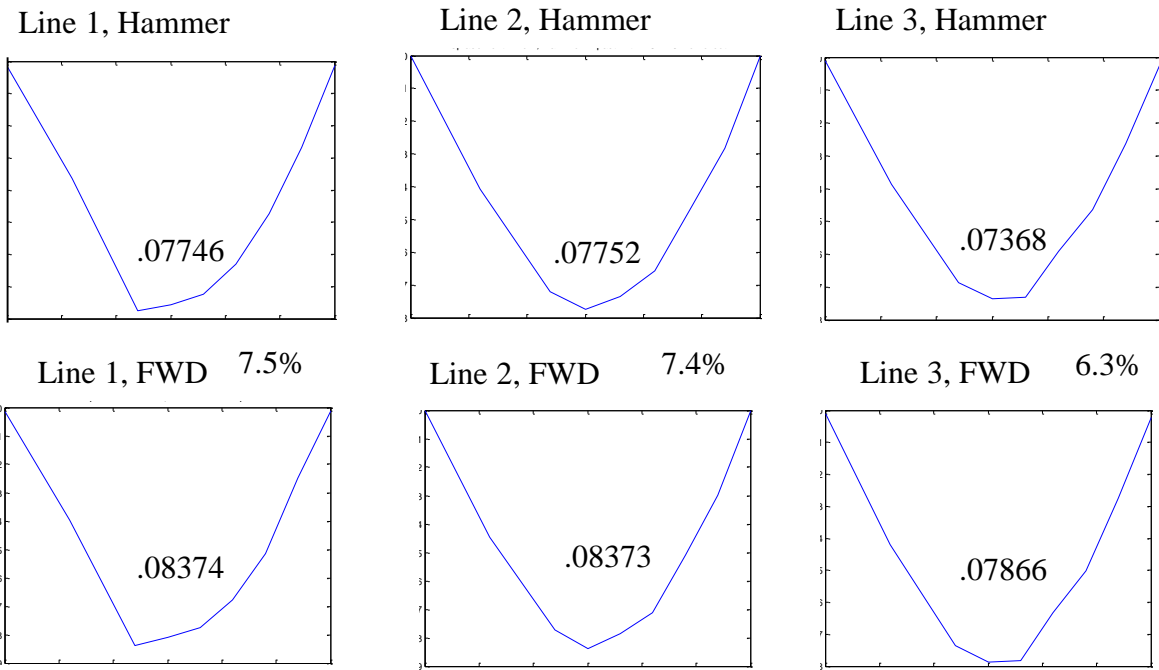
Figure 4.34: Displacement profiles and maximum displacement values from portable impact hammer and FWD impacts (curve fit and scaled) along upstream truss, longitudinal deck centerline, and downstream truss.
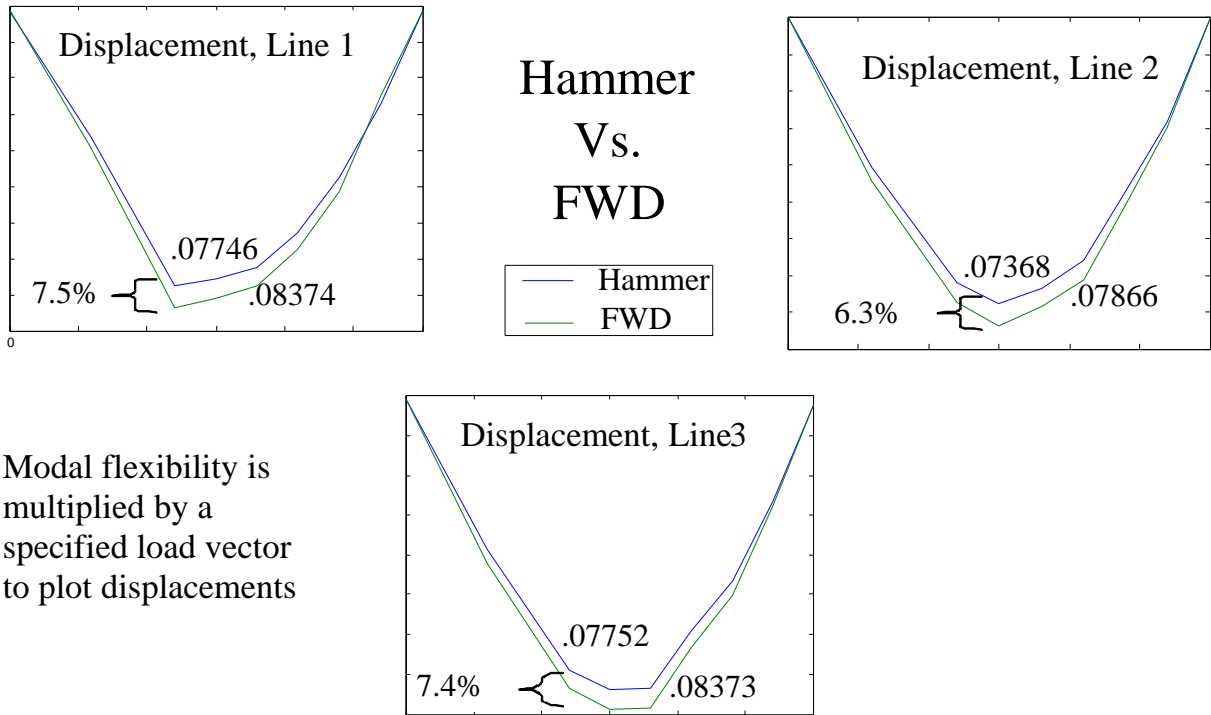
Figure 4.35: Maximum percent difference in displacement profiles from impact hammer and modified FWD impacts (curve fit and scaled) for upstream truss, longitudinal deck centerline, and downstream truss.

Unlike the Hartbarger Bridge, conclusions can be drawn between the impact hammer and the FWD as impact force sources for calculating modal flexibility. Without increasing the measured FWD impact to its actual drop weight of 9,000 lbs, the bridge appears to be more flexible than from the hammer impact measurements. This is because the accelerometers are responding to the full impact force being supplied by the FWD device, while the force plate is actually measuring a smaller impact force (some of the force bypasses the force sensor through the elastomer bumpers). This affects the resulting FRFs, which are calculated by dividing the measured displacement (computed from accelerations) by the measured force and the force measurement used in the calculation is smaller than its actual value. When the FWD impact force

is scaled to the 9,000 lb force dropped from the FWD, the maximum displacements are only slightly smaller than those computed from the portable impact hammer measurements.

4.12   CONCLUSIONS

Having analyzed the data for both of the tested bridges, conclusions can now be drawn on the analyzed results. Each bridge was subject to MRIT by two different impact devices, the FWD and a portable impact hammer. The portable impact hammer was used in both bridges to supply impacts to many more sensor locations that were used with the FWD device. This generally led to the identification of more columns in the FRF matrix being computed with the portable impact hammer than with the FWD device. The additional columns in the FRF matrix permit a better spatial representation of the global dynamic response of the bridge for impact testing. The portable impact hammer measurements on each bridge were used as a baseline for evaluating the quality of the vibration measurements from the FWD impacts.

A number of issues were encountered and multiple solutions attempted to minimize the potential for double impacts with the FWD device and to obtain accurate impact force measurements from this device. These efforts were marginally acceptable. In some cases, the doubles impacts were minimized through the use of a force plate that incorporated elastomer bumpers. A side effect resulting from the use of these devices was that some of the impact force from the FWD device would bypass the force sensor resulting in a smaller impact force being measured than was actually produced by the FWD. Measures were taken to mitigate the double impacts in the measured forces (curve fitting over the two peaks in the force measurements) and to scale the measured peak impact force to the known drop weight forces. These measures

yielded some improvements to the modal flexibility matrix determined using the FWD impact measurements. The FWD impact measurements were too limited and inconsistent for the Hartbarger Bridge testing to provide a meaningful comparison to the portable impact hammer results. The FWD impact measurements were significantly better for the Baptist Ford Bridge and the displacement profiles estimated using the FWD derived modal flexibility matrix were within 10% of the displacement profiles estimated using the portable impact hammer measurements.

These results could likely be improved with some additional time, effort and money spent on the design and validation of a force plate that will accurately and reliably measure the FWD impact forces. One potential solution using the existing elastomer bumpers could be to preload the force plate such that bumpers are pre-compressed and the top plate of the force plate assembly is in direct contact with the force sensor. A tripod arrangement of 3 force sensors could also be used to obtain a stable platform for the FWD load plate to rest on. The force measurements from the 3 sensors would be summed to obtain the total force produced by each FWD impact. Compressed gas type shock absorbers could be a potential solution for reducing the likelihood for double impacts from the FWD device. These devices are more expensive than the elastomer bumpers investigated in this study and were not compatible with the research budget; however, they may offer better and more controlled performance than what was observed using the elastomer bumpers for the force plate assembly.

Although the FWD impacts only produced a reasonable modal flexibility matrix for the Baptist Ford Bridge when the force measurements were modified, the device did provide reasonable identification of the modal parameters for both bridges, especially when the CMIF algorithm was used to analyze the input-output measurements. Such data still has value for quantitatively characterizing and describing the as-is condition of a bridge, and for evaluating

future changes in its condition. The modal parameters (natural frequencies, mode shapes, damping ratios) are properties of the structure and are directly related to the mass and stiffness of the bridge. If these parameters are tracked over time, significant changes in them would be indicative of changes to the mass or stiffness of the bridge due to damage or deterioration. This characterization is still more quantitative and perhaps meaningful to a structural engineer than qualitative evaluations of damage or deterioration obtained from visual inspections.

5.   CONCLUSION

The objective of the research discussed in this thesis was to evaluate the capabilities of using an FWD as a tool for the condition assessment of bridges. A full discussion of previous research was completed to show the history and progress of impact testing. Experiments were performed in the laboratory on a full grid model and cantilever model to validate the use of an impact hammer to excite and characterize a structure through its modal properties. Having confidence with the results from the laboratory tests, the methodology was performed on two bridges in the field. The purpose of using a FWD was to make use of an impact source that would allow for the testing to be performed rapidly with reliable results.

5.1   DISCUSSION OF LABORATORY WORK

The grid model discussed in this thesis underwent a full range of testing using both static loading and impact testing. The results from the static loadings were used to characterize the grid in terms of static flexibility. Comparing the static flexibility from load testing to modal flexibility by impact testing will validate the method. The modal flexibility by hammer impacts will be used to compare the FWD impacts in the field. The results from the grid were discussed in Chapter 3 of this thesis.

The displacement profiles for the three longitudinal girder lines permit a physical comparison of the static and modal flexibility matrices. Two impact tests were performed on separate occasions and the analysis yielded similar results. The displacement profiles obtained from the ULS plot directly on top of each other, while the displacement lines for the static test and the analytical model are also close to the impact tests. The difference between the results of

the static test and those of the impact tests vary between 15% and 20% on the three girders. This range is larger than what is desirable to draw an accurate estimation for the modal flexibility. In all cases, the girder displacement profiles obtained from the modal flexibility matrices were smaller than the static flexibility matrices (static load test and FE model). One possible reason for this difference is truncation error that occurs from using only eight modes to identify the modal flexibility matrix. The higher vibration modes of the grid were not successfully captured because of the spatial resolution of the instrumentation layout. Due to a limited amount of space for sensor placement, the number of sensors used did not allow for the higher mode shapes to be properly viewed. Having more modes will allow for a better approximation of the static flexibility. A more likely reason for the difference is probably due to the calibration of the force transducer in the impact hammer used for the MRIT program. The differences between the static and modal flexibility matrices could be reduced by a better calibration of the force transducer on the impact hammer used for the testing. Although there are differences in the displacements predicted by the static and modal flexibility matrices obtained from the grid model, the results were close enough to warrant confidence in the experimental and analytical approaches that were used in the evaluation of the grid structure. These results will allow for the use of a modal impact hammer as an impact source to compare the results from the FWD.

5.2   DISCUSSION OF FIELD WORK

Two bridges were located and full testing was completed on both the Hartbarger Bridge and the Baptist Ford Bridge. Having analyzed the data for both of the tested bridges, conclusions can now be drawn on the analyzed results. Each bridge was subject to MRIT by two different

impact devices, the FWD and a portable impact hammer. The portable impact hammer was used in both bridges to supply impacts to many more sensor locations that were used with the FWD device. This generally led to the identification of more columns in the FRF matrix being computed with the portable impact hammer than with the FWD device. The additional columns in the FRF matrix permit a better spatial representation of the global dynamic response of the bridge for impact testing. The portable impact hammer measurements on each bridge were used as a baseline for evaluating the quality of the vibration measurements from the FWD impacts.

5.3   RESULTS OF FIELD WORK

A number of issues were encountered and multiple solutions attempted to minimize the potential for double impacts with the FWD device and to obtain accurate impact force measurements from this device. These efforts were marginally acceptable. In some cases, the double impacts were minimized through the use of a force plate that incorporated elastomer bumpers. A side effect resulting from the use of these devices was that some of the impact force from the FWD device would bypass the force sensor resulting in a smaller impact force being measured than was actually produced by the FWD. Measures were taken to mitigate the double impacts in the measured forces (curve fitting over the two peaks in the force measurements) and to scale the measured peak impact force to the known drop weight forces. These measures yielded some improvements to the modal flexibility matrix determined using the FWD impact measurements. The FWD impact measurements were too limited and inconsistent for the Hartbarger Bridge testing to provide a meaningful comparison to the portable impact hammer results. The FWD impact measurements were significantly better for the Baptist Ford Bridge and

the displacement profiles estimated using the FWD derived modal flexibility matrix were within 10% of the displacement profiles estimated using the portable impact hammer measurements.

These results could likely be improved with some additional time, effort and money spent on the design and validation of a force plate that will accurately and reliably measure the FWD impact forces. One potential solution using the existing elastomer bumpers could be to preload the force plate such that bumpers are pre-compressed and the top plate of the force plate assembly is in direct contact with the force sensor. A tripod arrangement of 3 force sensors could also be used to obtain a stable platform for the FWD load plate to rest on. The force measurements from the 3 sensors would be summed to obtain the total force produced by each FWD impact. Compressed gas type shock absorbers could be a potential solution for reducing the likelihood for double impacts from the FWD device. These devices are more expensive than the elastomer bumpers investigated in this study and were not compatible with the research budget; however, they may offer better and more controlled performance than what was observed using the elastomer bumpers for the force plate assembly.

Although the FWD impacts only produced a reasonable modal flexibility matrix for the Baptist Ford Bridge when the force measurements were modified, the device did provide reasonable identification of the modal parameters for both bridges, especially when the CMIF algorithm was used to analyze the input-output measurements. Such data still has value for quantitatively characterizing and describing the as-is condition of a bridge, and for evaluating future changes in its condition. The modal parameters (natural frequencies, mode shapes, damping ratios) are properties of the structure and are directly related to the mass and stiffness of the bridge. If these parameters are tracked over time, significant changes in them would be indicative of changes to the mass or stiffness of the bridge due to damage or deterioration. This

153

characterization is still more quantitative and perhaps meaningful to a structural engineer than qualitative evaluations of damage or deterioration obtained from visual inspections.

5.4   CONCLUSION

The experimental characterization results indicated that the FWD can be an effective device for the dynamic testing of highway bridges. The FWD enabled the identification of natural frequencies and mode shapes almost identical to those by typical hammer testing. Also, the extracted modal flexibility was in agreement with modal flexibility extracted from the hammer test and static flexibility from the FE model.

The FWD has some positive qualities that make it attractive for the impact dynamic testing of bridges. First, many departments of transportation already have these devices. Second, the FWD produces an excitation force significantly larger than what can be produced by a standard hand-held impact hammer; the larger force leads to better signal to noise ratios in the measurements and more closely approximates service loads on the bridge. Finally, the FWD provides a fairly consistent impact force from hit to hit and from day to day, which is difficult and labor intensive to accomplish with a hand-held impact hammer.

The FWD has some shortcomings as an impact testing device. Most importantly, it produces a double impact that is difficult to mitigate. The device is designed to be used where the double impact is not of great importance, and eliminating the second hit does not appear to be easily rectified. For longer bridges with lower frequencies, the double impact is less important because the effect in the frequency domain is minor below 20 Hz. The FWD has accessibility issues and traffic control requirements that are not necessarily applicable to hammer testing. For

example, FWD use requires a lane closure at a minimum, and keeping the bridge free of traffic during the measurements is preferable. The width of the trailer prevents the FWD from being used very close to curbs, barriers, and so on. Thus, some additional planning may be required to co-locate impact and response measurements.

Finally, impact testing with the FWD generally is slower than with the hand-held impact hammer. The FWD requires more time to reset between hits at one location and requires considerably more time to relocate to the next impact location. The slower testing speed and the benefits of larger, more repeatable impact forces need to be considered when using an FWD for the impact dynamic testing of in-service bridges.

In general, results indicate that the FWD is an effective excitation device for the impact dynamic testing of bridges and permits the identification of some modal characteristics of the bridge provided by other EMA methods. The main benefits of this device include its ability to create large impact forces and to generate consistent forces. The FWD device definitely could be useful for screening bridges to detect significant performance or condition changes as reflected by global stiffness. Additional research and enhancements to the experimental FWD approach to mitigate the double impacts would be required if the objective is to reliably detect and quantify locations of damage or deterioration.

WORKS CITED

Bridging the Gap: Restoring and Rebuilding the Nation's Bridges, 2nd ed. AASHTO, Washington, D.C. 2008

Report Card for America's Infrastructure, 2009. ASC.

The Manual for Condition Evaluation of Bridges, 2nd ed. AASHTO, Washington, D.C., 2011

Alampalli, S., and J. Kunin. 2003. Load testing of an FRP bridge deck on a truss bridge. *Applied Composite Materials* 10 (2): 85-102.

Allemang, RJ, 1999. Vibrations: Experimental Modal Analysis. UC-SDRL.

Allemang, RJ, and DL Brown. 2006. A complete review of the complex mode indicator function (CMIF) with applications. Paper presented at Proceedings of ISMA International Conference on Noise and Vibration Engineering, Katholieke Universiteit Leuven, Belgium.

Turnage, R.S. and Baber, T.T. 2009. Field testing of the wolf creek curved girder bridge, part 1 vibration tests. Report No. FHWA/VTRC 09-CR13. Virginia Transportation Research Council, Charlottesville, VA.

Catbas, F., & Aktan, A., 2002. Condition and Damage Assessment: Issues and Some Promising Indices. *Journal of Structural Engineering*, 128:8, 1026-1036.

Catbas, F. N., D. L. Brown, and A. E. Aktan. 2006. Use of modal flexibility for damage detection and condition assessment: Case studies and demonstrations on large structures. *Journal of Structural Engineering* 132:11, 1699-1712.

Catbas, F.N. 2004. Parameter estimation for multiple-input multiple-output modal analysis of large structures. *Journal of Engineering Mechanics* 130 : 921-930.

Catbas, FN, M. Lenett, DL Brown, SW Doebling, CR Farrar, and A. Turer. 1997. Modal analysis of multi-reference impact test data for steel stringer bridges. Paper presented at Proceedings of SPIE, the International Society for Optical Engineering, 381-391.

Catbas, N., K. Ciloglu, A. Celebioglu, J. Popovics, and E. Aktan. 2001, August. Fleet health monitoring of large populations: Aged concrete t-beam bridges in pennsylvania. 6th Annual International Symposium on NDE for Health Monitoring and Diagnostics, 500-509. International Society for Optics and Photonics. Newport Beach, CA USA, March 4-8, 2001.

Doebling, SW, and LD Peterson. 1997. Computing statically complete flexibility from dynamically measured flexibility. *Journal of Sound and Vibration* 205 (5): 631-645.

Douglas, B. M., and Richardson, J.A. 1984, July "Maximum amplitude dynamic tests of a highway bridge". Paper presented at Proceedings of the 8th world conference: on earthquake engineering (Vol 6, pp 889-896).

Farrar, C. R., S. W. Doebling, P. J. Cornwell, and E. G. Straser. 1997. Variability of modal parameters measured on the alamosa canyon bridge. Paper presented at Proceedings of SPIE, the International Society for Optical Engineering.

Farrar, C. R., T. Duffey, P. J. Cornwell, and S. W. Doebling. 1999. Excitation methods for bridge structures. Paper presented at Society for Experimental Mechanics, Inc, 17 th International Modal Analysis Conference.

Hibbeler, R. C., Tan, K.H., & Nolan B. 2006. "*Structural analysis,"* sixth ed.Pearson Prentice Hall.

Hoadley, P. W., and J. P. Gomez. 1996. *Structural stiffness identification of bridge superstructures. Report* VTRC 96-R26.Virginia Transportation Research Council, Charlottesville, Va. 1996.

Hu, K-K, Niazi, K., Iyer, M., and Melhem, H. 1997. Bridge rating using KDOT FWD and the related methodologies. Report No. K-TRAN KSU-96-1, Kansas State University, Manhattan, KS.

KRÄMER, C., and S. DE. 1999. Comparison of ambient and forced vibration testing of civil engineering structures. Proceedings of IMAC (Vol. 17, pp 1030-1034).

Lenett, M., Catbas, N., Hunt, V., Aktan, A.E., Helmicki, A., & Brown, D., 1997. Issues in multi-reference impact testing of steel-stringer bridges. Proceedings - SPIE The International Society for Optical Engineerin. (374-380)

Levi, A., V. Hunt, A. Helmicki, and A. Aktan. 1997. Instrumented monitoring and diagnostic load testing of steel stringer bridges. Paper presented at PROCEEDINGS-SPIE THE INTERNATIONAL SOCIETY FOR OPTICAL ENGINEERING, (pp. 392-399). SPIE International Society For Optical.

Liu, C., and J. T. DeWolf. 2007. Effect of temperature on modal variability of a curved concrete bridge under ambient loads. *Journal of Structural Engineering* 133 : 1742-1751.

M+P. (2009). SO Analyzer Operating Manual. In m. international.

Moore, Mark, Brent M. Phares, B. Graybeal, D. Rolander, and G. Washer. *Reliability of visual inspection for highway bridges, volume I: Final report*. No. FHWA-RD-01-020,. 2001.

Pandey, AK, and M. Biswas. 1994. Damage detection in structures using changes in flexibility. *Journal of Sound and Vibration* 169 (1): 3-17.

Patjawit, A., and W. Kanok-Nukulchai. 2005. Health monitoring of highway bridges based on a global flexibility index. *Engineering Structures* 27 (9): 1385-1391.

Raghavendrachar, M., and A. E. Aktan. 1992. Flexibility by multireference impact testing for bridge diagnostics. *Journal of Structural Engineering* 118 : 2186-2203.

SAP 2000. 2010, Integrated Finite Element Analysis and Design of Structures Basic Analysis

Shih, C.Y., Tsuei, Y.G., Allemang, R.J., & Brown, D.L. 1988. Complex mode indicator function and its applications to spatial domain parameter estimation. Mechanical Systems and Signal Processing, 2(4), 367-377.

Toksoy, T., and AE Aktan. 1994. Bridge-condition assessment by modal flexibility. *Experimental Mechanics* 34 (3): 271-278.

Zhang, Z., and AE Aktan. 1998. Application of modal flexibility and its derivatives in structural identification. *Research in Nondestructive Evaluation,*Vol. 10 (1): 43-61.

Zhengsheng Li, PE, J. A. Swanson, A. J. Helmicki, and V. J. Hunt. 2005. Modal contribution coefficients in bridge condition evaluation. *Journal of Bridge Engineering* 10 : 169-178.